UNIVERSITY OF LIVERPOOL

APPROXIMATE STOCHASTIC TECHNIQUES FOR DIVERSE ENGINEERING DYNAMICS APPLICATIONS

THESIS SUBMITTED IN ACCORDANCE WITH THE REQUIREMENTS OF THE UNIVERSITY OF LIVERPOOL FOR THE DEGREE OF DOCTOR OF PHILOSOPHY

BY

NIKOLAOS GAZIS

NOVEMBER 2018

ABSTRACT

Approximate Stochastic Techniques for Diverse Engineering Dynamics Applications

By

Nikolaos Gazis

Generally, *deterministic* approaches are used in practice to analyze dynamic systems. Variations in loading conditions and material properties are taken into account by either selecting high, low or average values. Consequently, the uncertainty inherent in almost every dynamic analysis is considered just intuitively. To realistically capture the behavior of a dynamic system the intrinsic randomness must be appropriately modeled requiring concepts and methods of mathematical statistics and probability theory, as well as, random vibration theory. Undeniably, stochastic dynamics based approaches provide a more realistic modeling of the dynamic response of engineered systems allowing for enhanced design solutions. The prevailing approach used in the industry is the Monte Carlo simulation method. However, a well-known shortcoming of the method is the extensive computational cost required. Further, the class of problems of *nonlinear random vibrations* that lend themselves to exact solutions (e.g., via the associated Fokker-Planck-Kolmogorov equation) is extremely limited. Therefore, approximate approaches are desired for solving nonlinear stochastic dynamics problems. The current thesis seeks to exploit approximate stochastic dynamics tools to solve engineering dynamics problems encountered in practice. In particular, the primary focus is directed towards the recently developed Wiener path integral technique, which has been shown to poses certain advantages over alternative well-established solution methodologies, namely, computational efficiency and accuracy. Two applications are investigated: the stochastic response of nonlinear vibratory energy harvesters, and, the depth determination of ice gouging events. The accuracy/reliability of the approximate approaches is demonstrated via comparisons with pertinent Monte Carlo simulation data.

TABLE OF CONTENTS

LIST OF FIGURES

LIST OF TABLES

1 INTRODUCTION

By and large, *deterministic* approaches are used in the industry to analyze dynamic systems. Variations in loading conditions (i.e. wind, wave, earthquake, snow etc.) and material properties are taken into account by either selecting extremely high, low or average values. Observations and measurements of physical processes, however, show not only variability, but also stochasticity (Schueller, 2007). Further, researchers have concluded that accounting for the uncertainties in both the system parameters and the excitation can influence the structural performance. Igusa and Kiureghian, (1988) studied the reliability of primary/secondary structural systems (e.g. structures with secondary frames for equipment, tuned mass damper systems etc.) considering the uncertainties in both the physical properties of the system (i.e. mass, damping, stiffness etc.) and the excitation, and concluded that doing so significantly influenced the reliability of the system even when subjected to wide band random excitations. When assessing the seismic risk of structural systems equipped with linear and nonlinear dampers, Tubaldi et al. (2014) accounted for the uncertainties in model parameters in addition to the random seismic input and found that when accounting for parameter uncertainty there was a non-negligible influence on the structural performance. Further, when comparing conventional optimization design procedures (i.e. optimization methods that consider only the uncertainties in the excitation but not the system parameters) to robust ones (i.e. parameter uncertainty and uncertainty in the excitation are taken into account), Merano et al., (2010) found that robust optimization procedures provided solutions that differed from the conventional ones. Clearly, a more

realistic response is obtained when considering the inherent randomness in dynamic systems. Modeling the uncertainties and deriving the response requires utilizing concepts and methods of mathematical statistics and probability theory (e.g. Ang and Tang, 2007; Pishro-Nik, 2014), and random vibration theory (e.g Crandall and Mark, 1963; Roberts and Spanos, 2003; Lutes and Sarkani, 2004; Newland, 2005; Wirsching et al 2006).

1.1 LINEAR VS NONLINEAR SYSTEMS

Dynamic engineering systems can be modeled, to a first approximation, in terms of linear differential equations of motion, if the amplitude of motion is relatively small (Crandall and Mark, 1963; Roberts and Spanos, 2003). The adoption of a linear model is desirable as it is much easier to solve when compared to nonlinear models. Particularly, the principle of superposition, which allows for the derivation of the response using a straightforward summation procedure via Fourier's method in the frequency domain, or via the convolution integral in the time domain (see Crandall and Mark, 1963, and Section 2.3.1 for more details), is valid for linear systems but not for nonlinear systems. Further, according to the linear theory of random vibrations, the response of a linear system excited by a Gaussian process is also Gaussian (Crandall and Mark, 1963). This is important as the Gaussian or normal process can be described fully if the mean and variance of the process are known. There is no doubt that linear approximations can result in efficient solution procedures. However, it has been postulated that no real dynamic system is exactly linear, and failing to account for the effect of nonlinearities may lead to excessively conservative design solutions at best, or catastrophic failures at worst (Roberts and Spanos, 2003). In fact, nonlinear systems may have more than one equilibrium state, whereas

linear systems only have one equilibrium position. Further, the response of a nonlinear system can deviate considerably from the normal distribution.

A simple qualitative exercise can demonstrate the differences in responses between a linear and nonlinear system. Consider, for example, an oscillator with a nonlinear restoring force having the form of a third order polynomial:

$$\ddot{x} + 2\zeta\omega\dot{x} + \omega^2(x + ax^2 + bx^3) = f(t) \tag{1.1}$$

where ω is the natural frequency of the linear oscillator, ζ is the damping term, a and b control the intensity of the quadratic and cubic nonlinear terms, respectively, and $f(t)$ is the excitation modeled as a zero mean Gaussian white noise process possessing a power spectrum value of S_0. The displacement response probability density functions (PDFs) of the nonlinear system (Eq. 1.1) and the equivalent linear system (i.e. linear system having the same mean and standard deviation as the nonlinear system) are shown in Figure 1-1 for $\zeta = 0.1, \omega = 1, a = 10, \mathrm{b} = 1$ and $S_0 = 1$.

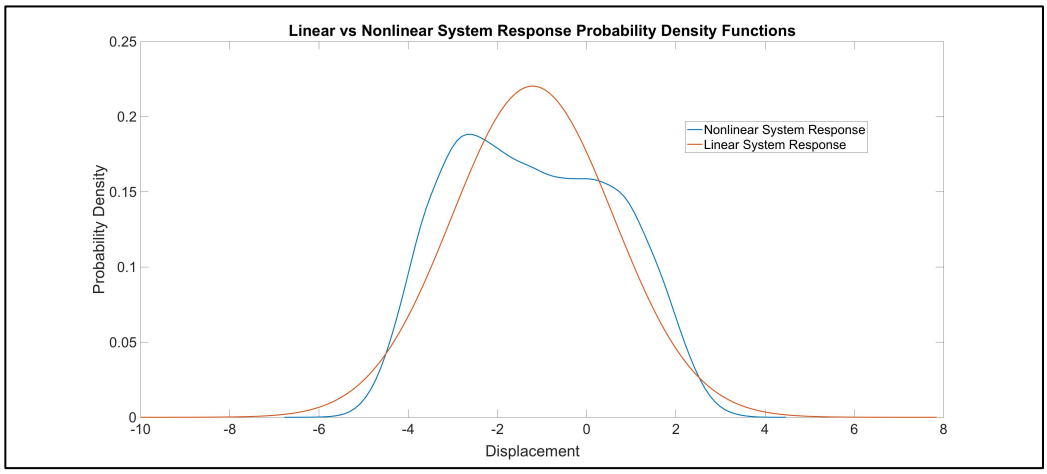

Figure 1-1: Linear vs. Nonlinear Response PDFs

It can be clearly seen in Figure 1-1 that the overall shapes of the response PDFs differ. Further, if extreme value statistics are sought, as is the case for reliability-based design, accurately estimating the shape of the tail ends of the response PDF curve becomes critical. For the current case the linear

approximation overestimates the response at the tail ends. Furthermore, the nonlinear system appears to exhibit bimodal behavior (i.e. response PDF has two peaks), which an equivalent linear system cannot accurately capture. Figure 1-2 shows the cumulative distribution functions for both the linear and nonlinear systems.

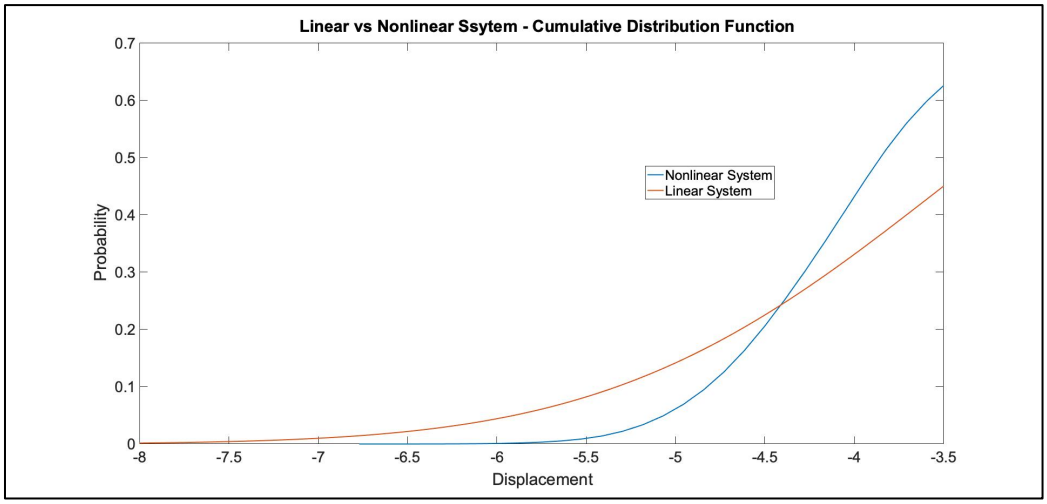

Figure 1-2: Cumulative Distribution Functions

As seen in Figure 1-2, the linear system over estimates the probability in the displacement range between -8 and -4.5, and underestimates the probability in the displacement range between -3.5 and -4.5.

It is obvious that a key requirement for any stochastic based solution method is the ability to accurately estimate the system response. Additionally, the method should be tractable which often requires that it is computationally efficient.

1.2 Stochastic-Based Solution Methods

The Monte Carlo simulation (MCS) method allows for the straightforward use of deterministic analysis procedures (Spanos and Zeldin, 1998; Rubinstein and Kroese, 2007; Au and Wang, 2014), and, based on the author's experience in industry, it is the method most commonly adopted for solving stochastic

dynamics problems in practice. The major advantage of the MCS method is that solutions can be obtained for any problem whose deterministic solution (either analytical or numerical) is known. The method is straightforward to implement, and, the approach is applicable for the estimation of both stationary and non-stationary response statistics. However, a well-known drawback of the MCS method is the extensive computational cost required. “Smart” MCS approaches have been developed (Au and Wang, 2014) to decrease the computation time. One such approach is the Subset Simulation method proposed by Au and Beck (2001). The idea behind their approach is to express the failure probability as a product of larger conditional failure probabilities by introducing intermediate failure events. The approach has been shown to be computationally efficient and accurate when compared to the direct MCS method (Schueller and Pradlwarter, 2007).

An exact solution to random vibration problems is theoretically obtained by solving the associated Fokker-Planck-Kolmogorov (FPK) equation and determining the exact response probability distribution (Caughey, 1963; Caughey and Ma, 1982). This requires that the response has the Markov property. Unfortunately, however, the class of problems of *nonlinear* random vibrations that lend themselves to exact solutions is extremely limited. Moreover, exact solutions are rare or nonexistent for non-stationary, or transient, probability distributions of Markovian models of nonlinear systems. Therefore, approximate tools are desired for solving nonlinear stochastic dynamics problems.

One such approximate tool is the *stochastic averaging technique* (Spanos, 1981b; Roberts and Spanos, 1986; Zhu, 1988). It can be applied to solve systems that are lightly damped and exposed to broadband excitations (nearly white noise). The main concept is to extend averaging techniques used in

deterministic vibrations to stochastic dynamics so as to obtain a first order differential equation of a Markovian model of an appropriate envelope of the response (Roberts and Spanos, 1986). The procedure can also be used to address both stationary and non-stationary problems. There are, however, considerable difficulties in applying the stochastic averaging technique to systems with more than one degree of freedom (see Kougioumtzoglou, 2013; and Spanos et al., 2018; for some indicative recent generalizations of stochastic averaging to account for non-stationary excitations and systems with fractional derivative elements).

A very popular approximate approach is the *statistical linearization technique*. It involves linearizing the equation of motion by replacing the original set of governing nonlinear equations with an equivalent set of linear equations; the difference between the sets being minimized in a statistical sense (Roberts and Spanos, 2003). It is an extremely versatile tool and relatively easy to implement. However, it can only yield first and second order moment statistics (e.g. mean, mean square, and power spectrum). This is due to the in-built assumption that the response is Gaussian. As such, it doesn't accurately provide an estimate of the shape of the extreme tail ends of the response probability density function. Nonetheless, the statistical linearization technique is ideally suited for initial stages of system design optimization as it provides simple response level indices, such as mean and mean square, in an efficient manner.

An alternative approach proposed by (Kougioumtzoglou and Spanos, 2009) comprises elements of both stochastic averaging and statistical linearization. Specifically, taking into account the equivalent time-dependent frequency and damping factor, a simple first-order ordinary differential equation is derived for the response variance, and a time-dependent Rayleigh distribution for the response amplitude is assumed. Analytical expressions can be derived for a

number of hysteretic and non-hysteretic nonlinear oscillators. It allows treating problems that involve non-separable and non-white excitation spectra without resorting to ad hoc pre-filtering or other spectral manipulation of the system excitation, as is the case for many of the existing linearization schemes. Though the approach is efficient and has been shown to yield fairly accurate results of the response variance of nonlinear systems, the exhibited accuracy may be inadequate for determining low probability events (e.g. failure probabilities). Further, more recent extensions of the statistical linearization technique can be found in a book by Socha (2008), while wavelet-based generalizations accounting also for fractional derivatives terms can be found in (Spanos and Kougioumtzoglou, 2012; Kong et al., 2014; Kougioumtzoglou and Spanos, 2016).

One of the promising frameworks for solving random vibration problems relates to the concept of the Wiener path integral (WPI). The WPI has strongly impacted the field of theoretical physics, however, the engineering community has so far ignored its potential as a powerful stochastic dynamics tool. Recently, in (Kougioumtzoglou and Spanos, 2012) an approximate analytical WPI technique was developed based on a variational formulation and on the concepts of stochastic averaging/linearization for addressing certain stochastic engineering dynamics problems. In this regard, relying on the concept of the most probable path an approximate expression was derived for the non-stationary response probability density function (PDF). Further, the aforementioned technique was enhanced in (Kougioumtzoglou and Spanos, 2014) circumventing the approximations associated with the stochastic averaging/linearization treatment of the previous development. The technique can account for multi-degree-of-freedom (MDOF) systems and for hysteretic nonlinearities, as well as for systems with fractional derivative terms (Di Matteo

et al., 2014). Furthermore, it has been extended for addressing certain one-dimensional mechanics problems with random material/media properties (Kougioumtzoglou, 2017) while preliminary results towards an error quantification analysis can be found in (Meimaris et al., 2017). From a computational efficiency perspective, recent work by Kougioumtzoglou et al. (2015) reduced the computational complexity by, potentially, several orders of magnitude as compared to the original formulation and numerical implementation of the technique. It is noted that the aforementioned WPI technique should not be confused with alternative numerical schemes (commonly referred to as numerical path integral schemes), which constitute, in essence, a discrete version of the Chapman–Kolmogorov (C–K) equation (Naess et al., 1993; Di Paola and Santoro, 2008; Pirrotta and Santoro, 2011; Kougioumtzoglou and Spanos, 2013a). In this regard, utilizing the C–K equation the basic characteristic of those schemes is that the evolution of the PDF is computed in short time steps; thus, rendering the schemes computationally demanding potentially. Similarly, a recently developed numerically oriented solution technique is the probability density evolution scheme (Li and Chen, 2009).

1.3 ENGINEERING APPLICATIONS

Two applications are considered in the current work, 1) the stochastic response of nonlinear vibratory energy harvesters (VEH), and 2) the depth determination of ice gouging events. Approximate stochastic dynamics tools are employed to solve the engineering problems, and special attention is paid to the adaptation of a recently developed approximate WPI technique that has been shown to be both efficient and accurate when compared to alternative well-established solution methodologies.

1.3.1 Stochastic Response of Nonlinear Vibratory Energy Harvesters

The motivation behind the development of VEHs is that compact and scalable electronic devices, such as wireless sensors, data transmitters and medical implants, are designed to function even with very low power levels. In this regard, VEHs aim at converting any available ambient energy into electricity, and eventually powering and enabling the independent operation of such devices. A main benefit of VEHs is that the need for re-charging and replacing batteries is circumvented. This is especially important considering in vivo biomedical implants such as pacemakers, where the replacement of batteries increases the risk of infection. Further, structural health monitoring applications have started benefiting from the utilization of wireless sensors powered by VEHs, resulting in reduced installation and maintenance costs as compared with alternative hard wired sensor configurations. Generally, VEHs use active materials (e.g. piezoelectric) and electromechanical coupling mechanisms to generate an electric potential in response to external/environmental excitations.

Most VEHs are subject to environmental excitations that have random and time-varying characteristics. Further, the few papers that consider stochastic excitations almost exclusively use the maximization of the average (mean) harvested power as the optimization criterion. Some papers have highlighted the need for considering higher-order or peak value statistics in the optimization process (see Daqaq et al, 2014; Adhikari et al., 2016). For example, placing restrictions on the probability the voltage remains above a certain level could be used to safeguard associated electronic circuits, or restrictions in terms of maximum displacement of the mechanical oscillator may be required in realistic situations due to limited available space, or to avoid potential mechanical failures.

A cantilever piezoelectric VEH system was adopted for the current study and was modeled as a SDOF system. The tip mass to distributed mass ratio is assumed to be sufficiently high enough for a SDOF system to accurately capture the response (Erturk and Inman, 2008a). Further, an uncoupled model is used since the electrical resistance is low (Erturk and Inman, 2008b). In other words, the mechanical oscillator influences the harvested circuit, but not vice versa. Further, both symmetrical and asymmetrical nonlinear restoring forces were considered. An exact solution to the nonlinear stochastic differential equation does not exist when assessing the non-stationary response. Therefore, approximate solutions are required. The results indicate that the adaptation of the recently developed approximate WPI technique for stochastic analysis is both computationally efficient and accurate when compared to the MCS data.

1.3.2 Ice Gouge Depth Determination

Ice gouging has been identified as a concern for oil and gas development in the arctic and thus has prompted efforts to develop mathematical models of the gouging event. Accurate theoretical models are desirable to circumvent the costly seabed survey campaigns. Therefore, it is important to understand the mechanics of the grounding berg, as well as, consider the uncertainty inherent in the environment. Sophisticated finite element method (FEM) based models have been developed to predict the ice gouge behavior, however, they require significantly more computational effort when compared to more analytical approaches. Further, FEM based methods can become computationally prohibited when utilized in conjunction with a stochastic framework. Therefore, approximate analytical treatments of the ice-gouge problem are appropriate.

The current work extends and generalizes a model proposed in (Lopez et al., 1981) circumventing some of its limitations. Further, a stochastic model is

developed taking into account the uncertainty in the environment, and the problem is solved using the WPI approach. The validity of the study is demonstrated by comparing the results to pertinent MCS data. The proposed approach is orders of magnitude less computationally demanding when compared to brute force MCS based approaches. The combination of a simplified model and the efficient WPI based solution establishes the proposed approach as a viable alternative to previous approaches, at least at a preliminary design level.

1.4 OBJECTIVES OF THESIS

There are three main objectives of the current thesis:

1. First, to provide a general overview of various tools currently available in the literature used to solve stochastic dynamics problems, including, a brief literature survey, and, the advantages and disadvantages of each method;
2. Second, to demonstrate the efficacy of the tools by applying them to two distinct stochastic dynamics problems. The two applications are diverse to exhibit the versatility of the approaches, and, to provide insight into when one approach is more advantageous over another. The results are compared with exact solutions when available or with pertinent MCS data;
3. Third, to show the capabilities of the WPI technique, and present the approach as a promising and efficacious solution tool in the field of stochastic engineering dynamics.

The originality of the thesis is demonstrated in the second and third objectives. In the case of the VEH, most studies to date consider the stationary response

and focus on optimizing the mean power output. The current study accurately and efficiently estimates the response PDF considering a non-stationary excitation with a focus on the estimation of low probability events (i.e. accurately estimating the shape of the tail ends of the response PDF curve). Further, the adaptation of the recently developed potent approximate WPI technique is presented for the stochastic response of VEHs possessing symmetric and asymmetric restoring forces.

Regarding the ice gouge depth determination problem, most of the theoretical models in the literature are deterministic, and thus, it can be argued that they cannot capture many aspects of the ice gouge mechanism, as the uncertainties inherent in the environment are not considered. In this regard, an existing phenomenological model is generalized and then extended to account for the uncertainties in the environment. The main advantages of the proposed approach are computational efficiency and accuracy, which hinge on the simplified model adopted to estimate the gouge depth coupled with the WPI based solution used to conduct the stochastic analysis.

1.5 THESIS OUTLINE

The following is an outline of the thesis.

Section 2 – Random Vibration Theory

A brief overview of random vibration theory is presented for the purpose of providing the appropriate background for the stochastic dynamic tools used to solve the engineering problems presented in this thesis.

Firstly, an introduction to probability theory and stochastic processes is presented. Then, the stochastic input-output relationship is shown, and, finally,

the response of a single degree of freedom (SDOF) system excited by a stationary stochastic process is solved.

Section 3 – Monte Carlo Simulation Method

The Monte Carlo Simulation method is presented in this section. A general introduction to the MCS method is outlined, and some pertinent literature is referenced. Special attention is paid to the spectral representation method and the simulation formula is presented. Next, an example is solved considering a nonlinear oscillator excited by a non-stationary stochastic excitation to demonstrate the MCS procedure.

Section 4 – Statistical Linearization

This section is concerned with the statistical linearization method. An overview of the method and relevant references are presented. The procedure is described by considering a simple system possessing a single nonlinear element. Then, the case of a Duffing oscillator excited by a stationary stochastic process is solved. The accuracy of the approach is demonstrated by comparing the results to the exact solution derived via the associated Fokker-Planck-Kolmogorov equation. Next, an extension of the linearization procedure is employed to handle non-stationary random excitations. The solution estimated using the approximate approach is compared with MCS data. Finally, the advantages and disadvantages related to the estimation of failure probabilities are discussed.

Section 5 – Wiener Path Integral

The Wiener Path Integral method is outlined in this section. A brief background and literature survey are presented. The WPI and most probable path formulation are shown. The case of a linear oscillator excited by a white noise

process is presented first, and it is demonstrated that an analytical solution for the most probable path can be determined without resorting to numerical treatment of the boundary value problem. Then an example is solved considering a Duffing oscillator excited by a white noise process. The accuracy of the approach is confirmed by comparing the transient and steady state responses to pertinent MCS data.

Section 6 – Stochastic Response of Vibratory Energy Harvesters

The subject of vibratory energy harvesting is presented in this section. A nonlinear model proposed by previous authors is adopted and the non-stationary responses of the VEH subjected to (time-modulated) white noise excitations are assessed. The statistical linearization and the WPI approaches are employed to derive the response of the nonlinear VEH with symmetrical restoring force, and the results are compared to MCS data. Next, the case considering an asymmetric restoring force is presented, and the accuracy of the WPI technique is demonstrated by comparing the results to pertinent MCS data.

Section 7 – Ice Gouge Depth Determination

The problem of ice gouging is presented in this section. A simplified model of the motion of a grounding iceberg for determining the gouge depth into the seabed is proposed. The uncertainties relating to the soil strength are modeled, and a nonlinear stochastic differential equation governing the evolution of the gouge length/depth in time is derived. The Wiener path integral based approach is employed. Finally, the accuracy/reliability of the approach is demonstrated via comparisons with pertinent MCS data.

Note: the author has published the results of this study in the peer-reviewed archival International journal ASME OMAE (Gazis et al., 2017).

Section 8 – Conclusions and Future Work

Conclusions from the current work are drawn, future work is presented and references follow.

2 RANDOM VIBRATIONS: A BRIEF OVERVIEW

A general overview of random vibrations is presented in this section for the purpose of providing the appropriate background for the stochastic dynamic tools used to solve the engineering applications presented in this thesis. For a more thorough description of random vibration theory see (Crandall and Mark, 1963; Roberts and Spanos, 2003; Lutes and Sarkani, 2004; Newland, 2005; Wirsching et al 2006; Li and Chen 2009).

When reviewing a vibration record a natural tendency is to look for a repeating pattern in order to characterize the record in some simple manner - the simplest being a sinusoid. If, however, there is no apparent pattern then the vibration record is sometimes referred to as a *random vibration*. In addition to the given record, the totality of the possible records that might equally have been produced under the same conditions should be considered. If an experiment was conducted to produce a record and a similar record results when repeating the experiment then the process is said to be *deterministic*. However, if the records continually differ from each other when repeating the experiment while maintaining the same conditions, then the process is said to be random (Crandall and Mark, 1963). Figure 2-1 provides examples of deterministic and random records.

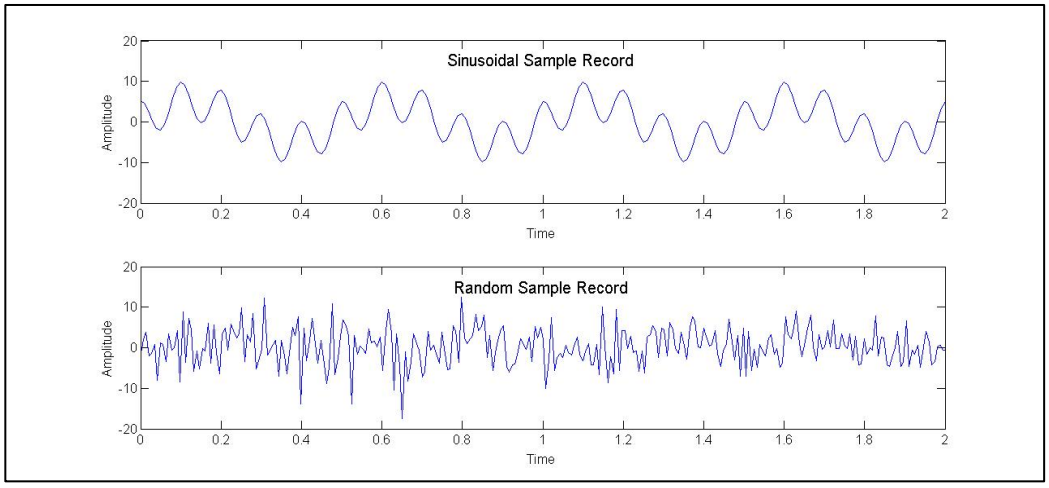

Figure 2-1: Sinusoidal and Random Sample Records

As can be seen in Figure 2-1, there is an apparent pattern in the top record (i.e. a combination of sinusoids), however, there does not appear to be a repeating pattern in the bottom record. A sinusoidal signal is characterized by its amplitude and its frequency. On the other hand, a random vibration signal can be characterized by an average amplitude and by a decomposition in frequency. The average amplitude most commonly employed is the root mean square (RMS) and the frequency decomposition is indicated by the mean square spectral density (Crandall and Mark, 1963). Further, other statistical parameters, such as the probability distribution function, can be provided for a more complete probabilistic description of a signal.

2.1 INTRODUCTION TO PROBABILITY THEORY

The probability of an event 'A' occurring may be written as $P(A)$. $'A'$ is considered a random event since it is not certain and not impossible, but has a chance of occurring. The quantity $P(A)$ is a numerical measure of that chance and is a number such that $0 \leq P(A) \leq 1$. The event A is certain if $P(A) = 1$ and is impossible if $P(A) = 0$. The following definitions are required to describe the relationship between events (Roberts and Spanos, 2003):

- $P(A, B, C, \ldots, N)$ is the probability that all the events $A, B, \ldots, N$ occur.
- $P(A + B + C \ldots + N)$ is the probability that at least one of the events occurs.
- $P(A|B)$ is the 'conditional probability' that the event A occurs, given that B has occurred.

Using the above notation, the following axioms governing probability theory are defined (Kolmogorov, 1956):

Let A be a random event and let $P(A)$ be the probability that event A occurs. Then, $P(A)$ is a number between 0 and 1:

$$0 \leq P(A) \leq 1 \tag{2.1}$$

Let S be the sample space containing all possible events (i.e. $S = A, B, C, \ldots, N$). Then, the probability of any event in the sample space occurring is 100%:

$$P(S) = 1 \tag{2.2}$$

If events $A, B, C, \ldots, N$ are disjoint events (i.e. there is no overlap between them), then

$$P(A + B + C \ldots + N) = P(A) + P(B) + P(C) \ldots + P(N) \tag{2.3}$$

In other words, the probability of the union of disjoint events is equal to the summation of their probabilities.

Further, the events A and B are considered 'independent' if $P(A|B) = P(A)$ and $P(A, B) = P(A)P(B)$. And, generally, the events $A, B, C, \ldots, N$ are independent if $P(A, B, \ldots, N) = P(A)P(B)P(C) \ldots P(N)$.

Furthermore, the probability that events A and B will occur is equal to the product of the probability of A occurring given that B has occurred, and the probability of B occurring:

$$P(A,B) = P(A|B)P(B) \tag{2.4}$$

2.1.1 Random Variables and Probability Distributions

The outcome of a random experiment is represented by a number, which is referred to as a *random variable*. A discrete random variable is one for which the sample space consists of integer values. In other words, the set of values a discrete random variable can take on (i.e. its "support") is part of a countable set (e.g. 6 possible outcomes for a rolling die). The support of a discrete random variable can be finite or infinite. The probability distribution of a discrete random variable is called a probability mass function (PMF). The PMF provides the probability the discrete random variable will take on a value in a given set.

A continuous random variable is one for which the sample space consists of a range of values on the real number line. The number of points on a real number line is theoretically infinite. The function that describes the distribution of probability density over the sample space of the continuous random variable is called the probability density function (PDF). For a continuous random variable, X, the PDF is designated $f_X(x)$. To find the probability of X occurring between a and b, $f_X(x)$ is integrated from a to b:

$$P(a < X < b) = \int_a^b f_X(x)dx \tag{2.5}$$

Further, the total area under the PDF is equal to unity:

$$\int_{-\infty}^{\infty} f_X(x)dx = 1 \tag{2.6}$$

In other words, there is 100% certainty that x is somewhere between $-\infty$ and $+\infty$ (under the implicit understanding that x is a real number).

The cumulative distribution function (CDF) is an alternate way to describe the probability density of a random variable. For a continuous random variable, X, the CDF defines the probability that X is less than or equal to a specific value:

$$F_X(x) = P(X \leq x) \tag{2.7}$$

and can be calculated by integrating the PDF for all values of X less than or equal to x:

$$F_X(x) = \int_{-\infty}^{x} f_X(x)dx \tag{2.8}$$

Conversely, the PDF may be found from the CDF by differentiation:

$$f_X(x) = \frac{dF_X(x)}{dx} \tag{2.9}$$

The mean (or expected value) of a random variable is

$$E[x] = \mu_X = \int_{-\infty}^{\infty} x f_X(x)dx \tag{2.10}$$

The variance is a measure of how "spread out" the distribution of the random variable is. It is the average of the deviation from the mean:

$$E[(x - \mu_X)^2] = \sigma_X^2 = \int_{-\infty}^{\infty} (x - \mu_X)^2 f_X(x)dx \tag{2.11}$$

In other words, the variance is the mean square minus the square of the mean:

$$\sigma_X^2 = E[x^2] - (E[x])^2 \tag{2.12}$$

The square root of the variance is the *standard deviation*. If the mean is zero, then, the variance is just the mean square, $E[x^2]$.

2.1.1.1 The Gaussian Distribution

In many practical problems the random variables of concern have a probability distribution that can be closely approximated by the ideal form known as the *normal* or *Gaussian* distribution. The theoretical basis for this observation is the so-called Central Limit Theorem, which states that if $A1, A2, \ldots, An$ are n independent random variables, with arbitrary distributions, then the sum of these variables, $a = A1 + A2 + \ldots + An$, is a random variable which tends to that of a Gaussian distribution as n becomes large. The importance of this result comes from the fact that many random variables in real life can be expressed as the sum of a large number of random variables and, by the *Central Limit Theorem*, one can argue that they will have distributions which are close to the Gaussian form.

The PDF of the Gaussian distribution is the following:

$$p(x) = \frac{1}{\sqrt{2\pi}\sigma} e^{\frac{-(x-\mu)^2}{2\sigma^2}} \tag{2.13}$$

An important property of Gaussian random variables is that any linear combination of such variables is also Gaussian.

2.1.1.2 Joint Distributions

The first-order PDF $f_X(x)$ specifies the probability $f_X(x)dx$ that a random variable lies in the range of values x to $x + dx$. A second-order PDF $f_{XY}(x, y)$ is defined in the same way but extends the number of random variables from one to two, in this case X and Y. The probability that the random variable X lies in the range of values x to $x + dx$ and that the random variable Y lies in the range of values y to $y + dy$ is given by $f_{XY}(x, y)dxdy$.

In order to determine the joint distribution that X occurs between a and b, and that Y occurs between c and d, $f_{XY}(x,y)dxdy$ is integrated from a to b and from c to d:

$$P(a < X \leq b) \; and \; P(c < Y \leq d) \; = \; \int_a^b \int_c^d f_{XY}(x,y)dxdy \tag{2.14}$$

The joint PDF $f_{XY}(x,y)dxdy$ may therefore be represented as a two-dimensional surface for which the volume contained underneath the surface is unity:

$$\int_{-\infty}^{\infty} \int_{-\infty}^{\infty} f_{XY}(x,y)dxdy = 1 \tag{2.15}$$

Further, the first order densities $f_X(x)$ and $f_Y(y)$ can be obtained from the joint density $f_{XY}(x,y)$ through integration:

$$f_X(x) = \; \int_{-\infty}^{\infty} f_{XY}(x,y)dy \tag{2.16}$$

and

$$f_Y(y) = \; \int_{-\infty}^{\infty} f_{XY}(x,y)dx \tag{2.17}$$

2.1.2 Functions of Random Variables

Given a function $Y = g(X)$, and suppose X is a random variable, then the results of function Y is also a random variable. The mean and variance of Y, μ_Y and σ_Y, can easily be computed by appropriately integrating the PDF of X. However, determining the actual distribution of Y, $f_Y(y)$, is more involved. The method employed to solve for the distribution of Y is referred to as the *change of variables or method of* transformation (Pishro-Nik, 2014).

Assuming the function $g(X)$ is differentiable and is a strictly increasing function, that is if $x_1 < x_2$, and $g(x_1) < g(x_2)$, then, the probability density function of the random variable Y is given by

$$f_Y(y) = f_X(g^{-1}(y)) \frac{d}{dy} g^{-1}(y) \quad (2.18)$$

Of course the method works for a function that is strictly decreasing as well. The proof is based on the consideration that the probability of obtaining a value of Y in the interval $[y = g(x),\ y + dy = g(x + dx)]$ is equal to the probability of obtaining a value of X in the interval $[x, x + dx]$. In other words,

$$P(y \leq Y \leq y + dy) = P(x \leq X \leq x + dx) = f_Y(y)dy = f_X(x)dx \rightarrow$$

$$f_Y(y) = f_X(x) \frac{dx}{dy} \quad (2.19)$$

For a function $Z = X + Y$ where X and Y are two independent random variables, the PDF of Z is given by convolution integral (Pishro-Nik, 2014):

$$f_Z(z) = \int_{-\infty}^{\infty} f_X(x)\, f_Y(z - x)\, dx \quad (2.20)$$

2.2 STOCHASTIC PROCESSES

As presented earlier, a random variable is a number that characterizes an event belonging to a complete set of events. A sample value is obtained every time a random experiment is performed. In other words, each experiment produces a number from the set of possible values. After a sufficient number of such observations, one will get an idea of the likelihood of various outcomes and can estimate the probability distribution and/or expected values of the random variable. As a natural extension, it may be envisioned that a function of time, instead of just a number, is obtained every time a random experiment is carried out. The sample function obtained will, in general, be different every time the experiment is performed, and there is thus an infinite set, or *ensemble,* of possible sample functions, or realizations. This infinite set is referred to as a stochastic or *random process*. Again, a sufficient number of observations will

allow for the estimate of probabilities and expected values related to the process. Figure 2-2 shows an example of six realization samples.

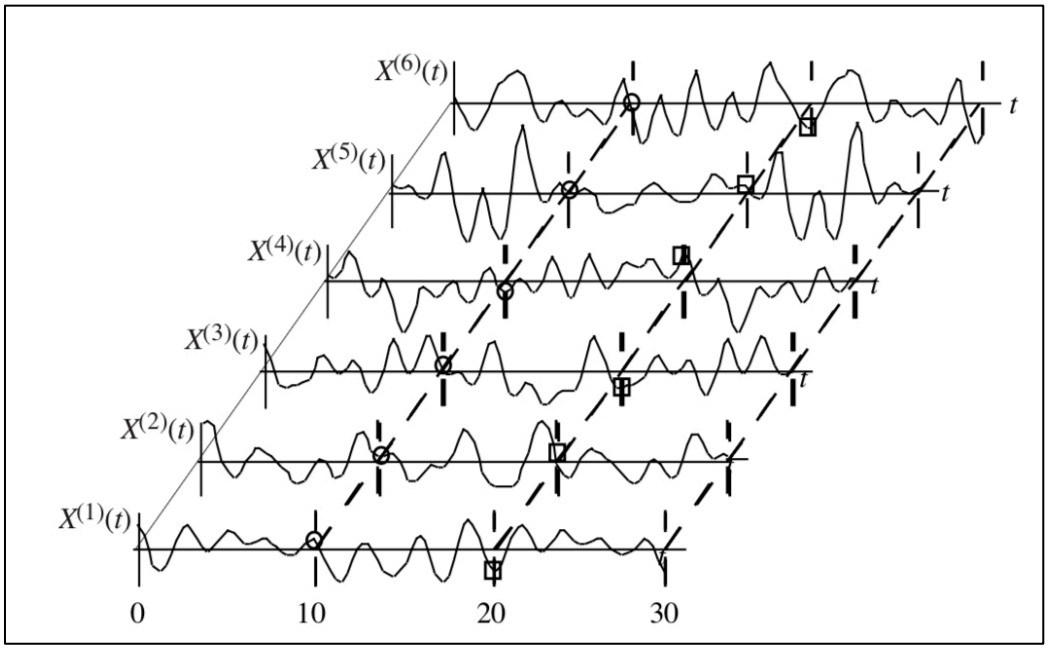

Figure 2-2: Sample of Realizations of Random Process

Note that the stochastic processes considered in the present study are continuous time, continuous state processes. In other words, the time variable and state space assume a continuous range of values. Stochastic processes can take the form of discrete time, discrete state, where both the time and state space belong to a countable set, or continuous time, discrete space, and discrete time, continuous space where one of the two values (either time or state space) belongs to a countable set while the other to a range of values.

2.2.1 Ensemble Averages, Mean, and Correlation

A random process consists of a (theoretically) infinite number of sample functions each of which can be thought of as resulting from a separate experiment. The set of functions of a random process is called the ensemble. Averages can be measured across all samples (i.e. ensemble average). For example, considering the random process $X(t)$ shown in Figure 2-2, the

probability distribution for X at time instance 10 can be calculated by considering all the values of the realizations at $t = 10$. Note that this is different from taking averages across a single sample function that is referred to as a *temporal average*. The distribution of values at any given time is called the marginal distribution of the process $X(t)$. The mean of the process at time t, $\mu_X(t)$, is calculated by taking the expected value across the ensemble, that is the ensemble average, using the marginal density function:

$$\mu_X(t) = E[X(t)] = \int_{-\infty}^{\infty} x\, f_{X(t)}(x)dx \tag{2.21}$$

Similarly, the variance at time t, $\sigma_X^2(t)$, is calculated across the ensemble as:

$$\sigma_X^2(t) = E[(X(t) - \mu_X(t))^2] = \int_{-\infty}^{\infty}[x - \mu_X(t)]^2\, f_{X(t)}(x)dx \tag{2.22}$$

The joint distribution of $X(t)$ at all times t provides a complete picture of the random processes. Any number of time instances may be considered for a joint distribution, for example, $X(t_1), X(t_2), X(t_3), \ldots, X(t_n)$, but the most practical case is to consider $X(t)$ at two time instances, $X(t_1)$ and $X(t_2)$.

An important joint measure in a random process is the correlation of the process with itself at two different times, $X(t_1)$ and $X(t_2)$. Denoted $R_X(t_1, t_2)$, this measure of correlation is called the *autocorrelation* function and is calculated as follows:

$$R_X(t_1, t_2) = E[X(t_1), X(t_2)] = \int_{-\infty}^{\infty} x_1 x_2 f_{X(t_1)X(t_2)}(x_1, x_2)\, dx \tag{2.23}$$

Another measure that is related to the autocorrelation function is the *autocovariance* function, $\sigma_{xx}(t_1, t_2)$, and is defined as:

$$\sigma_{xx}(t_1, t_2) = E\big[\{X(t_1) - \mu_\chi(t_1)\}\{X(t_2) - \mu_\chi(t_2)\}\big] = E[X(t_1), X(t_2)] - \mu_\chi(t_1)\mu_\chi(t_2) = R_X(t_1, t_2) - \mu_\chi(t_1)\mu_\chi(t_2) \tag{2.24}$$

Further, the autocorrelation coefficient function $\rho_{XX}(t_1, t_2)$ is defined as:

$$\rho_{XX}(t_1, t_2) = \frac{\sigma_{XX}(t_1,t_2)}{\sigma_X(t_1)\sigma_X(t_2)} \quad (2.25)$$

The autocorrelation function, autocovariance function, and autocorrelation coefficient function all provide measures of the linear dependence of $X(t_1)$ and $X(t_2)$. In general, this dependence varies with the particular times t_1 and t_2.

2.2.2 Stationary Stochastic Process

The probability distributions of all random processes representing physical phenomena evolve with respect to time due to the fact that all physically realizable processes have a beginning and an end. As such, the mean and variance of these processes depend on time, and the autocorrelation function depends on both t_1 and t_2. However, for many situations in random vibrations, the probability distributions do not appear to evolve over the time intervals of interest. Random processes whose distributions do not evolve with time are called *stationary random processes*. Formally, a process is strictly stationary if the joint distribution of $\{X(t_1), X(t_2), X(t_3), \ldots, X(t_n)\}$ is identical to the joint distribution of the same variables displaced an arbitrary amount of time h, that is, $\{X(t_1 + h), X(t_2 + h), X(t_3 + h), \ldots, X(t_n + h)\}$. This is a difficult condition to demonstrate in practice (Wirsching et al 2006). Figure 2-3 illustrates the requirements of a strictly stationary process i.e. the joint distribution $\{X(t_1), X(t_2)\}$ is equal to the joint distribution $\{X(t_1 + h), X(t_2 + h)\}$.

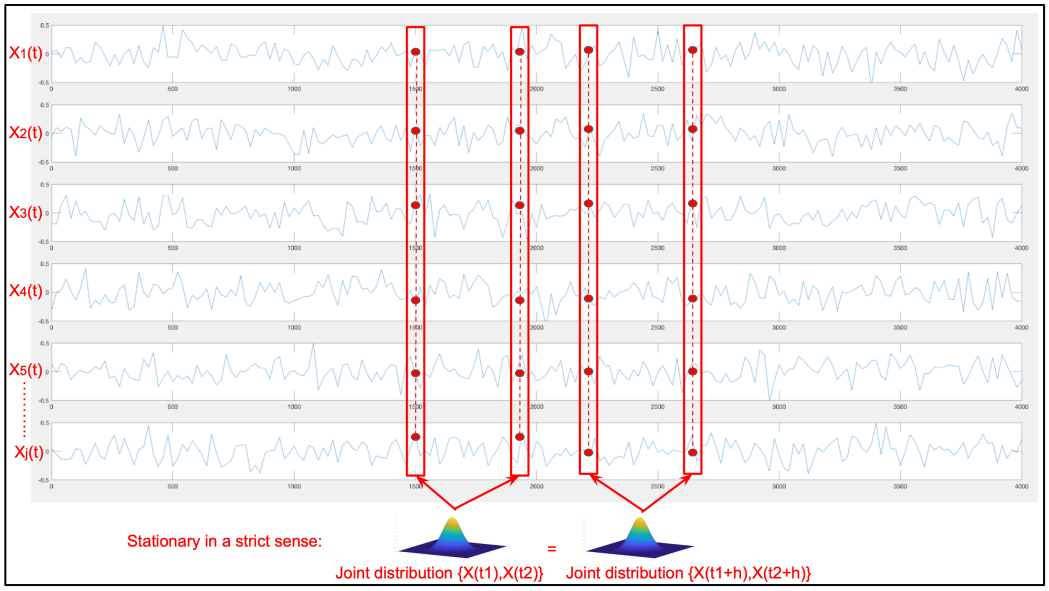

Figure 2-3: Strictly Stationary Process

A more practical form of stationarity occurs when the mean and variance of the process are constants, independent of time, and the autocorrelation function depends only upon the difference between t_1 and t_2. $R_X(t_1, t_2) = R_X(t_1 - t_2)$. This type of process is called weakly stationary or stationary in the wide sense. Figure 2-4 shows the requirements for a weakly stationary process i.e. the mean and variance taken across the ensemble at two different times need to be equal.

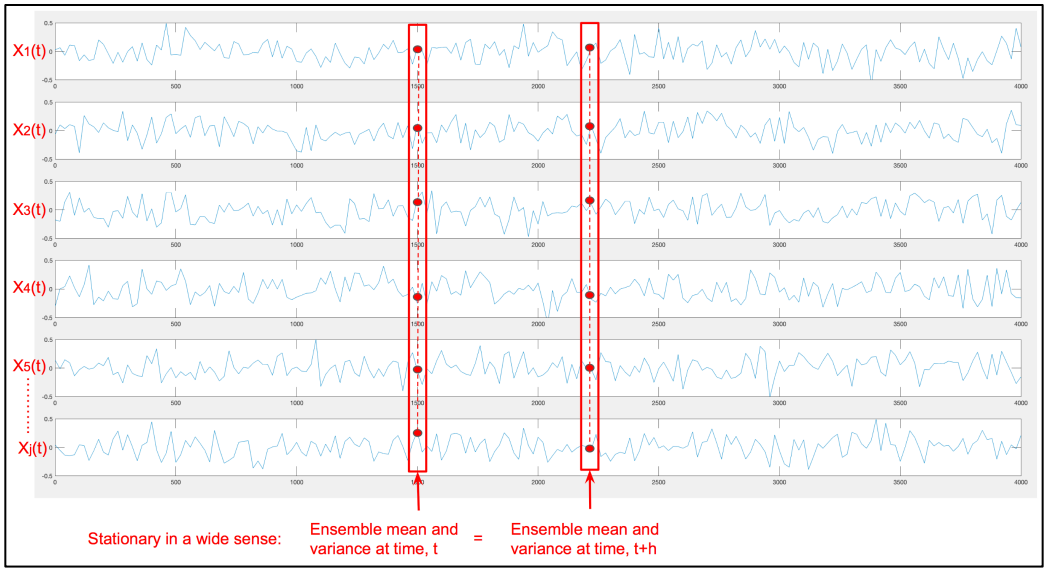

Figure 2-4: Weakly Stationary Process

For weakly stationary random processes the mean and the variance are expressed as constants:

$$\mu_X(t) = \mu_X \tag{2.26}$$

$$\sigma_X^2(t) = \sigma_X^2 \tag{2.27}$$

The stationary autocorrelation function is written in terms of the difference between $t_1 - t_2$, known as the lag, $\tau = t_1 - t_2$:

$$R_X(\tau) = R_X(t, t+\tau) = E[X(t)X(t+\tau)] \tag{2.28}$$

The stationary autocovariance and autocorrelation coefficient functions are given by:

$$\sigma_{XX}(\tau) = R_X(\tau) - {\mu_X}^2 \tag{2.29}$$

$$\rho_{XX}(\tau) = \frac{\sigma_{XX}(\tau)}{{\sigma_X}^2} \tag{2.30}$$

It is important to note that in the special case of a Gaussian process, stationarity in the wide sense also implies stationarity in the strict sense (Roberts and Spanos, 2003).

2.2.2.1 Derivative of Stationary Process

Assuming that the sample function $X(t)$ is differentiable and that the process $\dot{X}(t)$ is simply the family of derivatives of the sample function $X(t)$, the derivative of the autocorrelation function $R_X(\tau)$ with respect to τ is the following (Wirsching et al., 2006):

$$\frac{d}{d\tau}R_X(\tau) = \frac{d}{d\tau}E[X(t)X(t+\tau)] = \left[X(t)\frac{d}{d\tau}X(t+\tau)\right] = \left[X(t)\dot{X}(t+\tau)\right] = R_{X\dot{X}}(\tau) \tag{2.31}$$

$R_X(\tau)$ is an even function, that is, it is symmetric about the origin, and its maximum value is also at the origin. The derivative of $R_X(\tau)$ is zero at the origin, positive immediately left of the origin, and negative immediately right of the origin. Therefore, $R_{X\dot{X}}(\tau)$, the cross-correlation function of $X(t)$ and $\dot{X}(t)$, is an odd function and is equal to zero at the origin,

$$R_{X\dot{X}}(0) = 0 \tag{2.32}$$

which means that any stationary process $X(t)$ and its derivative $\dot{X}(t)$ are uncorrelated (i.e. statistically independent) at any given time, t.

2.2.2.2 Ergodic and Gaussian Processes

If the mean and correlation function estimated from a single realization (temporal averages) are the same as the ensemble averages, then the process is said to be ergodic (see Figure 2-5 for a depiction of an ergodic process).

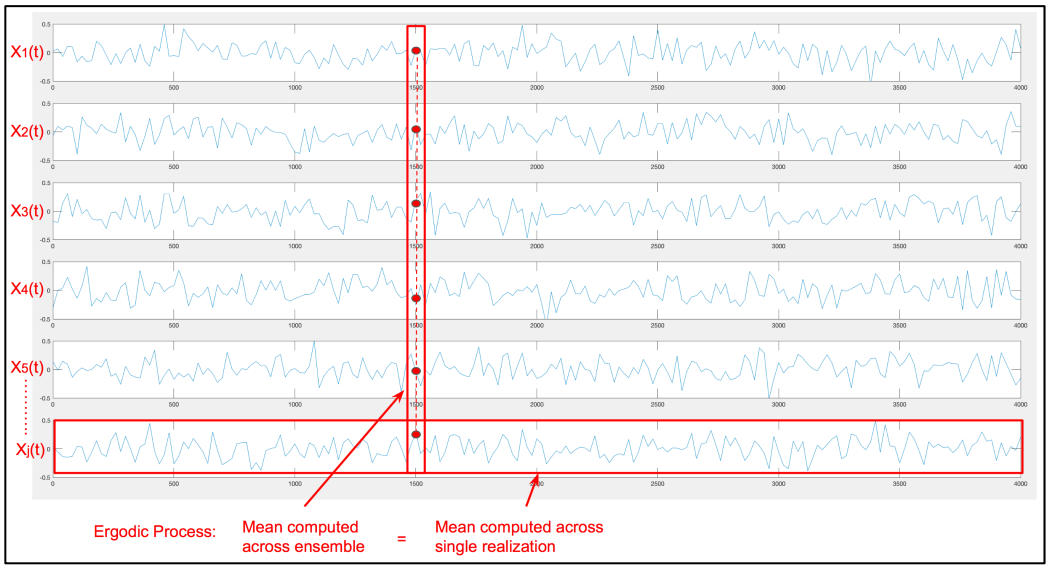

Figure 2-5: Ergodic Process

For a process to be ergodic, it must be stationary. However, the converse is not true; a stationary process is not necessarily ergodic.

Assuming a realization $X_j(t)$, a time average over sample j corresponding to the mean of the process can be written as

$$\mu_{X_j} = \frac{1}{T}\int_{-T/2}^{T/2} X_j(t)dt \tag{2.33}$$

The stochastic process, $X(t)$, is ergodic in mean value if μ_{X_j} tends to the ensemble mean (for a stationary process), $E[X(t)]$, as T tends to infinity regardless of the value of j. Similarly, $X(t)$ is ergodic in second moment if it is second moment stationary and

$$R_{XX}(\tau) = E[X(t+\tau)X(t)] = \lim_{T\to\infty}\frac{1}{T}\int_{-T/2}^{T/2} X_j(t+\tau)X_j(t)\,dt \tag{2.34}$$

There are as many types of ergodicity as there are stationarity. For any stationary characteristic of the stochastic process, one can define a corresponding time average, and ergodicity of the proper type will ensure that the two are the same (Lutes and Sarkani, 2004).

A random process $X(t) = \{X(t_1), X(t_2), X(t_3), \ldots, X(t_n)\}$ for any time instants $t_1, t_2, t_3, \ldots, t_n$ having a multivariate Gaussian distribution is referred to as a *Gaussian process.* Therefore, knowledge of $\mu_X(t)$ and $\sigma_X^2(t)$ for any set of time instants is sufficient to define a Gaussian process completely. Powerful simplifications are possible if the process is Gaussian (Wirsching et al., 2006):

- A normal random variable is completely characterized by its mean μ_X and variance σ_X^2 (as presented earlier); all higher moments of the density function are dependent on the variance. All joint probability distributions of a Gaussian random process are completely determined once the mean and autocorrelation function are know.

- If a Gaussian process is weakly stationary, it is also strictly stationary. Furthermore, if a Gaussian process is weakly ergodic, it is also strongly ergodic.
- The derivatives and integrals of a Gaussian process are also Gaussian processes.

2.2.3 Frequency Decomposition and Spectral Density

In linear vibration theory when studying the steady state response it is common to conduct Fourier analyses. This simplifies the problem as it permits the treatment of each single-frequency Fourier component separately and subsequently combining the components to obtain the total response.

2.2.3.1 Fourier Series and Fourier Integrals

A periodic function $f(t)$ of period T may be represented as a superposition of sinusoids in the following exponential Fourier series:

$$f(t) = \sum_{n=-\infty}^{\infty} c_n e^{ni\omega_0 t} \tag{2.35}$$

where $\omega_0 = 2\pi/T$ is the fundamental frequency and i represents an imaginary unit. The Fourier coefficients c_n can be evaluated directly from the relationship

$$c_n = \frac{1}{T}\int_{-T/2}^{T/2} f(t)e^{ni\omega_0 t}dt \tag{2.36}$$

If $f(t)$ is a non periodic function defined from $t = -\infty$ to $t = \infty$ and provided that $\int_{-\infty}^{\infty} |f(t)|dt < \infty$, such a function may be represented as a continuous superposition of sinusoids in the following exponential Fourier integral

$$f(t) = \frac{1}{2\pi}\int_{-\infty}^{\infty} F(\omega)e^{i\omega t}d\omega \tag{2.37}$$

where $F(\omega)$ is called the Fourier transform of $f(t)$ and may be evaluated directly from the relationship

$$F(\omega) = \int_{-\infty}^{\infty} f(t)e^{-i\omega t}dt \quad (2.38)$$

2.2.3.2 Spectral Density of Stochastic Process

For a stationary stochastic process $X(t)$, the concept of the power spectral density function (or power spectrum), denoted $S(\omega)$ may be defined as the Fourier transform of the autocorrelation function, $R(\tau)$;

$$S(\omega) = \int_{-\infty}^{\infty} R(\tau)e^{i\omega t}d\tau \quad (2.39)$$

Note that the units of spectral density are (mean square)/(unit of frequency).

Further, the inverse of the equation is

$$R(\tau) = \int_{-\infty}^{\infty} S(\omega)e^{-i\omega t}d\omega \quad (2.40)$$

The above two equations are the so-called Wiener-Khinchine relations (Wirsching et al., 2006). Furthermore, since $R(\tau)$ and $S(\omega)$ are even functions, the equations can be written as

$$S(\omega) = \int_{-\infty}^{\infty} R(\tau)\cos(\omega\tau)\,d\tau \quad (2.41)$$

and

$$R(\tau) = \int_{-\infty}^{\infty} S(\omega)\cos(\omega\tau)\,d\omega \quad (2.42)$$

When setting $\tau = 0$ the following is derived,

$$R(0) = E[x^2(t)] = \sigma_X^2 = \int_{-\infty}^{\infty} S(\omega)\cos(0)\,d\omega = \int_{-\infty}^{\infty} S(\omega)d\omega \quad (2.43)$$

Therefore, the total area under the spectral density function is the total mean square or variance of the process (assuming the mean is equal to zero).

The spectral densities of the derivatives of stochastic processes are the following (Roberts and Spanos, 2003):

$$S_{\dot{X}}(\omega) = \omega^2 S_X(\omega) \tag{2.44}$$

$$S_{X\dot{X}}(\omega) = -\omega^2 S_X(\omega) \tag{2.45}$$

$$S_{\ddot{X}}(\omega) = \omega^4 S_X(\omega) \tag{2.46}$$

The above equations are important because the mean square of the "velocity" and "acceleration" can be computed, respectively:

$$E[\dot{x}^2] = \int_{-\infty}^{\infty} \omega^2 S_X(\omega) d\omega \tag{2.47}$$

$$E[\ddot{x}^2] = \int_{-\infty}^{\infty} \omega^4 S_X(\omega) d\omega \tag{2.48}$$

2.3 TRANSMISSION OF RANDOM VIBRATION

When dealing with random vibrations problems, both the excitation and the response processes are modeled as stochastic processes. In other words, if the excitation is a random process, the response quantity will also be a random process. The goal is to predict the various statistical parameters of the response process given the probabilistic characteristics of the excitation process, and behavior of the equation of motion of the system.

2.3.1 General Input-Output Relationship

Linear time-invariant systems are described by linear differential equations with constant coefficients (e.g. a single degree of freedom (SDOF) system can be described by a second-order ordinary differential equation). For a specified deterministic input time history $x(t)$, it is possible to obtain a specified output time history $y(t)$, by integrating the differential equations of motion, subject to

initial conditions. Many techniques exist for solving linear differential equations with constant coefficients (see Shampine, 1994). Two procedures will be described below; using the *complex frequency response* together with the Fourier integral, and using the *impulse response* together with the convolution integral. These methods are related, as they are essentially the Fourier transform of each other.

2.3.1.1 Complex Frequency Response

The amplitude and phase of the response of a system generally depend on the frequency. A method for describing the frequency dependence of the amplitude and phase is to derive the complex frequency response function, $H(\omega)$. The complex frequency response is obtained analytically by substituting $x = e^{i\omega t}$ and $y = H(\omega)\, e^{i\omega t}$ in the equation of motion, cancelling the $e^{i\omega t}$ terms, and solving for $H(\omega)$ algebraically. Knowledge of the complex frequency response for all frequencies contains all the information necessary to obtain the response $y(t)$ to an arbitrary known excitation, $x(t)$. This is due to the principle of superposition that can be implemented for linear systems.

If the input $x(t)$ is periodic then it can be decomposed into sinusoids forming a Fourier series. The response to each sinusoid is provided by $H(\omega)$ and these responses, in turn, form a new Fourier series representing the output, $y(t)$. For an input $x(t)$ that is not periodic but has a Fourier transform,

$$X(\omega) = \int_{-\infty}^{\infty} x(t) e^{i\omega t} dt \tag{2.49}$$

each frequency component yields the Fourier transform of the response, $y(t)$,

$$Y(\omega) = H(\omega) X(\omega) \tag{2.50}$$

Superposing all individual responses via the Fourier integral yields the response,

$$y(t) = \frac{1}{2\pi}\int_{-\infty}^{\infty} Y(\omega)e^{i\omega t}d\omega \quad (2.51)$$

2.3.1.2 Impulse Response

A solution for the response of a time-invariant system can be obtained by superposing unit solutions in the time-domain as well. The impulse response function $h(t)$ provides the response of the system at time t to a unit impulse applied at time 0. An arbitrary input $x(t)$ may be viewed as being made up of a continuous series of small impulses. The "impulse" corresponding to the input $x(t)$ between times τ and $\tau + d\tau$ has the magnitude $x(\tau)d\tau$. The response to a unit impulse at time $t = \tau$ is the impulse response function, $h(t-\tau)$. The contribution of the impulse response to the total response of the system is $h(t-\tau)x(\tau)d\tau$. The total response $y(t)$ at time t may be obtained by summing up all the individual outputs to all the "impulses" which make up the time history of $x(t)$. The individual outputs are superposed via the convolution integral,

$$y(t) = \int_{-\infty}^{t} x(\tau)h(t-\tau)d\tau \quad (2.52)$$

Since the impulse response function, $h(t-\tau)$, vanishes when $\tau > t$, the upper limit can be replaced with ∞ without changing the value of the integral.

$$y(t) = \int_{-\infty}^{\infty} x(\tau)h(t-\tau)d\tau \quad (2.53)$$

The impulse response, $h(t)$, and the complex frequency response, $H(\omega)$, form a Fourier transform pair (Wirsching et al., 2006):

$$H(\omega) = \int_{-\infty}^{\infty} h(t)\, e^{-i\omega t}dt \quad (2.54)$$

and

$$h(t) = \frac{1}{2\pi}\int_{-\infty}^{\infty} H(\omega)\, e^{i\omega t} d\omega \quad (2.55)$$

2.3.2 Stochastic Input-Output Relationship

The general input-output relationship can be extended to account for stochastic inputs. As mentioned above, if the input is a stationary random process, then the output will also be a stationary random process ($x(t)$ and $y(t)$ are now random processes of the input and output, respectively). First and second order statistical properties of the response can easily be derived from knowledge of the system and the statistical properties of the excitation.

2.3.2.1 Mean Value of Response

An alternative form of the response can be written as

$$y(t) = \int_{-\infty}^{\infty} x(t-\theta)h(\theta)d\theta \quad (2.56)$$

where $\theta = t - \tau$.

To obtain the mean of the response, $E[y(t)]$, the mean of the convolution integral is taken,

$$E[y(t)] = \int_{-\infty}^{\infty} E[x(t-\theta)]h(\theta)d\theta \quad (2.57)$$

where $E[x(t-\theta)]$ is the mean of the input process. Since the mean of the input is a constant for stationary random processes, the mean of the output process is given in terms of the mean of the input:

$$E[y(t)] = E\,[x(t)] \int_{-\infty}^{\infty} h(\theta)d\theta = \mu_X \int_{-\infty}^{\infty} h(\theta)d\theta \quad (2.58)$$

Further, the integral $\int_{-\infty}^{\infty} h(\theta)d\theta$ is a constant equal to $H(0)$ found by setting $\omega = 0$ in Eq. 2.54.

Note that if the mean value of input process is zero, then the mean value of the response is also zero (for stationary stochastic processes).

2.3.2.2 Autocorrelation and Spectral Density of Response

The same procedure used to solve for the mean value of the response can be used to solve for the autocorrelation function of the response:

$$y(t)y(t+\tau) = \int_{-\infty}^{\infty}\int_{-\infty}^{\infty} x(t-\theta_1)x(t+\tau-\theta_2)h(\theta_1)h(\theta_2)d\theta_1 d\theta_2 \quad (2.59)$$

Taking the ensemble average,

$$E[y(t)y(t+\tau)] = E[\int_{-\infty}^{\infty}\int_{-\infty}^{\infty} x(t-\theta_1)x(t+\tau-\theta_2)h(\theta_1)h(\theta_2)d\theta_1 d\theta_2] \quad (2.60)$$

Noting that $E[x(t-\theta_1)x(t+\tau-\theta_2)]$ is just the autocorrelation function of the input process with a time lag of $\tau+\theta_1-\theta_2$, the autocorrelation function of the response is

$$R_y(\tau) = \int_{-\infty}^{\infty}\int_{-\infty}^{\infty} R_x(t+\theta_1-\theta_2)h(\theta_1)h(\theta_2)d\theta_1 d\theta_2 \quad (2.61)$$

The spectral density of the response, $S_y(\omega)$, is related to autocorrelation through the Wiener-Khintchine relation:

$$S_y(\omega) = \int_{-\infty}^{\infty} R_y(\tau)e^{-i\omega t}d\tau \quad (2.62)$$

The right hand side of the equation is a triple integral which can be manipulated in a form in order to take advantage of the Wiener-Khintchine relation again (Crandall and Mark, 1963):

$$S_y(\omega) =$$

$$\frac{1}{2\pi}\int_{-\infty}^{\infty} h(\theta_1)e^{i\omega t}d\theta_1 \int_{-\infty}^{\infty} h(\theta_2)e^{i\omega t}d\theta_2 \int_{-\infty}^{\infty} R_x(\tau+\theta_1-\theta_2)e^{-i\omega(\tau+\theta_1-\theta_2)}dt \quad (2.63)$$

The first and second integrals above are frequency response functions (the negative sign in the first integral giving the complex conjugate of the frequency response), and, taking advantage of the Wiener-Khintchine relation, the third integral yields the spectral density function of the input process. Given the above, the spectral density of the response can be written as,

$$S_y(\omega) = H(-\omega)\, S_x(\omega)\, H(\omega) \tag{2.64}$$

Noting that the product of $H(\omega)$ and its complex conjugate is the square of its magnitude, the equation above may be rewritten as

$$S_y(\omega) = |H(\omega)|^2\, S_x(\omega) \tag{2.65}$$

2.3.2.3 Mean Square of Response

The mean square of the stationary response process $y(t)$ is denoted $E[y^2]$, and can be derived from the autocorrelation function of the response, $R_y(\tau)$, or the spectral density of the response, $S_y(\omega)$. If the input autocorrelation function $R_x(\tau)$ is known then the mean square of the response is

$$E[y^2] = R_y(0) = \int_{-\infty}^{\infty}\int_{-\infty}^{\infty} R_x(\theta_1 - \theta_2)h(\theta_1)h(\theta_2)d\theta_1 d\theta_2 \tag{2.66}$$

And, if the spectral density of the input process is known then the mean square of the response is

$$E[y^2] = \int_{-\infty}^{\infty} S_y(\omega)d\omega = \int_{-\infty}^{\infty} |H(\omega)|^2\, S_x(\omega)d\omega \tag{2.67}$$

Analytical solutions of the above integral exist for various forms of $H(\omega)$ and can be found in (Crandall and Mark, 1963; Roberts and Spanos, 2003; Lutes and Sarkani, 2004; Newland, 2005; Wirsching et al., 2006, Li and Chen 2009).

2.4 RESPONSE OF SDOF SYSTEM TO STATIONARY RANDOM EXCITATION

To illustrate the preceding ideas, an example of a SDOF system excited by a stationary random excitation is presented. The equation of motion is

$$m\ddot{y} + c\dot{y} + ky = -m\ddot{y}_0 \tag{2.68}$$

where m, c, and k are the mass, damping coefficient and stiffness of the system, respectively, and $\ddot{y}_0$ is the excitation represented by a Gaussian, zero-mean white noise process possessing a power spectral density of S_0. The response of the system $y(t)$ is sought.

Dividing through by the mass of the system yields the following

$$\ddot{y} + 2\zeta\omega_n\dot{y} + {\omega_n}^2 y = -\ddot{y}_0 \tag{2.69}$$

where $\zeta = c/(2\sqrt{km})$, and $\omega_n = \sqrt{k/m}$.

The impulse response function is obtained by solving Eq. 2.69 when $\ddot{y}_0 = \delta(t)$. The effect of the impulse is to give an initial value to $\dot{y}$ resulting in the following form of y (Crandall and Mark, 1963):

$$y(t) = e^{-\zeta\omega_n t}(C_1 \sin\left(\sqrt{1-\zeta^2}\right)\omega_n t + C_2 \cos\left(\sqrt{1-\zeta^2}\right)\omega_n t) \tag{2.70}$$

where C_1 and C_2 are constants of integration to be evaluated from the initial conditions. The initial conditions are obtained when considering Eq. 2.69 at $t = 0$. Since the right hand side is a negative δ the left hand side also has the same behavior. Therefore, $\dot{y}$ starts off with a unit negative step and y begins with a negative slope. Thus, the initial conditions immediately after impulse are

$y(+0) = 0$ and $\dot{y}\,(+0) = -1$, and the constants are $C_1 = (\omega_n\sqrt{1-\zeta^2})^{-1}$ and $C_2 = 0$. Finally, the impulse response, $h(t)$, is

$$h(t) = \begin{cases} 0, \ for\ t < 0 \\ \frac{e^{-\zeta\omega_n t}}{\omega_n\sqrt{1-\zeta^2}}\sin\left(\sqrt{1-\zeta^2}\right)\omega_n t\,, \ for\ t > 0 \end{cases} \tag{2.71}$$

The mean square of the response can be derived by evaluating Eq. 2.66 considering the input autocorrelation function, $R_x(\tau) = 2\pi S_0\delta(\tau)$, and the impulse response function given in Eq. 2.71. The resulting response autocorrelation function is:

$$R_y(\tau) = \int_0^\infty \int_0^\infty (2\pi S_0\delta(\tau + \theta_1 - \theta_2)) \frac{e^{-\zeta\omega_n(\theta_1+\theta_2)}}{\omega_n(1-\zeta^2)}\sin\left(\sqrt{1-\zeta^2}\right)\omega_n\theta_1 \sin\left(\sqrt{1-\zeta^2}\right)\omega_n\theta_2\, d\theta_1 d\theta_2 \tag{2.72}$$

The evaluation of the above integral is provided in (Crandall and Mark, 1963; Roberts and Spanos, 2003) as well as other textbooks, therefore only the solution is provided here:

$$R_y(\tau) = \frac{\pi}{2}\frac{S_0}{\zeta{\omega_n}^3} e^{\zeta\omega_n\tau}\left(\cos\left(\sqrt{1-\zeta^2}\right)\omega_n\tau - \frac{\zeta}{\sqrt{1-\zeta^2}}\sin\left(\sqrt{1-\zeta^2}\right)\omega_n\tau\right) \tag{2.73}$$

Setting $\tau = 0$ in Eq. 2.73 yields the mean square of the response,

$$E[y^2] = R_y(0) = \frac{\pi}{2}\frac{S_0}{\zeta{\omega_n}^3} \tag{2.74}$$

Alternatively, the complex frequency response function $H(\omega)$ is derived by substituting $f(t) = e^{i\omega t}$ and $y = H(\omega)e^{i\omega t}$:

$$H(\omega) = \frac{1}{({\omega_n}^2 - \omega^2 + 2\iota\zeta\omega_n\omega)} \tag{2.75}$$

The spectral density of the response is:

$$S_y(\omega) = |H(\omega)|^2 S_x(\omega) = |H(\omega)|^2 S_0 \quad (2.76)$$

and, the mean square of the response is:

$$E[y^2] = \int_{-\infty}^{\infty} S_y(\omega) d\omega = \int_{-\infty}^{\infty} |H(\omega)|^2 S_0 d\omega = S_0 \int_{-\infty}^{\infty} |H(\omega)|^2 d\omega \quad (2.77)$$

The integral above can be solved analytically. For $H(\omega)$ having the form:

$$H(\omega) = \frac{(i\omega B_1 + B_0)}{(A_0\omega^2 + \iota\omega A_1 + A_0)} \quad (2.78)$$

the integral has the following analytical solution (Crandall and Mark, 1963):

$$\int_{-\infty}^{\infty} |H(\omega)|^2 d\omega = \pi \frac{({B_0}^2/A_0)A_2 + B_1^2}{(A_1 A_2)} \quad (2.79)$$

where $A_0 = {\omega_n}^2$, $A_1 = 2\zeta\omega_n$, $A_2 = 1$, $B_0 = 1$ and $B_1 = 0$.

Therefore, the mean square of the displacement response is:

$$E[y^2] = S_0 \int_{-\infty}^{\infty} |H(\omega)|^2 d\omega = S_0 \pi \frac{({B_0}^2/A_0)A_2 + B_1^2}{(A_1 A_2)} = \frac{\pi S_0}{2\zeta {\omega_n}^3} \quad (2.80)$$

As seen above, both methods, solving for the autocorrelation function or the spectral density, produce the same result for the mean square response. Further, according to Eq. 2.47, the mean square of the velocity response is

$$E[\dot{y}^2] = \int_{-\infty}^{\infty} \omega^2 S_y(\omega) d\omega = \frac{\pi S_0}{2\zeta\omega_n} \quad (2.81)$$

2.5 SUMMARY AND DISCUSSION

A brief overview of linear random vibration theory has been presented above. The case of a linear system was used to present the general background, and, special attention was paid to Gaussian excitations. As described above, if the excitation to a linear system is Gaussian, then, according to the linear theory of random vibrations, the response will also be Gaussian. This is useful as it

enables one to compute various statistics of the response in terms of a few statistical parameters, as the Gaussian distribution can be completely characterized by its mean μ_x and variance ${\sigma_x}^2$.

Although it is sometimes appropriate to model an engineering system as linear, it is important to note that no real system is exactly linear (Spanos and Roberts, 2003). Nonlinearities can come about in many different forms, and usually become progressively more significant as the amplitude of the vibrations increase. Further, if the excitation to a nonlinear system is Gaussian, the response will not be Gaussian. Even for small nonlinearities, the difference between the linear and nonlinear response is apparent when evaluating the shape of the tail ends of the response PDF curve. Often, when designing mechanical and structural systems, the probability of exceeding a specific threshold is sought in order to reduce costs. This requires knowledge of the shape of the tail ends of the response PDF. Therefore, it is vital to properly account for the effects of even small nonlinearities. Of course, for large nonlinearities even the general shape of the response PDF curve may differ from that of a linear system.

3 MONTE CARLO SIMULATION METHOD

3.1 INTRODUCTION

The Monte Carlo simulation (MCS) method can be used to estimate the exact response statistics of randomly excited systems within a desired confidence level. The basis of the MCS is related to the fact that the stochastic differential equation governing the motion of the system can be interpreted as an infinite set of deterministic differential equations. For each member of this set, the input is a sample function of the excitation process, and the output is the corresponding sample function of the response process. The MCS is conducted by solving the set of deterministic equations and interpreting the responses of the set in a statistical manner. The major advantage of the MCS is that solutions can be obtained for any problem whose deterministic solution (either analytical or numerical) is known. Figure 3-1 shows a graphic representation of the MCS.

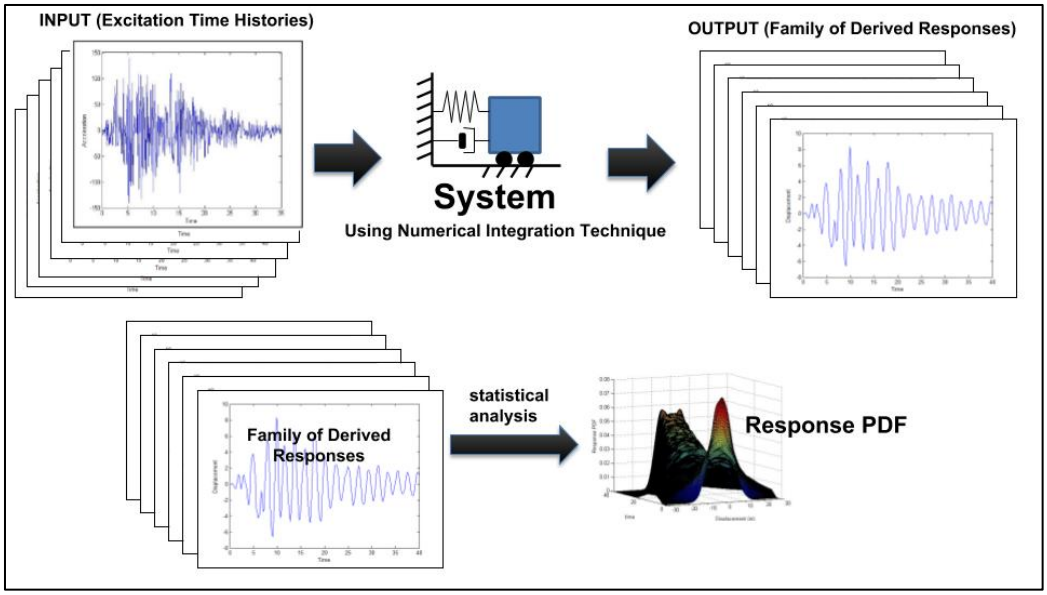

Figure 3-1 Monte Carlo Simulation Method

The most important part of the MCS methodology is the generation of sample functions of the stochastic processes. This is achieved by employing an algorithm to produce a set of pseudo-random numbers that fit a specified probability density function. The simulated input sample functions (i.e. random process excitations) must accurately describe the probabilistic characteristics of the corresponding stochastic processes that may be stationary or non-stationary, homogeneous or nonhomogeneous, one-dimensional or multidimensional, univariate or multivariate, Gaussian or non-Gaussian. Further, the sample function is generated with a pre-selected frequency content and temporal variation of intensity, by appropriately processing the set of pseudo-random numbers (Spanos and Zeldin, 1998). After generating a single sample of the random excitation the response is computed by any of the commonly available numerical integration techniques used to solve differential equations (Shampine, 1994). The process of generating a sample input function and computing the response is repeated and the system response statistics are updated. Obviously, this approach is applicable for the estimation of both stationary and non-stationary response statistics.

Of course the more simulations that are conducted, the closer the estimated response statistics are to the theoretical values. The accuracy of the approach is inversely proportional to the square root of the number of sample functions computed. Thus, to improve the accuracy by a factor of 10 it is necessary to increase the amount of simulations by a factor of 100 (Roberts and Spanos, 2003). The number of sample records that are necessary for a reasonable estimation of the first and second order moments (e.g. mean, mean square, and power spectrum) is of the order of five hundred (Roberts and Spanos, 2003). Further, to estimate the failure probabilities (e.g. the shape of the tail ends of the response PDF) within commonly acceptable engineering confidence levels, 10^6 or greater simulations may be required. In fact, analysis of reliability of structural systems for gravity dead and live loads suggests that the limit state probability of individual steel members and connections is on the order of 10^{-5} to 10^{-4} per year (Galambos et al., 1982). For redundant steel frame systems, the probability of failure is on the order of 10^{-6} to 10^{-5} (AISC, 2016). The *de minimis* risk, that is, the level below which the risk is of regulatory or legal concern and the economic or social benefits of risk reduction are small, is on the order of 10^{-7} to 10^{-6} per year (Pate-Cornell, 1994). The requirement for a very low level of probability can render the computational cost quite significant, especially for multi-degree of freedom (MDOF) vibratory systems.

3.2 SPECTRAL REPRESENTATION METHOD

A commonly employed method for generating realizations compatible with a prescribed power spectrum within the context of MCS is the *spectral representation* method. The method is a versatile and robust procedure for synthesizing random fields, it is quite straightforward to implement, and it is

widely used in practical applications (Spanos and Zeldin, 1998). A detailed derivation of the method can be found in (Shinozuka and Deodatis, 1991).

Assuming $f_0(t)$ is a real-valued homogeneous stationary stochastic process with mean value equal to zero, autocorrelation function, $R_{f_0 f_0}(\tau)$, and two-sided power spectrum, $S_{f_0 f_0}(\omega)$, (Shinozuka and Deodatis, 1991) have shown that the ensemble expected value and ensemble autocorrelation function, $E[f(t)]$ and $R_{ff}(\tau)$, of the simulated stochastic process, $f(t)$, are identical to the corresponding targets, $E[f_0(t)] = 0$ and $R_{f_0 f_0}(\tau)$, respectively.

The stochastic process $f_0(t)$ can be simulated using the following formula:

$$f(t) = \sqrt{2}\sum_{n=0}^{N-1} A_n \cos(\omega_n t + \Phi_n) \tag{3.1}$$

where,

$$A_n = \sqrt{2S_{f_0 f_0}(\omega_n)\Delta\omega}, \quad n = 1,2,3,\ldots N-1 \tag{3.2}$$

$$\omega_n = n\Delta\omega, \quad n = 1,2,3,\ldots N-1 \tag{3.3}$$

$$n\Delta\omega = \frac{\omega_u}{N} \tag{3.4}$$

and

$$A_0 = 0 \tag{3.5}$$

In Eq. 3.4, ω_u is an upper cutoff frequency beyond which the power spectral density is assumed to be zero. Also, Φ_n in Eq. 3.1 represents a random phase angle distributed uniformly of the interval $[0,2\pi]$. The simulated stochastic process, $f(t)$, is periodic with period,

$$T_0 = \frac{2\pi}{\Delta\omega} \tag{3.6}$$

3.2.1 Accuracy and Computational Cost of MCS Method

Next, the accuracy and computational cost of the MCS method is examined by solving a Duffing oscillator excited by a zero-mean white noise process and comparing the results to the exact theoretical solution obtained by solving the associated Fokker-Planck-Kolmogorov (FPK) equation (a discussion regarding the FPK equation of a Duffing oscillator excited by zero-mean white noise process is presented in Section 4.3).

The equation of motion for a Duffing oscillator is

$$\ddot{y} + 2\zeta\omega_n\dot{y} + g(y) = f(t) \tag{3.7}$$

where $g(y) = {\omega_n}^2(y + \lambda y^3)$, λ is the magnitude of nonlinearity, $f(t)$ is the excitation represented by a Gaussian, zero-mean white noise process possessing a power spectral density of S_0.

Three MCSs were conducted considering 1,000, 10,000 and 100,000 simulations. The following parameters were used in the example: $\zeta = 0.1$, $\omega_n = 1$, $\lambda = 1.5$, and $S_0 = 0.0637$. The normalized histograms and the exact displacement response PDFs are shown in Figure 3-2. Zoomed in portions of the tail ends of the curve are also shown.

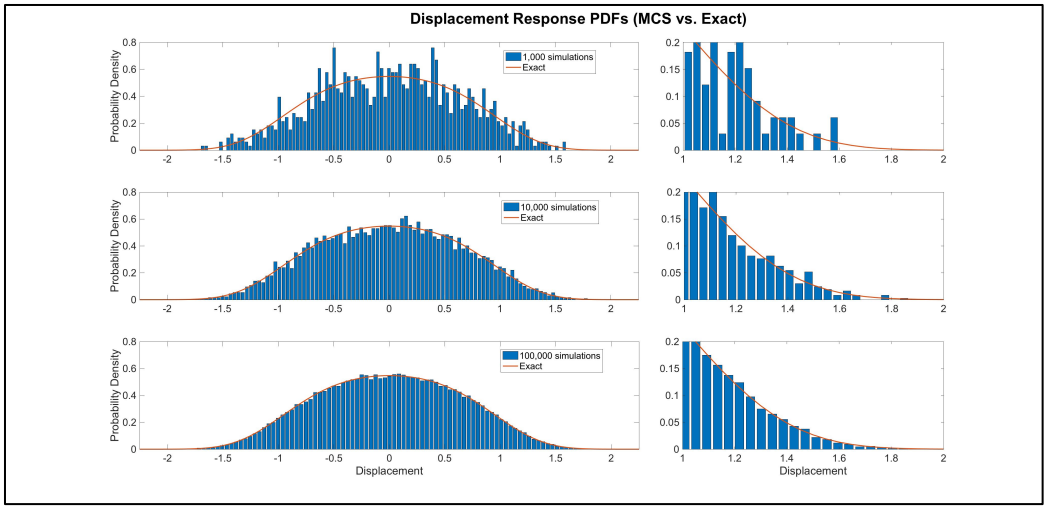

Figure 3-2: MCS vs. Exact (1k, 10k, and 100k simulations)

As seen in Figure 3-2, the accuracy of the MCS increases as the number of simulations increase. **Table 3-1** shows the estimated standard deviation of the displacement response, the estimated probability of the displacement response exceeding 2.0, and the computational time required for each case.

Table 3-1: MCS Accuracy and Computational Time

Number of Simulations	Estimated Standard Deviation of Displacement Response	Estimated Probability of Displacement >2.0	Computational Time
1,000	0.6488	0	5 minutes
10,000	0.6389	0	50 minutes
100,000	0.6379	3.0 x 10^-5	500 minutes
Exact	0.6377	3.8 x 10^-4	Closed form solution
Note: To estimate the probability of exceeding a displacement of 2.0, one of the bins of the histogram was centered at 2.0 and a bin width of 0.01 was used.			

As seen in **Table 3-1**, 10,000 simulations are adequate for the estimation of the standard deviation of the response. However, even 100,000 simulations are not enough to estimate extreme value statistics (i.e. probability of exceeding a displacement of 2.0). There were no response realizations that exceeded a displacement of 2.0 when running 1,000 and 10,000 simulations, while 3 response realizations exceeded a displacement of 2.0 when running 100,000 simulations.

3.3 NON STATIONARY EXCITATION

Structural systems are often subjected to extreme events and excitations such as seismic motions, winds, ocean waves, blasts, and impact loads, which inherently possess non-stationary characteristics. Further, the non-stationary characteristics of the system response are important from an analysis and design perspective. Representation of these excitation phenomena by non-stationary stochastic processes is therefore necessary to accurately capture system/structure behavior (e.g., Soong and Grigoriu 1993; Li and Chen, 2009; Spanos and Kougioumtzoglou 2012, 2014; Kougioumtzoglou and Spanos 2009).

3.3.1 Numerical Example – Non-Stationary Case

An example is presented considering a system excited by a non-stationary stochastic process. Specifically, a Duffing oscillator excited by a time modulated Gaussian white noise process will be solved using the spectral representation method.

The equation of motion is

$$\ddot{y} + 2\zeta\omega_n\dot{y} + g(y) = \theta(t)f(t) \tag{3.8}$$

where $g(y) = {\omega_n}^2(y + \lambda y^3)$, λ is the magnitude of nonlinearity, $f(t)$ is a Gaussian, zero-mean white noise process possessing a power spectral density of S_0, and $\theta(t)$ is a deterministic time modulation function having the following form

$$\theta(t) = te^{-\beta t} \tag{3.9}$$

where $\beta = 1/(2T_n)$ and $T_n = 2\pi/\omega_n$.

The time-modulated white noise PSD has the following form

$$PSD = |\theta(t)|^2 S_0 \tag{3.10}$$

Figure 3-3 shows a plot of the PSD of the excitation for $S_0 = 0.0637$ and $\omega_n = 1$.

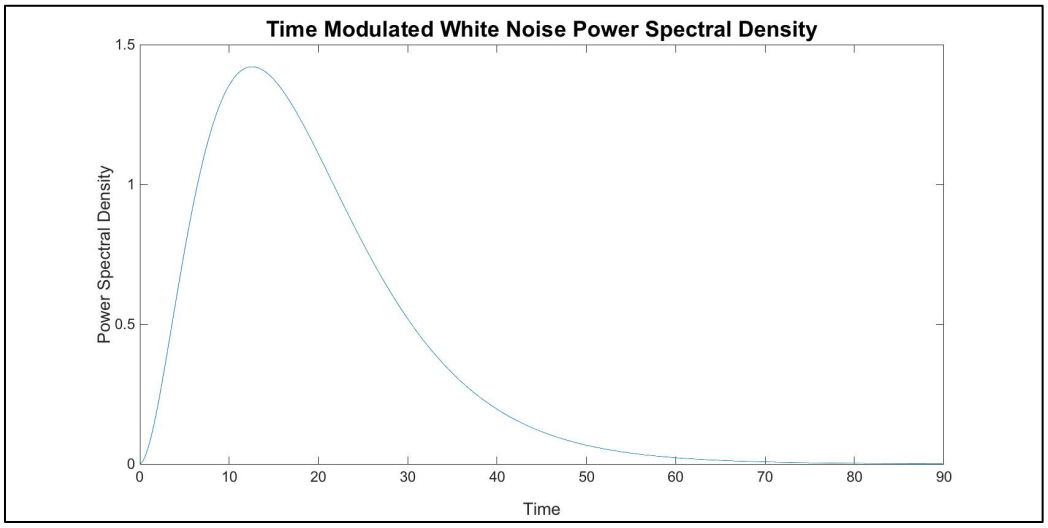

Figure 3-3: Time Modulated White Noise Power Spectral Density

Figure 3-4 shows a sample excitation function derived using the spectral representation method described above.

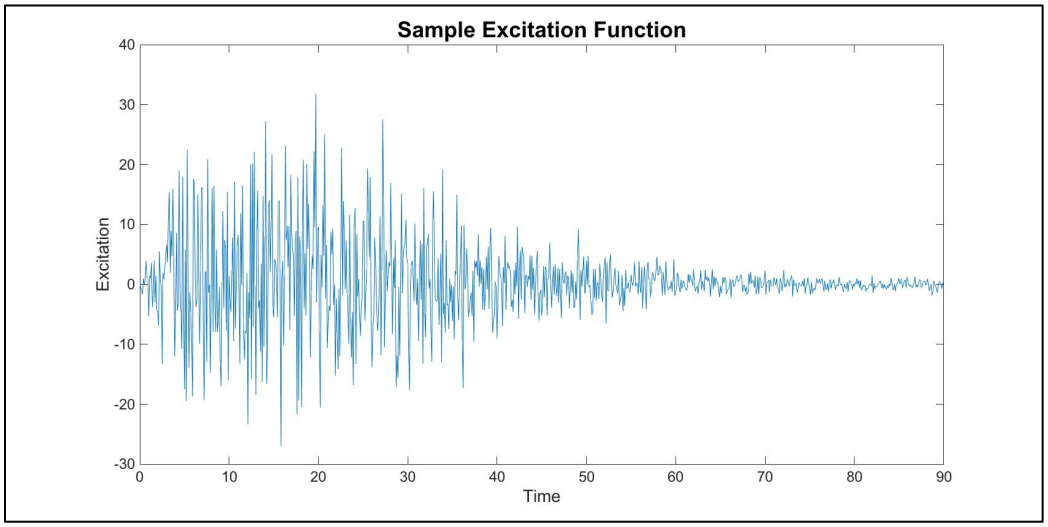

Figure 3-4: Sample Excitation Function

As described in Section 2.2.3.2 the total area under the spectral density function is the total mean square or variance of the process. Therefore the variance can be derived from the following

$$var(t) = |\theta(t)|^2 2\omega_u S_0 \tag{3.11}$$

The equation above was multiplied by 2 to account for the negative frequency range.

Figure 3-5 shows a comparison of the variances computed analytically and with the MCS method (50,000 simulations).

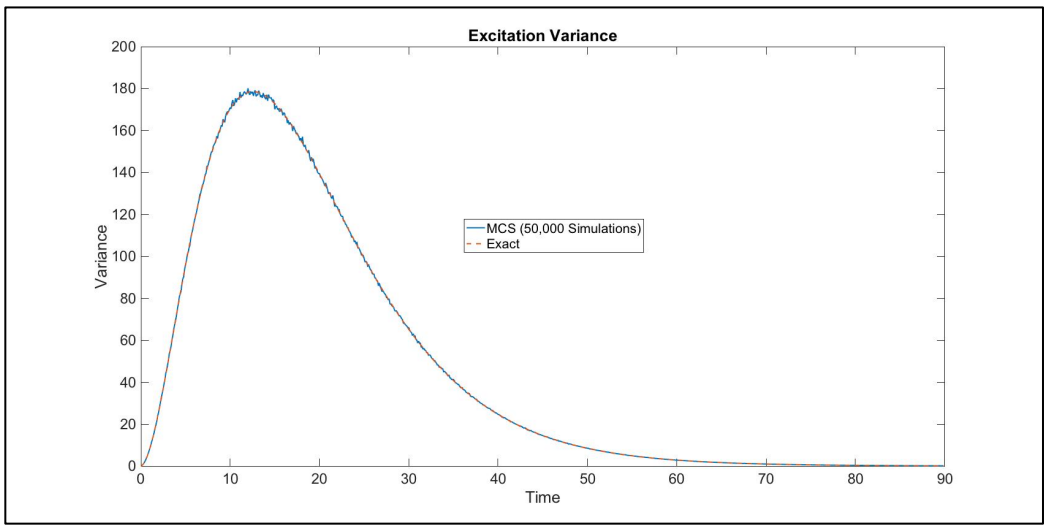

Figure 3-5: Variance of Power Spectral Density (MCS vs. Exact)

It is apparent that the simulation variance closely follows the variance found analytically, confirming the compatibility of the time histories with the time modulated PSD. Obviously, as the number of simulation samples approach infinity, the simulation variance converges to that found analytically.

The standard deviation of the displacement and velocity responses are shown in Figure 3-6 and Figure 3-9, respectively, for $\omega_n = 1, \zeta = 0.1, S_0 = 0.0637, \text{and } \lambda = 1.5$. The displacement and velocity response PDFs at different time instants are shown in Figure 3-7 and Figure 3-10, respectively, and the complete displacement and velocity response PDFs are shown in Figure 3-8 and Figure 3-11, respectively.

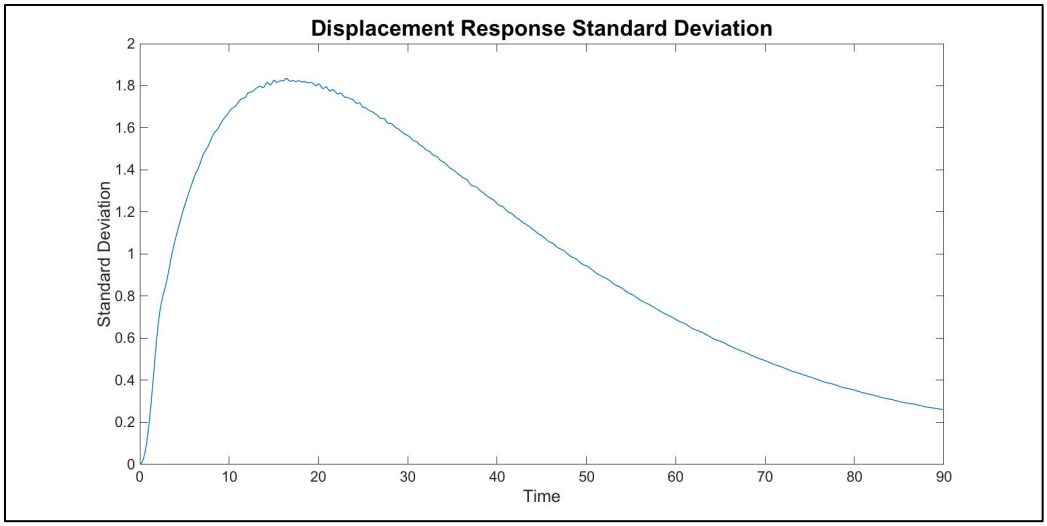

Figure 3-6: Standard Deviation of Displacement Response

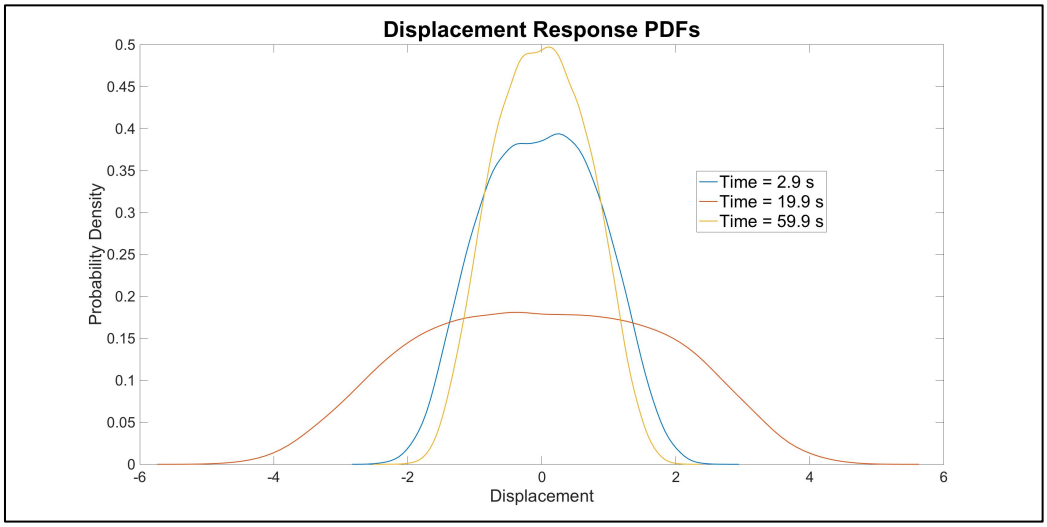

Figure 3-7: Displacement Response PDFs at Different Time Instances

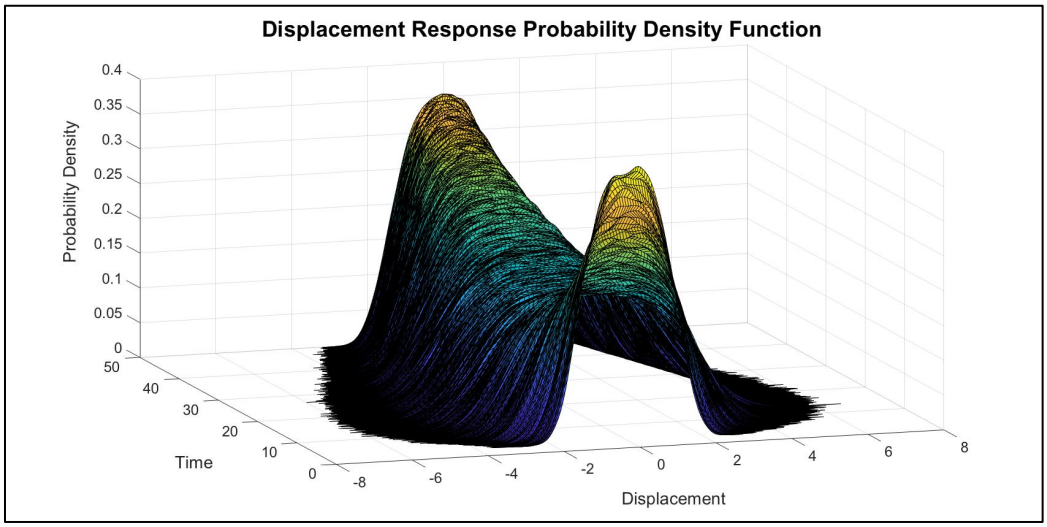

Figure 3-8: Displacement Response PDF

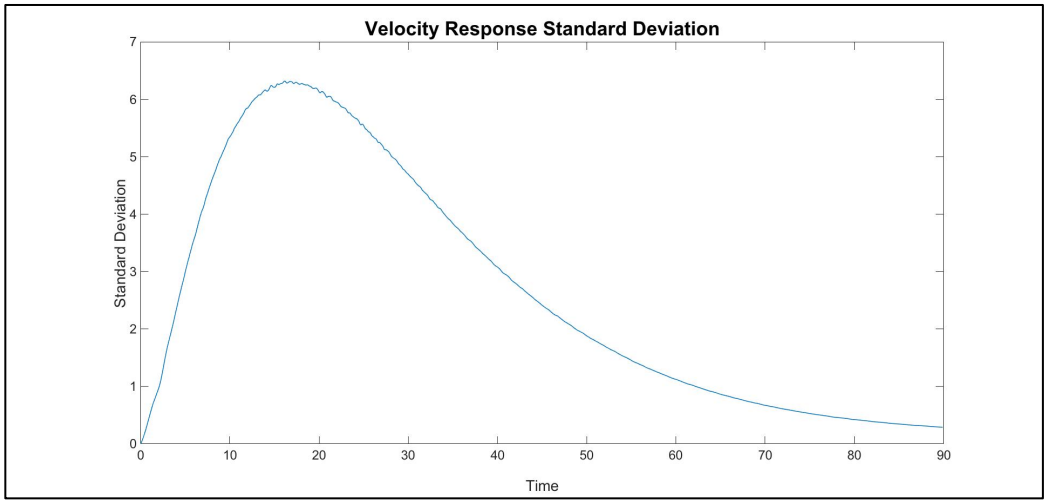

Figure 3-9: Standard Deviation of Velocity Response

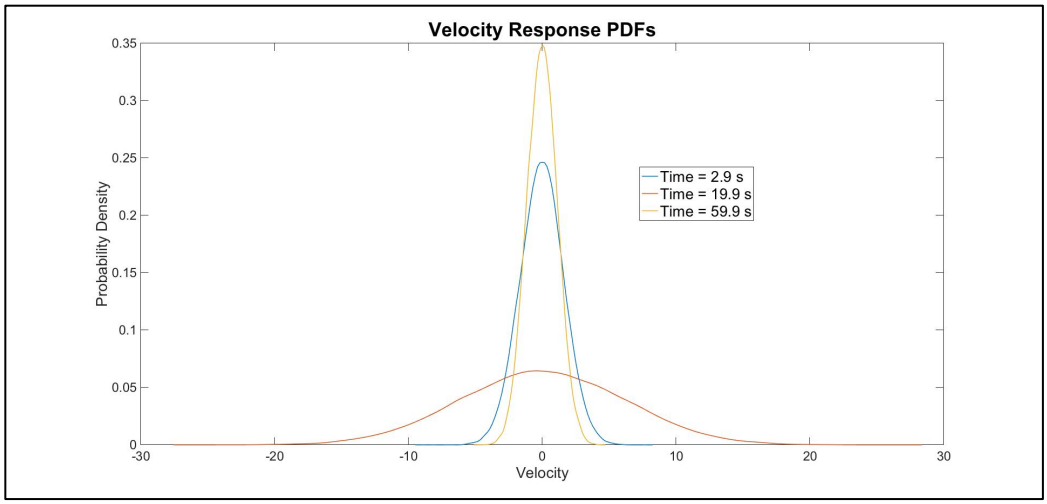

Figure 3-10: Velocity Response PDFs at Different Time Instances

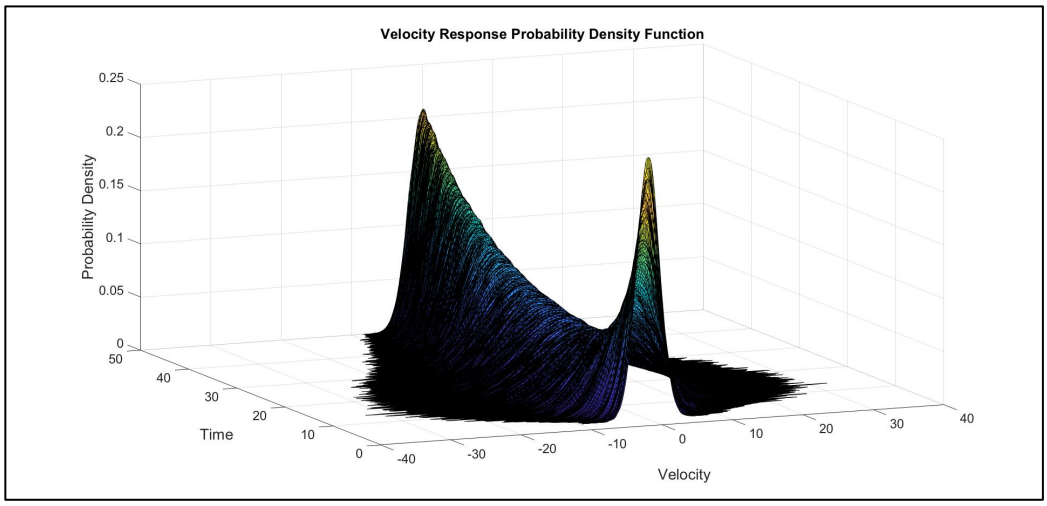

Figure 3-11: Velocity Response PDF

3.4 DISCUSSION

The MCS method is straightforward to implement and extremely versatile. However, in order to obtain reliable estimates of response variables, a sufficiently large sample size should be used in the analysis. This fact renders the method computationally expensive. This is particularly true in response analyses involving the estimation of rare events (e.g. failure probabilities). Spanos (1981a) has estimated that the cost of simulation studies is typically 100 to 1000 times that of an approximate analysis using statistical linearization techniques. It has been found that the cost of simulation increases linearly with sample size while the accuracy improves in proportion to the square root of sample size (Spanos & Lutes 1987). Nevertheless, given the strides made over the last few decades in computer power, and its simplicity, it can be seen that the MCS method will continue to be the most prevalent stochastic dynamics tool used in practice. In fact, “smart” MCS approaches have been developed recently (Au and Wang, 2014) to decrease the computation time.

One such approach is the Subset Simulation method proposed by Au and Beck (2001). The idea behind their approach is to express the failure probability as a product of larger conditional failure probabilities by introducing intermediate failure events. With a proper choice of intermediate failure events, the conditional probabilities involved, become sufficiently large so that they can be estimated efficiently by direct Monte Carlo simulation. Therefore, the problem of evaluating a small failure probability in the original probability space is replaced by a sequence of simulations of more frequent events in the conditional probability spaces. The conditional probabilities, however, cannot be evaluated efficiently by common techniques, and therefore a Markov chain MCS method based on the Metropolis algorithm is used (Au and Beck, 2001; Schueller et al.,

2004). The approach has been shown to be computationally efficient and accurate when compared to the direct MCS method (Schueller and Pradlwarter, 2007). In fact, Agdas et al. (2011) compared the subset simulation method with the direct MCS method via a theoretical case study and showed that 999,900 simulations were required to compute a probability of failure of 0.0001 using the direct MCS method while 65,250 simulations were required using the subset simulation method to achieve the same level of accuracy.

4 STATISTICAL LINEARIZATION

4.1 INTRODUCTION

An approximate method used to solve nonlinear stochastic problems in structural dynamics is the *Statistical Linearization* technique. It is a tool that linearizes the equation of motion by replacing the original set of governing nonlinear equations with an equivalent set of linear equations; the difference between the sets being minimized in a statistical sense (Roberts and Spanos, 2003). The nonlinear system is replaced by a linear system in such a way that some average measure of the equation difference is minimized for all possible solutions of the associated linear system. For systems with small nonlinearities, it is evident that the approximate solution obtained by statistical linearization will become asymptotic to the exact solution in the limit as the nonlinearity parameter approaches zero (Iwan and Mason, 1980).

The method can easily be generalized to handle multi-degree of freedom (MDOF) systems including those where hysteretic elements are incorporated. Also, the technique can deal with non-white excitations and can be generalized for non-stationary excitations and responses (Iwan and Mason, 1980; Spanos, 1981a; Roberts, 1981). Further, more recent extensions of the statistical linearization technique can be found in a book by Socha (2008), while wavelet-based generalizations accounting also for fractional derivatives terms can be found in (Spanos and Kougioumtzoglou, 2012; Kong et al., 2014; Kougioumtzoglou and Spanos, 2016).

Although the method is highly flexible and efficient to apply, in its standard implementation can only yield first and second order moment statistics (e.g. mean, mean square, and power spectrum). This is due to the in-built assumption that the response is Gaussian. Consequently, it cannot accurately predict the influence of nonlinearities on the probability of the system failing in some prescribed manner. In other words, it doesn't accurately provide an estimate of the shape of the extreme tail ends of the response PDF curves.

Although it may not accurately predict failure probabilities, the statistical linearization approach is orders of magnitude more efficient than the MCS method. Further, when designing structural/mechanical systems, the initial stages usually involve studies of the influence of various system parameters on the overall response. In other words, the mean and mean-square characteristics of the response are usually sufficient for initial design stages. The statistical linearization approach is ideally suited for these cases.

4.1.1 Linearization of Single Nonlinear Element

A simple example of a function with a single nonlinear element is solved below using the statistical linearization method to demonstrate the general idea of the approach.

A nonlinear function is considered:

$$y(t) = g[x(t)] = x(t)^3 \tag{4.1}$$

It should be noted, that the distribution of the output, $y(t)$, in Eq. 4.1 can be related to that of the input, $x(t)$, fairly directly, without resorting to approximate techniques by applying the change of variables technique described in Section 2.1.2.

Assuming both the input and output are zero mean, Eq. 4.1 can be approximated as

$$y_e = a\,x \tag{4.2}$$

where a is a constant (for convenience, the time argument is dropped from the equations above). A value for the parameter a can be chosen to minimize the difference between the nonlinear element output and the linear element output:

$$\varepsilon = y - y_e = g(x) - a\,x \tag{4.3}$$

If ε is suitably minimized, the system governed by Eq. 4.2 is referred to as the 'equivalent linear system'. In other words, the statistics of y_e may be used as approximations to the statistics of the output of the nonlinear element, $g(x)$. A minimization criterion that has been found to give good results is based on minimizing the expected value of ε^2, $E[\varepsilon^2]$ (Roberts and Spanos, 2003). Adopting this method, the value of a is sought by minimizing $E[\varepsilon^2]$:

$$E[\varepsilon^2] = E[(g(x) - a\,x)^2] \tag{4.4}$$

which can be minimized by solving,

$$\frac{d}{da}E[\varepsilon^2] = 0 \tag{4.5}$$

This leads to the following:

$$E[(g(x)x)] - aE[x^2] = 0 \tag{4.6}$$

and

$$a = \frac{E[(g(x)x)]}{E[x^2]} = \frac{E[(g(x)x)]}{\sigma_x{}^2} \tag{4.7}$$

An important relationship for Gaussian vectors is summarized in the following formula (Kazakov, 1965):

$$E[g(x)x] = E[x^2]E[\frac{dg}{dx}] \tag{4.8}$$

Taking advantage of the relationship in Eq. 4.8, a can be expressed as

$$a = E[\frac{dg}{dx}] = E[3x^2] = 3E[x^2] = 3{\sigma_x}^2 \tag{4.9}$$

Therefore, the equivalent linear system is

$$y_e = 3{\sigma_x}^2 \, x \tag{4.10}$$

and, the standard deviation of the linearized equation is

$$\sigma_{y_e} = 3{\sigma_x}^3 \tag{4.11}$$

As mentioned above, the nonlinear equation can be solved directly and has an analytical solution of which the standard deviation is (Roberts and Spanos, 2003):

$$\sigma_y = \sqrt{15}\,{\sigma_x}^3 \tag{4.12}$$

A comparison of the standard deviation of both the nonlinear and equivalent linear systems is shown in Figure 4-1 below.

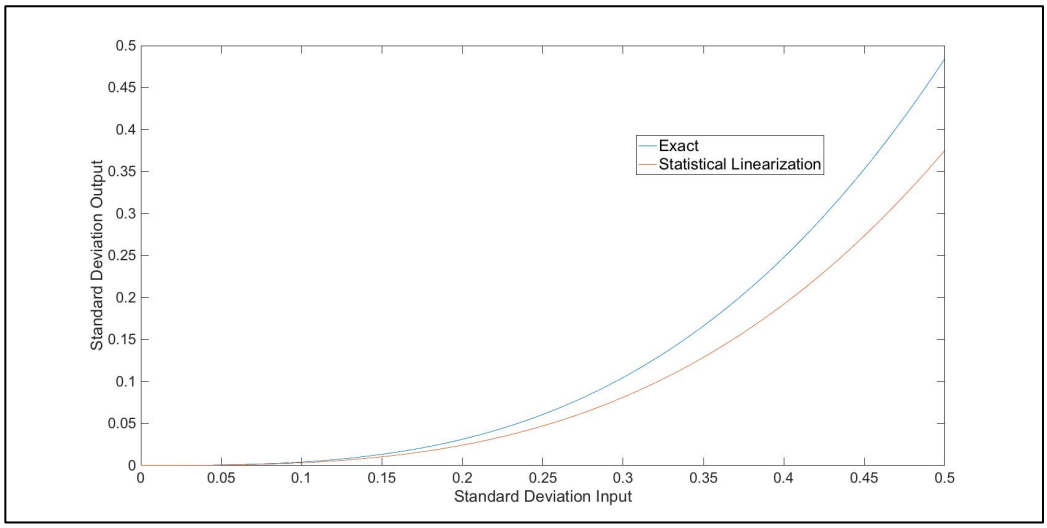

Figure 4-1: Standard Deviation Comparison (Nonlinear and Equivalent Linear Systems)

As seen in Figure 4-1, for smaller values of σ_x the equivalent linear system output σ_{y_e} is close to the nonlinear (exact) σ_y. As σ_x increases, the percent error also increases.

4.2 LINEARIZATION OF DUFFING OSCILLATOR

Next, an example is presented considering a Duffing oscillator excited by a stationary stochastic process. The approach presented above considering a single nonlinear element in isolation is extended to consider the nonlinear component as part of the overall system.

The equation of motion for a Duffing oscillator is

$$\ddot{y} + 2\zeta\omega_n\dot{y} + g(y) = f(t) \tag{4.13}$$

where $g(y) = {\omega_n}^2(y + \lambda y^3)$, λ is the magnitude of nonlinearity, $f(t)$ is the excitation represented by a Gaussian, zero-mean white noise process possessing a power spectral density of S_0.

The equivalent linear system takes the following form:

$$\ddot{y} + 2\zeta\omega_n\dot{y} + {\omega_{eq}}^2 y = f(t) \tag{4.14}$$

The term $g(y)$ is replaced with ${\omega_{eq}}^2 y$ where ω_{eq} is the natural frequency of the equivalent linear system. To derive ω_{eq} the difference between the linear and nonlinear stiffness, $\varepsilon = g(y) - {\omega_{eq}}^2 y$, must be minimized in a mean square sense:

$$\frac{d}{d{\omega_{eq}}^2} E[\varepsilon^2] = 0 \tag{4.15}$$

Taking advantage of the relationship $E[g(y)y] = E[y^2]E[\frac{dg}{dy}]$ (Kazakov, 1965) and solving for ω_{eq} yields the following expression:

$$\omega_{eq}{}^2 = \frac{E[(g(y)y)]}{\sigma_y{}^2} = \frac{E[y^2]E[\frac{dg}{dy}]}{\sigma_y{}^2} = E\left[\frac{dg}{dy}\right] = \omega_n{}^2(1 + 3\lambda\sigma_y{}^2) \quad (4.16)$$

Thus, the equivalent linear system is

$$\ddot{y} + 2\zeta\omega_n\dot{y} + \omega_n{}^2(1 + 3\lambda\sigma_y{}^2)y = f(t) \quad (4.17)$$

The complex frequency response function $H(\omega)$ is derived by substituting $f(t) = exp(i\omega t)$ and $y = H(\omega)exp(i\omega t)$:

$$H(\omega) = \frac{1}{(\omega_n{}^2(1+3\lambda\sigma_y{}^2) - \omega^2 + 2i\omega\zeta\omega_n)} \quad (4.18)$$

The spectral density and mean square of the displacement response are, respectively:

$$S_y(\omega) = |H(\omega)|^2 S_0 \quad (4.19)$$

and

$$E[y^2] = \int_{-\infty}^{\infty} S_y(\omega)d\omega = \int_{-\infty}^{\infty} |H(\omega)|^2 S_0 d\omega = S_0 \int_{-\infty}^{\infty} |H(\omega)|^2 d\omega \quad (4.20)$$

And, the spectral density and mean square of the velocity response are, respectively:

$$S_{\dot{y}}(\omega) = \omega^2 S_y(\omega) \quad (4.21)$$

and

$$E[\dot{y}^2] = \int_{-\infty}^{\infty} S_{\dot{y}}(\omega)d\omega = S_0 \int_{-\infty}^{\infty} \omega^2 S_y(\omega)d\omega \quad (4.22)$$

The integral in Eq. 4.20 can be solved analytically and has the following solution (see Section 2.4):

$$S_0 \int_{-\infty}^{\infty} |H(\omega)|^2 d\omega = S_0 \pi \frac{\left(\frac{{B_0}^2}{A_0}\right) A_2 + {B_1}^2}{A_1 A_2} \quad (4.23)$$

where $A_0 = {\omega_n}^2 \left(1 + 3\lambda {\sigma_y}^2\right), A_1 = 2\zeta\omega_n, A_2 = 1, B_0 = 1 \; and \; B_1 = 0.$

Therefore, the mean square of the displacement response is:

$$E[y^2] = {\sigma_y}^2 = \frac{\pi S_0}{(1+3\lambda {\sigma_y}^2) 2\zeta {\omega_n}^3} \quad (4.24)$$

and the mean square of the velocity response is:

$$E[\dot{y}^2] = {\sigma_{\dot{y}}}^2 = \frac{\pi S_0}{2\zeta\omega_n} \quad (4.25)$$

4.3 ACCURACY OF STATISTICAL LINEARIZATION METHOD

The accuracy of the statistical linearization method can, in general, be assessed by two approaches. One approach is to compare the results to those obtained by MCS, and the other approach is to compare them with the exact theoretical results obtained by solving the associated Fokker-Planck-Kolmogorov (FPK) equation. However, the class of nonlinear random vibration problems for which the appropriate FPK equation can be solved exactly is limited. SDOF systems for which the stationary solution of the associated FPK equation can be determined requires that the mass, damping and stiffness of the oscillator be a function of displacement and velocity of a very specific form (Roberts and Spanos, 2003). Also, the approach is dependent on the limitation assumption that the system's response is a Markov process restricting consideration to those cases where the excitation processes can be modeled adequately in terms of white noise processes.

4.3.1 Markov Processes

A Markov process is one whose current state only depends on the state immediately preceding it. For example, when considering a random process $x(t)$ that has been sampled at times $\{t_1, t_2, t_3, \dots\}$ the PDF of x at time t_n is only dependent on the preceding value of x:

$$P\,(x_n, t_n) \;=\; P\,(x_n, t_n | x_{n-1}, t_{n-1}) \tag{4.26}$$

If not a Markov process then the probability of x at time t_n could be conditional on all the past values of x:

$$P\,(x_n, t_n) \;=\; P\,(x_n, t_n | x_{n-1}, t_{n-1}; x_{n-2}, t_{n-2} \dots x_1, t_1; x_0, t_0) \tag{4.27}$$

Analytical white noise is, by definition, a Markov process.

4.3.2 Exact Solution of Duffing Oscillator Subjected to White Noise

For the case of a Duffing oscillator excited by white noise, the exact solution to the associated FPK equation is attainable (Caughey, 1963; Lin, 1967; Roberts and Spanos, 2003).

The corresponding FPK equation is the following:

$$\frac{\partial P(x_1,x_2,t)}{\partial t} = -x_2 \frac{\partial P(x_1,x_2,t)}{\partial x_1} + 2\zeta\omega_n x_2 \frac{\partial P(x_1,x_2,t)}{\partial x_2} + F(x_1)\frac{\partial P(x_1,x_2,t)}{\partial x_2} + \pi S_0 \frac{\partial^2 P(x_1,x_2,t)}{\partial^2 x_2} \tag{4.28}$$

where $x_1 = y,\ x_2 = \dot{y}, F(x_1) = {\omega_n}^2(x_1 + \lambda {x_1}^3)\ and\ P(x_1, x_2, t)$ is the joint probability density function of the response. For the stationary case, the PDF is time invariant, therefore $\frac{\partial P(x_1,x_2,t)}{\partial t} = 0$ and $P(x_1, x_2, t) = P(x_1, x_2)$, and the displacement and velocity are statically independent (see Section 2.2.2.1); i.e.,

$P(x_1, x_2) = P(x_1)P(x_2)$. Solving the FPK equation yields the following for the response displacement and velocity PDFs, respectively (Caughey, 1963):

$$P(x_1) = C_1 \exp\left[\left(\frac{-2\zeta\omega_n}{\pi S_0}\right)\left(\frac{\omega_n{}^2 x_1{}^2}{2} + \frac{\omega_n{}^2 \lambda x_1{}^4}{4}\right)\right] \tag{4.29}$$

and

$$P(x_2) = C_2 \exp\left[\left(\frac{-2\zeta\omega_n{}^2}{\pi S_0}\right)\left(\frac{x_2{}^2}{2}\right)\right] \tag{4.30}$$

where the constants required to satisfy the condition of unity are

$$C_1{}^{-1} = \int_{-\infty}^{\infty} \exp\left[\left(\frac{-2\zeta\omega_n}{\pi S_0}\right)\left(\frac{\omega_n{}^2 x_1{}^2}{2} + \frac{\omega_n{}^2 \lambda x_1{}^4}{4}\right)\right] dx_1 \tag{4.31}$$

and

$$C_2{}^{-1} = \int_{-\infty}^{\infty} \exp\left[\left(\frac{-2\zeta\omega_n{}^2}{\pi S_0}\right)\left(\frac{x_2{}^2}{2}\right)\right] dx_2 \tag{4.32}$$

Note that the displacement response PDF (Eq. 4.29) is not Gaussian.

Further, the variance of the displacement response can be determined by solving the following

$$\sigma_{x_1}{}^2 = \int_{-\infty}^{\infty}\int_{-\infty}^{\infty} x_1{}^2 P(x_1)P(x_2)dx_1 dx_2 \tag{4.33}$$

the solution of which is (Roberts and Spanos, 2003):

$$\sigma_{x_1}{}^2 = \left(\frac{\pi\rho}{2}\right)^{1/2}\left(\frac{\rho}{2}\right)^{-3/4} D_{-3/2}\left(\frac{1}{\sqrt{2\rho}}\right) K_{1/4}{}^{-1}\left(\frac{1}{8\rho}\right) \tag{4.34}$$

where $\rho = \lambda\sigma_{x_0}{}^2$, $\sigma_{x_0}{}^2 = \frac{\pi S_0}{2\zeta\omega_n{}^3}$ (i.e. the variance of the corresponding linear system), $D_{-3/2}$ is a parabolic cylinder function, and $K_{1/4}$ is a modified Bessel function (Abramowitz and Stegun, 1972).

4.3.3 Numerical Example (Stationary Case)

Figure 4-2 shows the exact standard deviation and the approximate solution derived using the statistical linearization technique for $\omega_n = 1, \zeta = 0.1, S_0 = 0.0637$, and varying the nonlinear coefficient, λ. As seen in Figure 4-2, the estimated standard deviation approaches the exact value as the nonlinearity term decreases.

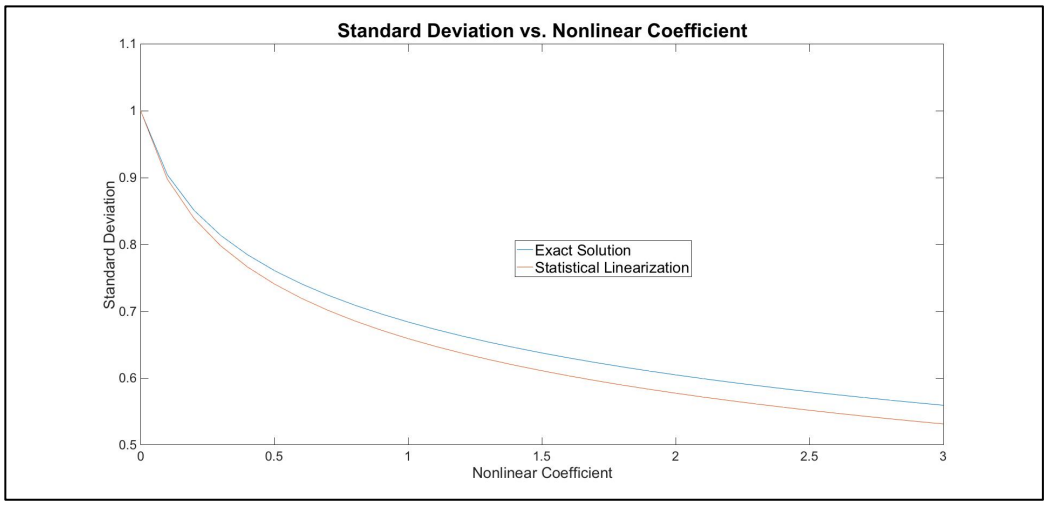

Figure 4-2: Variation of standard deviation with nonlinear coefficient, λ

The statistical linearization method can be used to derive response PDFs due to the in-built assumption of Gaussianity (i.e. Gaussian random variables are fully characterized by their mean and variance). Figure 4-3 shows the displacement response PDFs for the exact solution, MCS data, and the solution obtained by the statistical linearization for $\lambda = 1.5$.

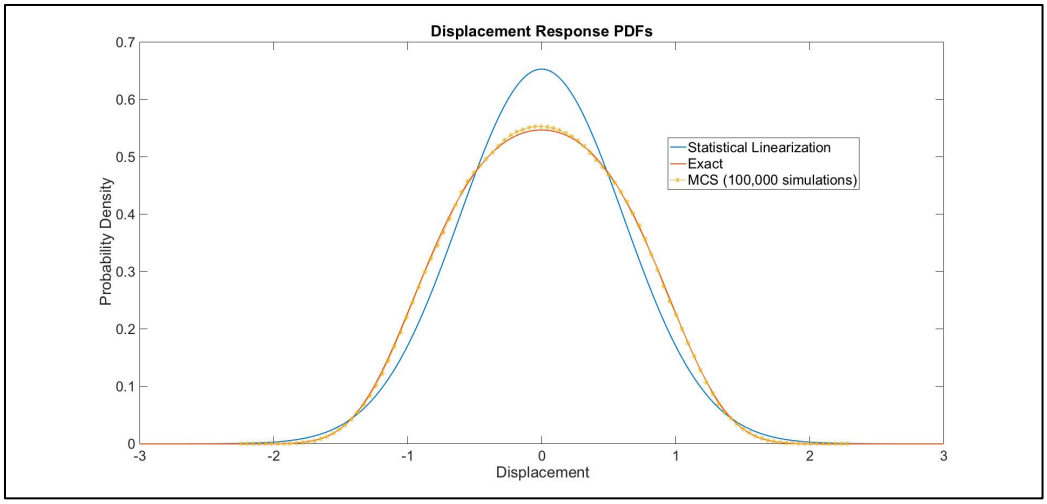

Figure 4-3: Displacement Response PDFs

As seen in Figure 4-3, the response PDF derived using the statistical linearization method slightly deviates from the exact solution. This deviation is noticeable when taking a closer look at the tail ends (see Figure 4-4). As discussed previously, the shape of the tail ends is important for determining failure probabilities.

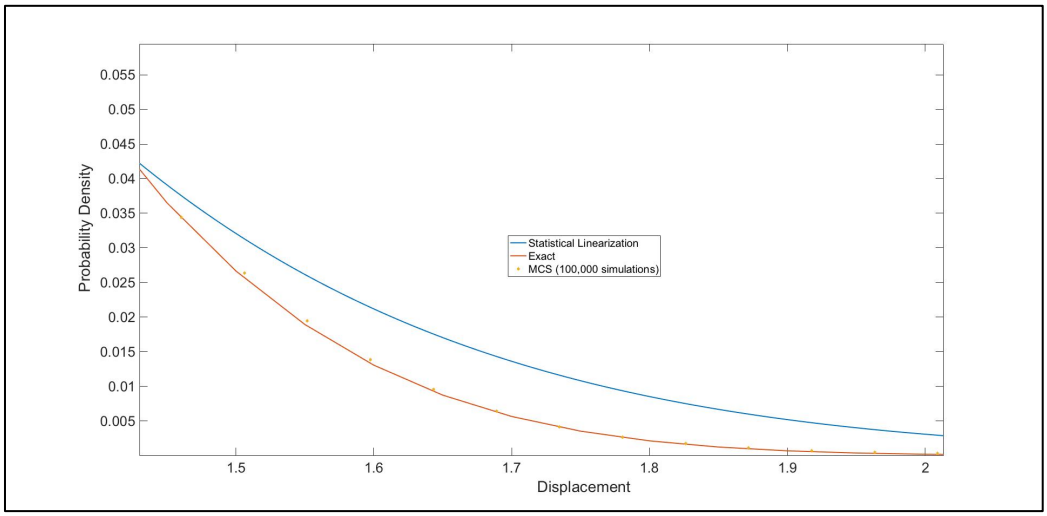

Figure 4-4: Displacement Response PDFs (tail end)

4.4 NON-STATIONARY EXCITATIONS

The statistical linearization method described above can be adapted for the case of non-stationary excitations. However, the elements of the equivalent

linear system are no longer time invariant. This poses some complications that are coped with by employing suitable extensions of the linearization procedure (e.g. Iwan and Mason, 1980; Roberts and Spanos, 2003). Since the linearized elements are time-dependent for the non-stationary case, a set of nonlinear differential equations must be solved, rather than algebraic equations, as is the case for stationary excitations.

The case of a Duffing oscillator subjected to a non-stationary stochastic process will be solved to demonstrate the approach. Again, the equation of motion for a Duffing oscillator reads:

$$\ddot{y} + 2\zeta\omega_n\dot{y} + g(y) = \theta(t)f(t) \tag{4.35}$$

where $g(y) = {\omega_n}^2(y + \lambda y^3)$, λ is the magnitude of nonlinearity, $f(t)$ is a stationary stochastic process, and $\theta(t)$ is a deterministic time modulation function. The equivalent linear system, as derived previously, is

$$\ddot{y} + 2\zeta\omega_n\dot{y} + {\omega_n}^2\left(1 + 3\lambda{\sigma_y}^2\right)y = \theta(t)f(t) \tag{4.36}$$

Recasting the equivalent linear system equation in state variable form (Roberts and Spanos, 2003) by defining a state vector, $z(t)$, where

$$z(t) = \begin{bmatrix} y \\ \dot{y} \end{bmatrix} \tag{4.37}$$

The system equation can be written in first-order form,

$$\dot{z} = G(t)z + f \tag{4.38}$$

where

$$G = \begin{bmatrix} 0 & 0 \\ -{\omega_n}^2\left(1 + 3\lambda{\sigma_y}^2\right) & -2\zeta\omega_n \end{bmatrix} \tag{4.39}$$

and

$$f = \begin{bmatrix} 0 \\ \theta(t)f(t) \end{bmatrix} \tag{4.40}$$

The covariance function of $z(t)$ is

$$V(t) = E[z(t)z^T(t)] \tag{4.41}$$

Differentiating both sides of Eq. 4.41,

$$\dot{V} = E[\dot{z}z^T] + E[z^T\dot{z}] \tag{4.42}$$

Substituting Eq. 4.38 into Eq. 4.42,

$$\dot{V} = G(t)V^T + VG(t)^T + U(t) + U(t)^T \tag{4.43}$$

where

$$U(t) = E[zf^T] \tag{4.44}$$

Eq. 4.43 is commonly known as the Lyapunov equation (Spanos, 1981a).

Next, by letting $Y(t)$ be the solution to the homogeneous equation,

$$\dot{Y} = G(t)Y \tag{4.45}$$

the solution of Eq. 4.38 may be written in terms of $Y(t)$,

$$z(t) = Y(t)\int_0^t Y^{-1}(s)f(s)ds \tag{4.46}$$

Note $Y(s)$ is a vector. Using Eq. 4.46 for $z(t)$, $U(t)$ can be expressed as

$$U(t) = Y(t)\int_0^t Y^{-1}(s)w_f(t,s)ds \tag{4.47}$$

where $w_f(t,s)$ is the covariance matrix of f,

$$w_f(t,s) = E[f(t)f^T(s)] \tag{4.48}$$

Considering the case of a white noise excitation, the spectral density function $S_f(\omega) = S_0$, and Eq. 4.48 becomes

$$w_f(t,s) = 2\pi S_0 \delta(s-t) \tag{4.49}$$

Therefore, $U(t)$ can be written as

$$U(t) = \frac{1}{2}\Theta(t) \tag{4.50}$$

where

$$\Theta(t) = \begin{bmatrix} 0 & 0 \\ 0 & \theta(t) 2\pi S_0 \theta^T(t) \end{bmatrix} \tag{4.51}$$

Substituting Eq. 4.50 into Eq. 4.43 yields,

$$\dot{V} = G(t)V^T + VG(t)^T + \Theta(t) \tag{4.52}$$

Denoting the elements of V as v_{ij}, Eq. 4.52 can be written in matrix form,

$$\frac{d}{dt}\begin{bmatrix} v_{11} & v_{12} \\ v_{21} & v_{22} \end{bmatrix} =$$

$$\begin{bmatrix} 0 & 0 \\ -{\omega_n}^2\left(1 + 3\lambda {\sigma_y}^2\right) & -2\zeta\omega_n \end{bmatrix} \begin{bmatrix} v_{11} & v_{12} \\ v_{21} & v_{22} \end{bmatrix} +$$

$$\begin{bmatrix} v_{11} & v_{12} \\ v_{21} & v_{22} \end{bmatrix} \begin{bmatrix} 0 & 0 \\ -{\omega_n}^2\left(1 + 3\lambda {\sigma_y}^2\right) & -2\zeta\omega_n \end{bmatrix} + 2\pi S_0 \theta^2(t) \begin{bmatrix} 0 & 0 \\ 0 & 1 \end{bmatrix} \tag{4.53}$$

Eq. 4.53 is equivalent to the following set of differential equations,

$$\dot{v_{11}} = \frac{d}{dt}E[y^2] = 2v_{12}$$

$$\dot{v_{12}} = \frac{d}{dt}E[y\dot{y}] = v_{22} - {\omega_n}^2(1 + 3\lambda v_{11})v_{11} - 2\zeta\omega_n v_{12}$$

$$\dot{v_{22}} = \frac{d}{dt}E[\dot{y}^2] = -2[{\omega_n}^2 v_{12}(1 + 3\lambda v_{11}) + 2\zeta\omega_n v_{22}] + 2\pi S_0 \theta^2(t) \tag{4.54}$$

where $v_{12} = v_{21}$.

The solution to Eq. 4.54 can be obtained by standard numerical methods such as the Runge–Kutta scheme (Shampine, 1994).

4.4.1 Numerical Example (Non Stationary Case)

For this particular example, a time modulation function having the following form is considered,

$$\theta(t) = k(e^{-at} - e^{-bt}) \tag{4.55}$$

in which $a = 0.25$, $b = 0.5$, and k is a normalization constant so that $\theta_{max} = 1$.

Note that for the non-stationary case, the joint response PDF is time variant (i.e. $\frac{\partial P(x_1,x_2,t)}{\partial t} \neq 0$ in Eq. 4.28) which complicates the problem significantly, and an analytical solution of the associated FPK equation does not exist (Roberts and Spanos, 2003). Therefore, the results obtained by solving Eq. 4.54 are compared with MCS data, and are shown in Figure 4-5 and Figure 4-6 for the following system parameters: $\omega_n = 3.61, \zeta = 0.01, \lambda = 0.5$ and $S_0 = 0.1$.

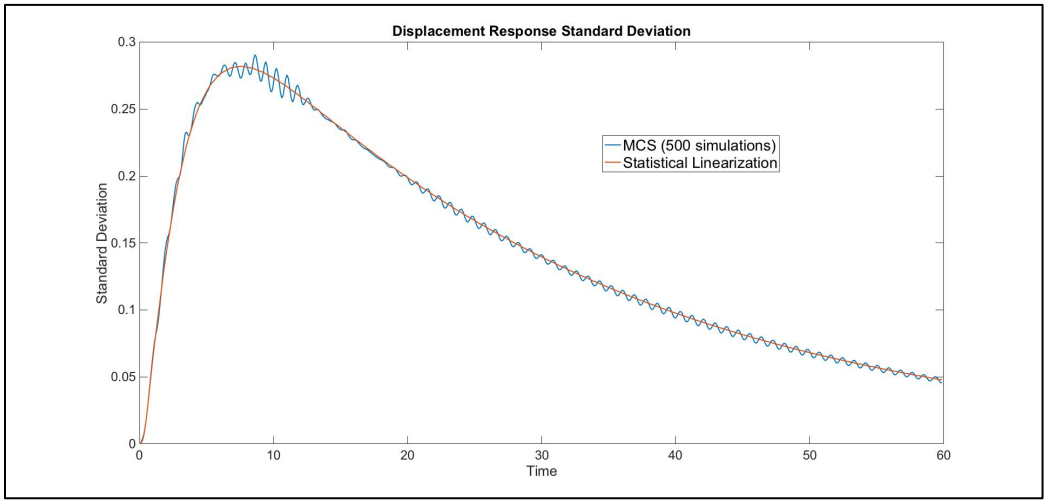

Figure 4-5: Displacement Response Standard Deviation

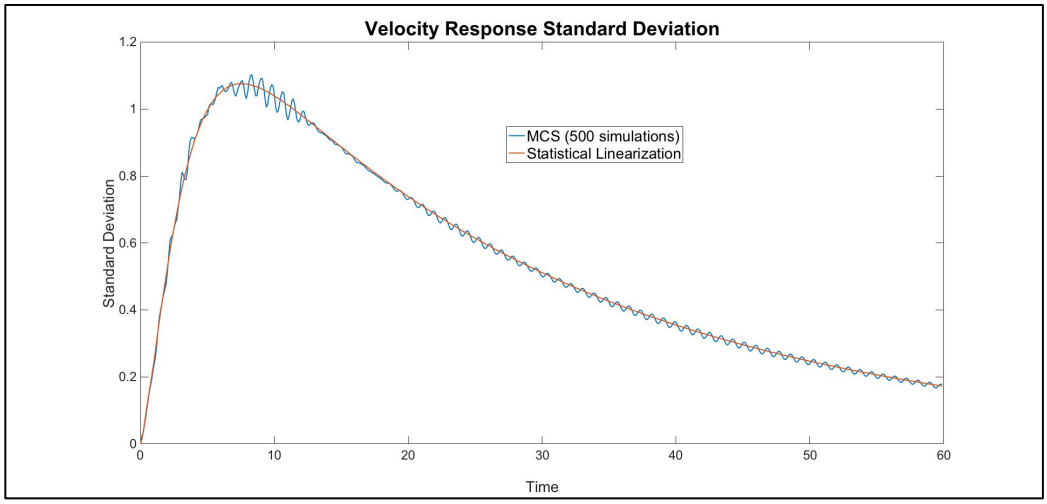

Figure 4-6: Velocity Response Standard Deviation

As seen in Figure 4-5 and Figure 4-6, the statistical linearization approach is in good agreement with the MCS data.

Using the in-built assumption of the Gaussianity, the displacement and velocity response PDFs are derived and presented in Figure 4-7 and Figure 4-8.

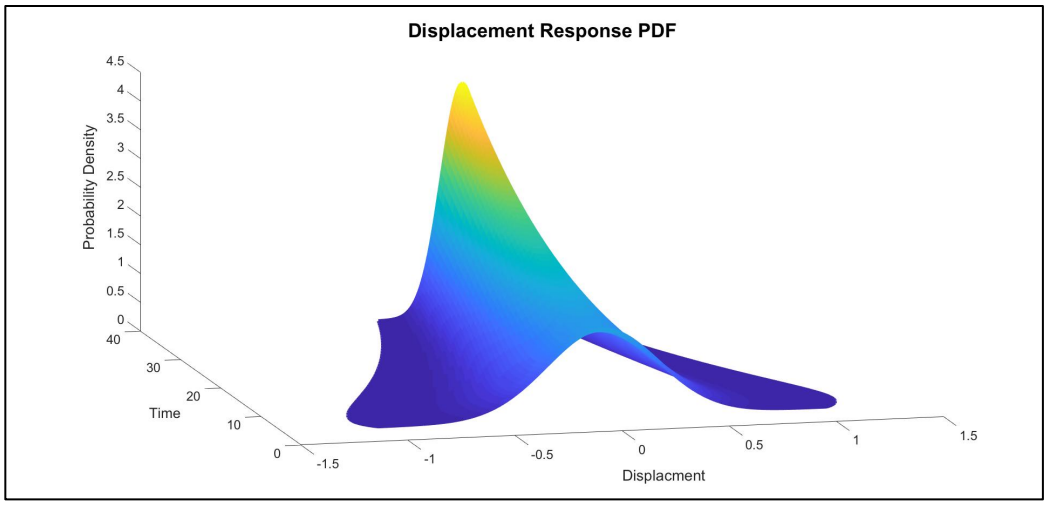

Figure 4-7: Displacement Response PDF

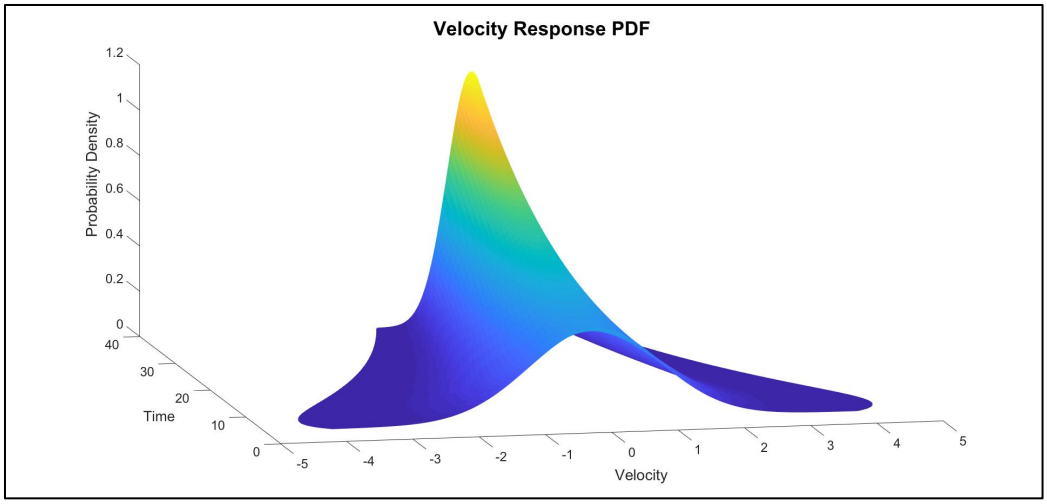

Figure 4-8: Velocity Response PDF

4.5 DISCUSSION

According to (Iwan and Mason, 1980), the variance computed using the statistical linearization technique is within approximately 15% of the exact value even for arbitrarily large values of λ. Of course for small nonlinearities the statistical linearization approach yields accurate results as is demonstrated in Figure 4-2.

It has been shown above that the distribution of the response can be estimated using the inbuilt assumption of Gaussianity (e.g. Figure 4-3, Figure 4-7 and Figure 4-8). However, it is important to note that the influence of nonlinearities on the distribution cannot be predicted using the statistical linearization technique. Therefore, caution should be exercised when computing failure probabilities as the tail ends of the response PDF curve can deviate considerably from the exact solution when nonlinearities are high (Roberts and Spanos, 2003). Nonetheless, the approach is extremely efficient to implement, and provides fairly good estimates of first and second moment statistics (e.g. mean and mean-square responses) when the damping is low. As such, the statistical linearization method is ideally suited for the beginning stages of

projects (i.e. front-end engineering and design) when the design parameters are not well established yet, complex systems can be simplified, and first and second moment statistics are sought.

To improve the statistical linearization technique, non-Gaussian closure (NGC) techniques have been developed (Beaman and Hedrick, 1981; Crandall, 1980; 1985; Ibrahim, 1985; Roberts and Spanos, 2003). The NGC technique involves constructing a non-Gaussian probability distribution with adjustable parameters for the response and using moment relationships derived from the equation of motion to obtain differential or algebraic equations for the unknown parameters. When the parameters are found, the resulting probability distribution can be used to provide the necessary response statistics (Noori et al.; 1987). Crandall (1980) developed a NGC technique by assuming a truncated Gram-Charlier expansion for the response PDF. Noori et al. (1987) compared the NGC technique by (Crandall, 1980) to the statistical linearization technique and found that for low nonlinearity cases both techniques produced similar results and compared well with the exact solution. When comparing the results considering high nonlinearities, the NGC technique showed a slight improvement over the statistical linearization technique. However, Noori et al. (1987) concluded that for the examples considered, the NGC technique does not justify its selection over the statistical linearization approach due to the associated complexity and increased computational time.

5 WIENER PATH INTEGRAL (WPI)

5.1 INTRODUCTION

The Monte Carlo simulation has been, perhaps, the most versatile tool for determining response and reliability statistics of stochastic systems. However, there are cases, for instance when large-scale complex systems are concerned or when the quantity of interest has a relatively small probability of occurrence, for which the use of MCS techniques can be computationally demanding, or even prohibitive. Thus, there is a need for developing alternative efficient approximate analytical and/or numerical solution techniques (see Kougioumtzoglou, 2013; Spanos and Kougioumtzoglou, 2014; Kougioumtzoglou and Spanos, 2013b for some recent references).

One of the promising frameworks relates to the concept of the Wiener path integral (WPI). In this regard, note that although the WPI has strongly impacted the field of theoretical physics, the engineering community has so far ignored its potential as a powerful uncertainty quantification tool. The concept of path integral was introduced by (Wiener, 1921) and was reinvented in a different form by (Feynman, 1948) to reformulate quantum mechanics. A more detailed treatment of path integrals, especially of their applications in physics, can be found in a number of books such as in (Chaichian and Demichev, 2001). Recently, in (Kougioumtzoglou and Spanos, 2012) an approximate analytical WPI technique was developed based on a variational formulation and on the concepts of stochastic averaging/linearization for addressing certain stochastic engineering dynamics problems. In this regard, relying on the concept of the

most probable path an approximate expression was derived for the non-stationary response probability density function (PDF). Further, the aforementioned technique was extended in (Kougioumtzoglou and Spanos, 2014) to account for multi-degree-of-freedom (MDOF) systems as well as for hysteretic nonlinearities. In (Di Matteo et al, 2014) the technique was further enhanced and generalized to treat linear and nonlinear systems endowed with fractional derivatives terms. Furthermore, the method has been extended for addressing certain one-dimensional mechanics problems with random material/media properties (Kougioumtzoglou, 2017) while preliminary results towards an error quantification analysis can be found in (Meimaris et al., 2017). From a computational efficiency perspective, recent work by Kougioumtzoglou et al. (2015) reduced the computational complexity by, potentially, several orders of magnitude as compared to the original formulation and numerical implementation of the technique.

The basic elements of the WPI technique are presented in more detail below. The technique is then applied to the stochastic response of nonlinear vibratory energy harvesters, and, to the depth determination of ice gouging events in subsequent sections.

5.2 WPI FORMULATION AND MOST PROBABLE PATH

The transition PDF, $p\left(x_f, \dot{x}_f, t_f | x_i, \dot{x}_i, t_i\right)$, denotes the probability of a transition from a point in state space $(x_i, \dot{x}_i)$ at time t_i to a point in state space $(x_f, \dot{x_f})$ at time t_f where $t_f > t_i$. Adopting the notation of (Chaichian and Demichev, 2001), $C\{x_i, \dot{x}_i, t_i; x_f, \dot{x}_f, t_f\}$ denotes the set of all trajectories (or paths) a particle can take starting at point $(x_i, \dot{x}_i)$ and having end point $(x_f, \dot{x_f})$. To obtain the transition PDF that the particle starting at $(x_i, \dot{x}_i)$ ends up at $(x_f, \dot{x}_f)$, the

probabilities over the set, $C\{x_i, \dot{x}_i, t_i; x_f, \dot{x}_f, t_f\}$, of all possible trajectories must be summed. This summation over the set of continuous trajectories is a functional integral called the Wiener path integral (Kougioumtzoglou and Spanos, 2012). Unlike an ordinary integral where there is a function to be integrated over a continuous range of values, in a functional integral, the domain of integration is a range of functions.

The WPI possesses a probability distribution on the path space as its integrand, which is denoted by $W[x(t)]$ and is called the probability density functional. Essentially, the probability density functional assigns a probability to each path, as all paths are not equally probable. This Figure 5-1 shows a graphical depiction of the set of paths $C\{x_i, \dot{x}_i, t_i; x_f, \dot{x}_f, t_f\}$.

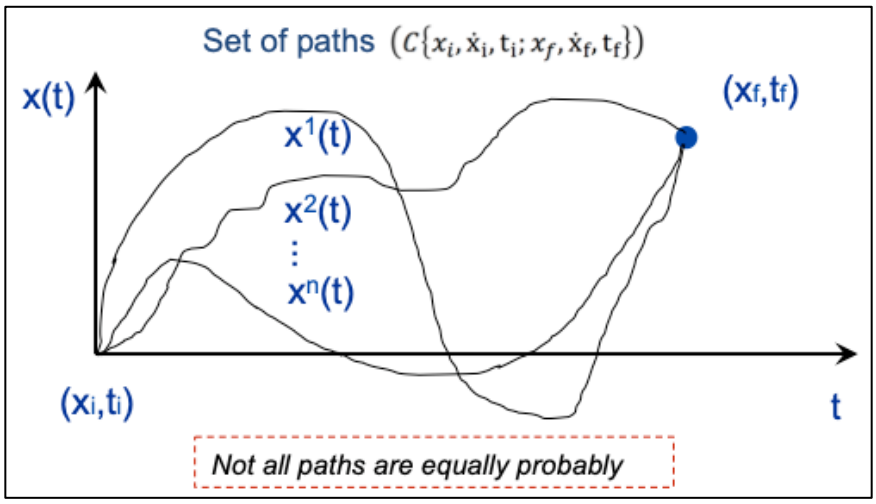

Figure 5-1: Sample Paths

In other words, the total probability that x will start from x_i at time t_i and end up at x_f at time t_f takes the form of a functional integral that sums up the respective probabilities of each and every path (i.e. probability density functional) that the process can possibly follow.

In this manner, the transition PDF $p(x_f, \dot{x}_f, t_f | x_i, \dot{x}_i, t_i)$ is given by

$$p(x_f, \dot{x}_f, t_f | x_i, \dot{x}_i, t_i) = \int_{\{x_i, \dot{x}_i, t_i\}}^{\{x_f, \dot{x}_f, t_f\}} W[x(t)][dx(t)]. \quad (5.1)$$

This can be construed as a number of successive probabilities for each point of the path, or the probability of a compound event (see Psaros et al., (2018) for more details).

Further, note that even if the probability density functional is constructed, the analytical solution of the WPI of Eq. 5.1 is a rather challenging, if not an impossible task. Thus, to circumvent the aforementioned challenge, several research efforts have focused on developing approximate techniques for determining the transition PDF, $p(x_f, \dot{x}_f, t_f | x_i, \dot{x}_i, t_i)$. In this regard, researchers invoked a variational formulation and defined a Lagrangian function $L(x, \dot{x}, \ddot{x})$ for determining the most probable path that connects the points $(x_i, \dot{x}_i, t_i)$ and $(x_f, \dot{x}_f, t_f)$. Figure 5-2 shows a depiction of the most probable path.

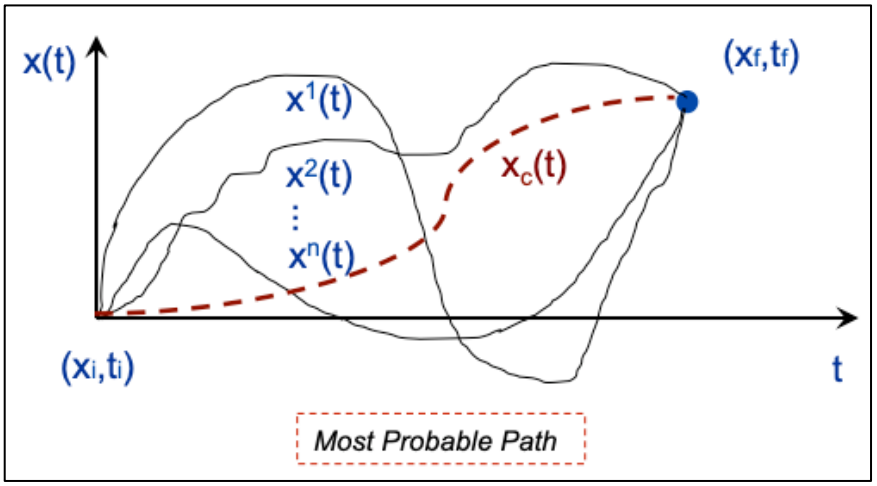

Figure 5-2: Most Probable Path

In this manner, a variational principle can lead to the associated Euler-Lagrange equation to be solved for the most probable path. See (Kougioumtzoglou and Spanos, 2012; Kougioumtzoglou and Spanos, 2014) for a more detailed presentation.

Specifically, utilizing the Lagrangian function and considering Eq. 5.1 yields (e.g. Caichian and Demichev, 2001)

$$W[x(t)] = Dexp\left(-\int_{t_i}^{t_f} L(x,\dot{x},\ddot{x})dt\right) \tag{5.2}$$

where D is a normalization coefficient. The largest contribution to the Wiener path integral comes from the trajectory for which the integral in the exponential (Eq. 5.2) becomes as small as possible. Variational calculus rules (e.g. Ewing, 1985) dictate that this trajectory with fixed end points satisfies the extremality condition

$$\delta \int_{t_i}^{t_f} L(x_c,\dot{x_c},\ddot{x_c})dt = 0. \tag{5.3}$$

This condition leads to the E-L equation

$$\frac{\partial L}{\partial x_c} - \frac{\partial}{\partial t}\frac{\partial L}{\partial \dot{x_c}} + \frac{\partial^2}{\partial t^2}\frac{\partial L}{\partial \ddot{x_c}} = 0, \tag{5.4}$$

with the four boundary conditions

$$x_c(t_i) = x_i, \dot{x}_c(t_i) = \dot{x}_i, x_c(t_f) = x_f, \dot{x}_c(t_f) = \dot{x}_f, \tag{5.5}$$

where $\mathrm{x_c}$ represents the most probable trajectory. Next, solving the boundary value problem (BVP) of Eq. 5.4 together with the conditions of Eq. 5.5 (e.g. De Coster and Habets, 2006) yields a solution for the transition PDF $p(x_f,\dot{x}_f,t_f|x_i,\dot{x}_i,t_i)$ in the form

$$p(x_f,\dot{x}_f,t_f|x_i,\dot{x}_i,t_i) = D\ exp\left[-\int_{t_i}^{t_f} L(x_c,\dot{x}_c,\ddot{x}_c)dt\right]. \tag{5.6}$$

It can be readily seen that for fixed time points $\mathrm{t_i}$ and $\mathrm{t_f}$, D can be determined by merely applying the normalization condition

$$\int_{-\infty}^{\infty}\int_{-\infty}^{\infty} p(x_f,\dot{x}_f,t_f|x_i,\dot{x}_i,t_i)dx_f d\dot{x}_f = 1. \tag{5.7}$$

The primary approximation of the technique relates to the fact that only the most probable path $\mathrm{x_c}$ is considered in the evaluation of the functional integral of Eq. 5.1 instead of all the possible paths $\mathrm{C\{x_i, \dot{x}_i, t_i; x_f, \dot{x}_f, t_f\}}$. The concept of the most probable path can be viewed as something equivalent to the fact that the most probable value of a random variable is the one corresponding to the peak of the PDF.

5.3 WPI NUMERICAL IMPLEMENTATION ELEMENTS

It is worth noting that for linear systems, the boundary value problem of Eq. 5.4 and Eq. 5.5 can be solved analytically, yielding an explicit closed-form expression for the most probable path $\mathrm{x_c}$ (see Section 5.3.1). Unfortunately, for the case of nonlinear systems (e.g. the vibratory energy harvester problem presented in Section 6 and the ice gouging problem presented in Section 7), the BVP of Eq. 5.4 and Eq. 5.5 cannot, in general, be solved analytically; thus, a numerical solution technique needs to be implemented. In this regard, for a given time instant $\mathrm{t_f}$ and a given vector value $\left(x_f, \dot{x}_f\right)$, a numerical solution of Eq. 5.4 and Eq. 5.5 yields a single point of the response PDF via Eq. 5.6. Typically, an effective domain of values is assumed for the response PDF $p\left(x_f, \dot{x}_f, t_f | x_i, \dot{x}_i, t_i\right)$; namely, for the $\mathrm{i th}$ components $\mathrm{x_{i,f}}$ of $\mathrm{x_f}$ and $\mathrm{\dot{x}_{i,f}}$ of $\mathrm{\dot{x}_f}$ it is assumed that $x_{i,f} = \in \left[x_{i,f,min}, x_{i,f,max}\right]$, $x^j{}_{i,f} = x_{i,f,min} + (j-1)\Delta x_{i,f}$, $j = 1, \dots, n$ with $\Delta x_{i,f} = \left(x_{i,f,max} - x_{i,f,min}\right)/(n-1)$ and $\dot{x}_{i,f} = \in \left[\dot{x}_{i,f,min}, \dot{x}_{i,f,max}\right]$, $\dot{x}^j{}_{i,f} = \dot{x}_{i,f,min} + (j-1)\Delta \dot{x}_{i,f}$, $j = 1, \dots, n$ with $\Delta \dot{x}_{i,f} = \left(\dot{x}_{i,f,max} - \dot{x}_{i,f,min}\right)/(n-1)$, respectively.

5.3.1 Numerical Example – Linear System

The WPI approach is now applied to a linear oscillator excited by a Gaussian, zero-mean white noise process.

The equation of motion of the system is

$$\ddot{x} + 2\zeta\omega_n\dot{x} + {\omega_n}^2 x = f(t) \tag{5.8}$$

where $f(t)$ is a Gaussian, zero-mean white noise process possessing a power spectral density of S_0.

The probability density functional for the white noise process $f(t)$ is given by (e.g. Chaichian and Demichev, 2001)

$$W[f(t)] = Dexp\left(-\int_{t_i}^{t_f} \frac{1}{2}\frac{f(t)^2}{2\pi S_0} dt\right) \tag{5.9}$$

Next, Eq. 5.8 is substituted into Eq. 5.9 and the probability density functional W[f(t)] is interpreted as the probability density functional $W[x(t)]$ for $x(t)$, yielding

$$W[f(t)] = Dexp\left(-\int_{t_i}^{t_f} \frac{1}{4\pi S_0}(\ddot{x} + 2\zeta\omega_n\dot{x} + {\omega_n}^2 x\ )^2 dt\right). \tag{5.10}$$

Thus, the corresponding Lagrangian is given by

$$L(x, \dot{x}, \ddot{x}) = \frac{1}{4\pi S_0}(\ddot{x} + 2\zeta\omega_n\dot{x} + {\omega_n}^2 x\ )^2. \tag{5.11}$$

Substituting Eq. 5.11 into Eq. 5.4 and considering Eq. 5.5 leads to the E-L equation,

$$\frac{d^4 x_c}{dt^4} + (2{\omega_n}^2 - 4\zeta^2{\omega_n}^2)\frac{d^2 x_c}{dt^2} + {\omega_n}^4 x_c = 0 \tag{5.12}$$

along with the boundary conditions

$x_c(0) = 0, \dot{x}_c(0) = 0, x_c(t_f) = x_f$ and $\dot{x}_c(t_f) = \dot{x}_f$. Note Eq. 5.12 can be easily solved analytically to obtain an expression for the most probable trajectory.

Specifically, seeking a solution in the form $e^{\Lambda t}$ and substituting into Eq. 5.12 yields the quadratic equation

$$\Lambda^4 + (2{\omega_n}^2 - 4\zeta^2{\omega_n}^2)\Lambda^2 + {\omega_n}^4 \tag{5.13}$$

Eq. 5.13 is solved next to obtain

$$\Lambda_1 = \zeta\omega_n\left(1 + i\sqrt{\frac{1}{\zeta^2} - 1}\right) \tag{5.14}$$

$$\Lambda_2 = \zeta\omega_n\left(1 - i\sqrt{\frac{1}{\zeta^2} - 1}\right) \tag{5.15}$$

$$\Lambda_3 = -\zeta\omega_n\left(1 + i\sqrt{\frac{1}{\zeta^2} - 1}\right) \tag{5.16}$$

$$\Lambda_4 = -\zeta\omega_n\left(1 - i\sqrt{\frac{1}{\zeta^2} - 1}\right) \tag{5.17}$$

Thus, the expression for the most probable path x_c becomes

$$x_c(t) = C_1 e^{\Lambda_1 t} + C_2 e^{\Lambda_2 t} + C_3 e^{\Lambda_3 t} + C_4 e^{\Lambda_4 t} \tag{5.18}$$

where C_1, C_2, C_3, and C_4 are constants to be determined by the boundary conditions. Note that for the case of a linear oscillator an analytical solution for the most probable path can be determined without resorting to numerical treatment of the boundary value problem of equations 5.4 and 5.5 rendering the developed WPI technique highly efficient.

Further, the solution to the problem can be determined in closed form. Eq. 2.80 provides the exact mean square of the displacement response, which, of course, is Gaussian (see Section 2).

The stationary response is computed considering the following system parameters: $\omega_n = 1, \zeta = 0.1$, and $S_0 = 0.0637$. Figure 5-3 shows the displacement response PDFs derived using the WPI approach and the exact solution.

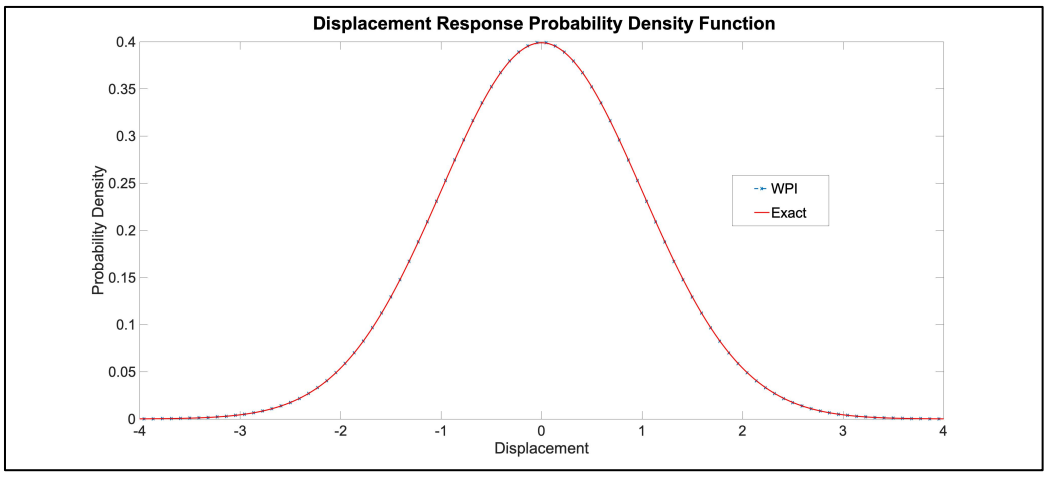

Figure 5-3: Displacement Response PDFs – Linear Oscillator (WPI vs. Exact)

As seen in Figure 5-3, a high level of accuracy is achieved using the WPI approach.

5.3.2 Numerical Example – Non Linear system

The WPI approach is now applied to a Duffing oscillator excited by a stationary stochastic process. Again, the equation of motion of the Duffing system is

$$\ddot{x} + 2\zeta\omega_n\dot{x} + {\omega_n}^2(x + \lambda x^3) = f(t) \tag{5.19}$$

where λ is the magnitude of nonlinearity and $f(t)$ is a Gaussian, zero-mean white noise process possessing a power spectral density of S_0.

The probability density functional for the white noise process $f(t)$ is given by (e.g. Chaichian and Demichev, 2001)

$$W[f(t)] = Dexp\left(-\int_{t_i}^{t_f} \frac{1}{2}\frac{f(t)^2}{2\pi S_0} dt\right) \tag{5.20}$$

Next, Eq. 5.19 is substituted into Eq. 5.20 and the probability density functional W[f(t)] is interpreted as the probability density functional $W[x(t)]$ for $x(t)$, yielding

$$W[f(t)] = Dexp\left(-\int_{t_i}^{t_f} \frac{1}{4\pi S_0}(\ddot{x} + 2\zeta\omega_n\dot{x} + {\omega_n}^2(x + \lambda x^3)\ )^2 dt\right). \quad (5.21)$$

Thus, the corresponding Lagrangian is given by

$$L(x, \dot{x}, \ddot{x}) = \frac{1}{4\pi S_0}(\ddot{x} + 2\zeta\omega_n\dot{x} + {\omega_n}^2(x + \lambda x^3))^2. \quad (5.22)$$

Substituting Eq. 5.22 into Eq. 5.4 and considering Eq. 5.5 leads to the E-L equation,

$$\frac{d^4x_c}{dt^4} + (2{\omega_n}^2 - 4\zeta^2{\omega_n}^2 + \lambda 6{\omega_n}^2{x_c}^2)\frac{d^2x_c}{dt^2} + \left({\omega_n}^4 + \lambda 6{\omega_n}^2{\dot{x}_c}^2\right)x_c + \lambda 4{\omega_n}^4{x_c}^3 + \lambda^2 3{\omega_n}^4{x_c}^5 = 0 \quad (5.23)$$

along with the boundary conditions

$x_c(0) = 0, \dot{x}_c(0) = 0, x_c(t_f) = x_f$ and $\dot{x}_c(t_f) = \dot{x}_f$. The most probable path, x_c, can be determined by solving the BVP of Eq. 5.23 numerically (e.g. De Coster and Habets, 2006). The Matlab algorithm “bvp4c” was employed below to solve the BVPs. It is a finite difference code that implements the three-stage Lobatto IIIa formula (Shampine et al., 2003).

5.3.2.1 Stationary Response of Duffing Oscillator

The stationary response is computed considering the following system parameters: $\omega_n = 1, \zeta = 0.1, S_0 = 0.0637$, and $\lambda = 1.5$. Figure 5-4 shows the displacement response PDFs derived using the WPI approach (i.e. $n = 40$) and the exact solution (i.e. solving the associated FPK equation).

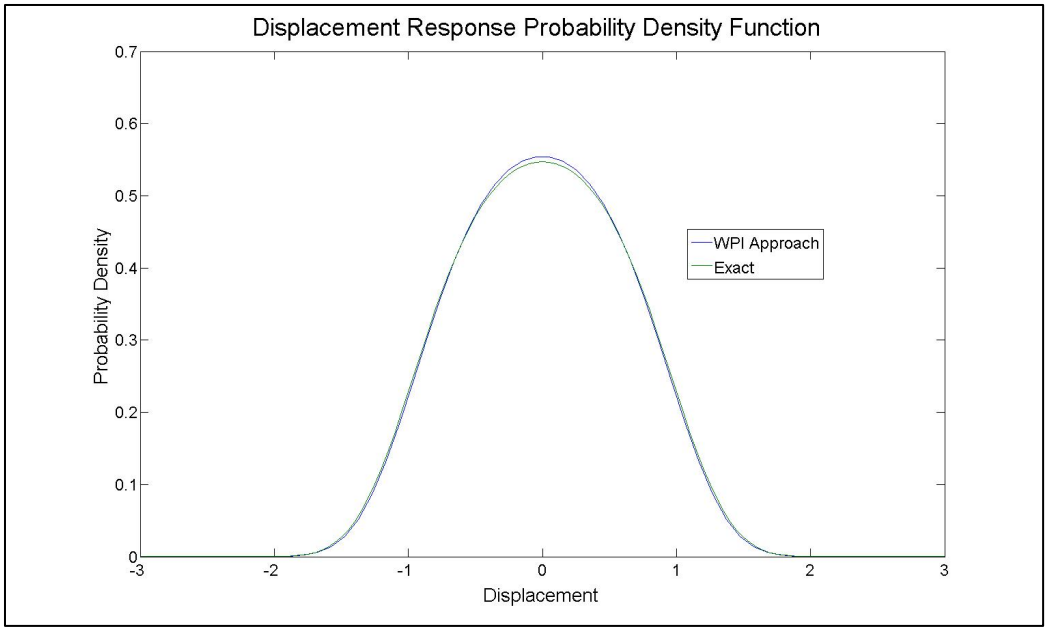

Figure 5-4: Displacement Response PDFs – Duffing Oscillator (WPI vs. Exact)

As seen in Figure 5-4, a high level of accuracy is achieved using the WPI approach.

In order to confirm that the system has reached stationarity, the variances, ${\sigma_i}^2$ and ${\sigma_{i+h}}^2$, are computed for two consecutive time instants, i and $i+h$. Then, the change in variance, ε, is assessed as follows:

$$\frac{\left|{\sigma_{i+h}}^2 - {\sigma_i}^2\right|}{{\sigma_i}^2} = \varepsilon \tag{5.24}$$

If the change in variance, ε, is sufficiently small, then stationarity has been reached.

5.3.2.2 Non Stationary Response of Duffing Oscillator

The non-stationary response (i.e. transient phase) can be derived using the WPI approach. An exact solution for the response of the transient phase is not attainable by solving the FPK equation. Therefore, the results derived using the WPI method are compared to MCS (50,000 realizations). Figure 5-5 shows the displacement response PDFs at different time instances.

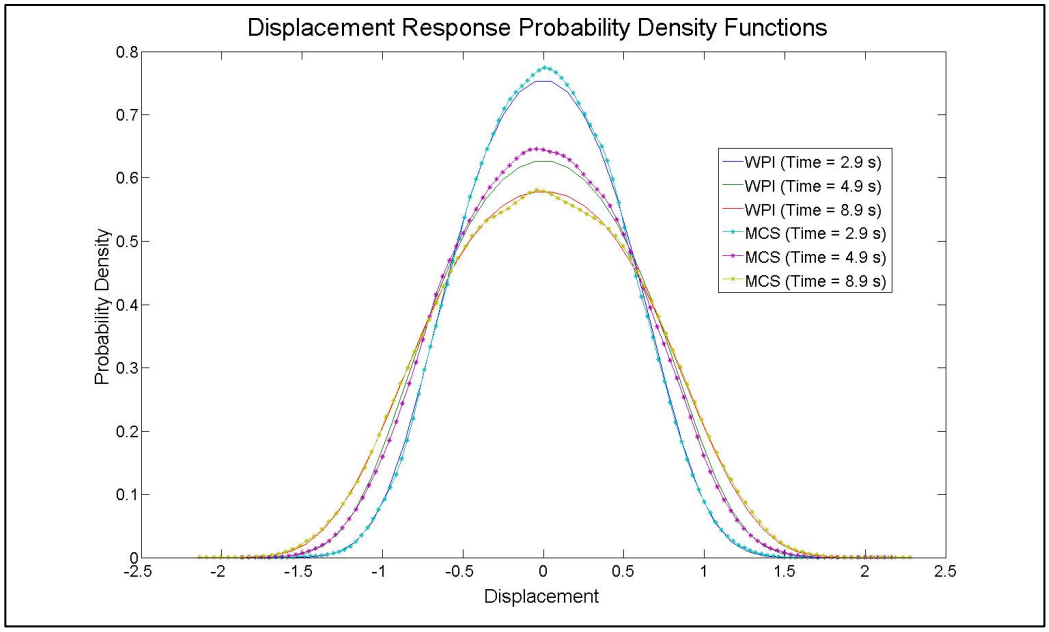

Figure 5-5: Non-Stationary (Transient Phase) Displacement Response PDFs

As seen in Figure 5-5, comparison with MCS data demonstrates a satisfactory level of accuracy.

5.4 DISCUSSION

The WPI approach took approximately 30 minutes to solve for each time instant using $n = 30$ (i.e. $n^2 = 900$ boundary value problems). By contrast, the MCS method took approximate 5.5 hours for 50,000 simulations. It is apparent that the WPI approach yields accurate results, and is more efficient that the MCS method.

Note that although for low-dimensional systems (e.g. the example above) the WPI technique can be significantly more efficient than the MCS method (Kougioumtzoglou and Spanos, 2013), its standard implementation proves computationally cumbersome for relatively high-dimensional MDOF systems. A novel WPI technique formulation/implementation was developed in (Kougioumtzoglou et al., 2015) that has drastically decreased the associated computational cost by several orders of magnitude, as compared to both the

standard WPI technique and the MCS approach. It involves combining the localization capabilities of the WPI solution framework with appropriately chosen expansions for approximating the system response PDF. In fact, the example of a Duffing oscillator was considered in (Kougioumtzoglou et al., 2015) and the same degree of accuracy was achieved as the example above except 15 BVPs were required as opposed to 900.

Further, in recent work by (Psaros et al., 2018), the WPI technique was extended to account for non-white, non-Gaussian and non-stationary processes representing either the excitation of a MDOF dynamical system, or the media properties of a class of one-dimensional continuous systems. The excitation process was modeled as the output of a filter equation with Gaussian white noise as its input. This filter approximation allows for the implementation of the WPI technique in a straightforward manner even for arbitrary excitation power spectrum forms.

Although relatively accurate when compared to other techniques (e.g. statistical linearization), the WPI method is still approximate. The approximation is based on the fact that the most probable path is derived as opposed to the summation of all possible paths. There has been an ongoing effort to account for the fluctuations around the most probable path (see Chaichian and Demichev (2001)), which may increase the degree of accuracy.

6 STOCHASTIC RESPONSE OF NONLINEAR VIBRATORY ENERGY HARVESTERS

6.1 INTRODUCTION

The field of vibratory energy harvesting (VEH) has flourished in recent years as a promising alternative to common energy sources such as batteries. The motivation behind the development of VEHs is that compact and scalable electronic devices, such as wireless sensors, data transmitters and medical implants, are designed to function even with very low power levels. For example, wireless transponders for data transmission can operate efficiently with less than 1 Milliwatt of power (Daqaq et al, 2014). In this regard, VEHs aim at converting any available ambient energy into electricity, and eventually powering and enabling the independent operation of such devices. An additional benefit of using VEHs is that limitations related to batteries, such as the need for re-charging and replacement, are bypassed. This is especially important considering in vivo biomedical implants such as pacemakers, where the replacement of batteries increases the risk of infection. Additionally, structural health monitoring applications have started benefiting from the utilization of wireless sensors powered by VEHs (see Cheng et al., 2013; Tomicek et al., 2013), resulting in reduced installation and maintenance costs as compared with alternative hard wired sensor configurations. Generally, VEHs exploit the ability of active materials (e.g. piezoelectric) and electromechanical coupling mechanisms to generate an electric potential in response to

external/environmental excitations. For a more thorough review of the current applications of VEHs for micro power generation see (Beeby et al, 2006; Beeby et al., 2007; Adhikari et al., 2009; Daqaq et al., 2014;).

A commonly utilized VEH consists of a cantilever beam with piezoelectric patches attached near its fixed end. The beam is subjected to an external excitation at its base causing large strains near the clamped end, thus producing a voltage difference across the patches. Utilizing an appropriate circuit, the electric potential is converted into a current; hence, mechanical energy is transformed into electrical. Figure 6-1 shows a depiction of the cantilever beam model.

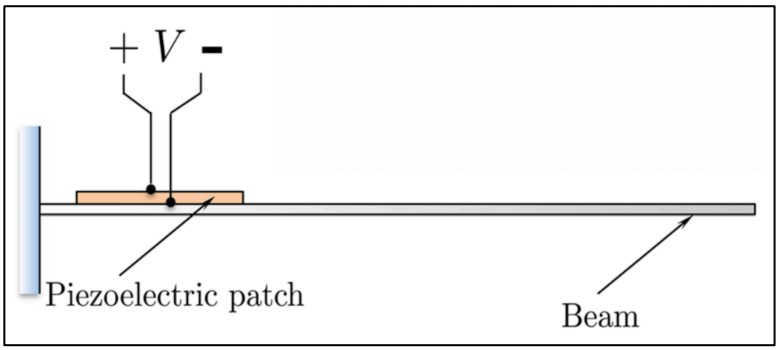

Figure 6-1: Cantilever Beam VEH Model (Daqaq et al., 2014)

Traditionally, VEHs have been modeled in the literature as linear systems excited by harmonic forces. This type of VEH relies on the theory of resonance. The beam's fundamental frequency is tuned to that of a given a priori known deterministic excitation frequency to generate maximum strain, and thus, maximum power output. A drawback of this method is that the steady state frequency bandwidth is relatively narrow. Also, any variations in the beam properties can 'detune' the VEH from the excitation frequency. Consequently, very tight manufacturer tolerances are required which can be costly. Further, a variation of the environmental excitation from its pre-assumed harmonic nature decreases the resonance phenomenon and hinders the energy output. Indeed,

most realistic excitations seen in the environment are not harmonic, or even deterministic. Observations and measurements of physical processes show not only variability, but also stochastic characteristics (Schueller, 2007). Further, common sources for vibrations in microsystems have white noise characteristics due to non-equilibrium thermal fluctuations, shot, and low-frequency noise (Daqaq et al., 2014). Therefore, tuning a linear VEH to an excitation frequency will generally lead to unsatisfactory energy output.

Researchers have intentionally introduced nonlinearities to the design of the VEH in an attempt to increase robustness and the coupling range between the excitation and the VEH. The approach commonly used introduces a nonlinear restoring force using magnetic forces (Daqaq et al., 2014; He and Daqaq, 2015). See Figure 6-2.

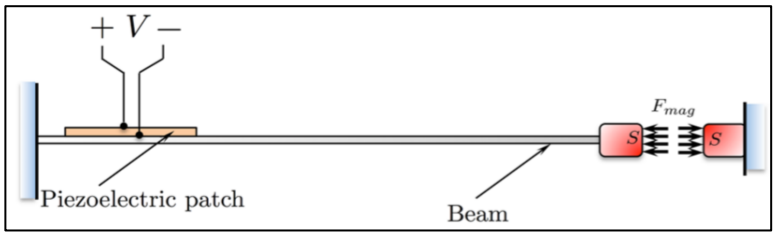

Figure 6-2: Nonlinear Cantilever Beam VEH Model (Daqaq et al., 2014)

The magnitude and nature of the nonlinearity can be updated through the design of the system. For example, changing the distance between the magnets or their strength can alter the relationship between the tip deflection and the restoring force. It should be noted that linear VEHs have been shown to produce higher average power levels than mono-stable Duffing harvesters with symmetric restoring forces, regardless of the magnitude of the nonlinearity or the spectral density of the excitation (Langley, 2014; He and Daqaq, 2016). However, (He and Daqaq, 2016) has shown that VEHs with asymmetric restoring forces may provide performance enhancements over linear devices or nonlinear devices with symmetric potentials.

6.2 VIBRATORY ENERGY HARVESTER SYSTEM MODEL

A SDOF system is adopted to represent the VEH in the current work. Ertuk and Inman (2008a, and 2008b) studied the difference in responses between a continuous Euler-Bernoulli beam model and SDOF model and showed that a SDOF approximation may yield highly inaccurate results for cantilever beams that have a low tip mass to beam mass ratio. Consequently, they introduced a more detailed model by providing correction factors for the SDOF system that account for distributed mass effects (Ertuk and Inman, 2008a). However, they concluded that the uncorrected SDOF model can be used safely when the tip mass is much larger than the beam distributed mass. Studies that use a SDOF model (e.g. Adhikari et al., 2009; Adhikari et al., 2016; Ali et al., 2010; Roundy et al., 2004; duToit and Wardle, 2007) implicitly assume that the tip mass is much larger than the distributed mass, and the same approach is adopted for the current work.

6.2.1 Coupled vs. Uncoupled VEH Models

The coupled differential equations governing the electromechanical system of the cantilever beam with piezoelectric patches (e.g. Figure 6-1) is (duToit and Wardle, 2007; Ali et al., 2010):

$$m\ddot{x} + c\dot{x} + g(x) + \theta y = -m\ddot{x}_b \tag{6.1}$$

and

$$\dot{y} + \frac{1}{C_p R} y = \frac{\theta}{C_p}\dot{x} \tag{6.2}$$

where x represents the displacement of the mass, m; c is the linear viscous damping coefficient; θ is a electromechanical coupling coefficient that measures

the coupling strength between the mechanical and electrical systems; $\ddot{x}_b$ is the base excitation; C_p and R are the capacitance and resistance coefficients, respectively; y is the induced voltage; and $g(x)$ represents the restoring force. Eq. 6.1 is simply the equation of motion governing the mechanical system, and Eq. 6.2 is obtained from the electrical circuit, where the voltage across the load resistance arises from the mechanical strain through the electromechanical coupling term and capacitance of the piezoceramic (Ali et al., 2010).

Several researchers have observed that when the $\frac{1}{C_p R}$ term in Eq. 6.2 is small the influence of the circuit dynamics on the mechanical subsystem becomes negligible (Daqaq et al., 2014; Erturk and Inman, 2008a; Erturk and Inman, 2008b). In fact, Erturk and Inman (2008b) compared the coupled model with the uncoupled model considering a range of load resistance values, R, and found that for a low load resistance both models generated similar power amplitudes.

In order to confirm this result, a parametric study was conducted by solving both the coupled and uncoupled equations for a range of load resistance values considering the system parameters presented in Table 6-1.

Table 6-1: System Parameters

Parameter	Value
$\boldsymbol{m}$	$9.12\times10^{-3}\ kg$
$\boldsymbol{k}$	$4.1\times10^{3}\ N\ m^{-1}$
$\boldsymbol{c}$	$0.218\ N\ s\ m^{-1}$
$\boldsymbol{C_p}$	$4.3\times10^{3}\ F$
$\boldsymbol{\theta}$	$-4.57\times10^{-3}\ N\ V^{-1}$

Values obtained from Table 1 in Ali et al., (2010) and are within the experimental parameters used in duToit and Wardle (2007).

A linear restoring force was modeled for the stiffness, and a direct harmonic excitation was considered with a frequency close to the natural frequency of the mechanical system and an amplitude of 2.5 m/s, which is the same forcing function considered in the experiments duToit and Wardle (2007) conducted. Figure 6-3 shows the power output as a function of resistance for both the coupled and uncoupled models.

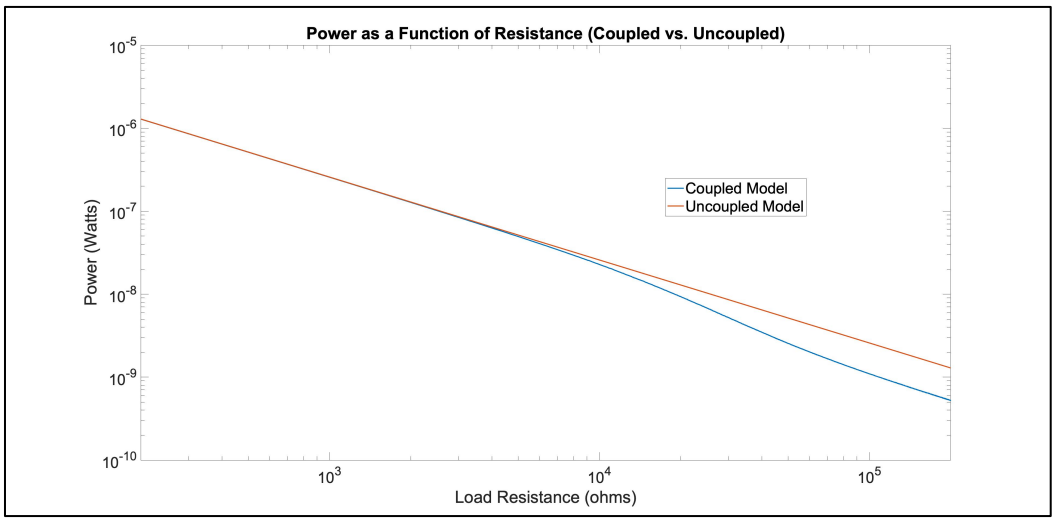

Figure 6-3: Variation of Electrical Power with Load Resistance (Coupled vs. Uncoupled models)

As seen in Figure 6-3, the power output of both models is similar for load resistance values less than 1,000 ohms. This result is consistent with results presented in Figure 7 of (Erturk and Inman, 2008b).

When the dynamics of the oscillator are decoupled from the circuit dynamics there is only a forward coupling effect. In other words, the mechanical oscillator influences the harvested circuit, but not vice versa. In this regard, the equation governing the system is recast as

$$m\ddot{x} + c_e\dot{x} + g(x) = -m\ddot{x}_b \tag{6.3}$$

where c_e is an effective damping term which considers the combined effect of the electrical and mechanical damping. Therefore, the electrical effect due to the presence of a resistive load is represented by an electrically induced viscous

damping coefficient in the mechanical equation of motion. Consequently, the mechanical system equation can be solved independently of the circuit dynamics.

6.2.2 Nonlinearities

As mentioned previously, nonlinearities can be introduced to the system using magnets as shown in Figure 6-2. In modeling the restoring force $g(x)$, a wide range of nonlinear behaviors can be captured by the 3rd order polynomial

$$g(x) = kx + \varepsilon x^2 + \delta x^3 \tag{6.4}$$

where k, ε, and δ control the intensity of the linear, quadratic, and cubic terms, respectively. Further, Eq. 6.4 leads to a bistable or monostable (depending on the magnitude of ε) asymmetric potential when $\delta \geq 0$, and to a monostable symmetric potential when $\varepsilon = 0$ (He and Daqaq, 2016).

The case of a symmetric potential (i.e. $g(x) = kx + \delta x^3$) will be considered first and the case of an asymmetric potential will be explored later in the chapter.

For the symmetric potential, Eq. 6.3 is recast as

$$\ddot{x} + \zeta_{eff}\dot{x} + {\omega_n}^2(x + \lambda x^3) = \ddot{x}_b \tag{6.5}$$

where $\zeta_{eff} = \frac{c_e}{m}$, $\omega_n = \sqrt{\frac{k}{m}}$ and $\lambda = \frac{\delta}{m{\omega_n}^2}$.

6.3 NON-STATIONARY RESPONSE

The solution to the associated FPK equation for the non-stationary response is not attainable. Therefore, approximate stochastic dynamics tools are desirable.

The current study considers a non-stationary excitation modeled as a time-modulated white noise process, and Eq. 6.5 is recast as

$$\ddot{x} + \zeta_{eff}\dot{x} + {\omega_n}^2 x + \lambda x^3 = \ddot{x}_b f(t) \tag{6.6}$$

where $\ddot{x}_b$ is a Gaussian, zero-mean white noise process possessing a power spectral density of S_0, and $f(t)$ is a time modulation function having the following form,

$$f(t) = k(e^{-at} - e^{-bt}) \tag{6.7}$$

in which a, and b are constants, and k is a normalization constant so that $f(t)$ does not exceed a value of 1.

It is worth noting that this type of excitation is typical of wind loading where there is an initial "buildup" phase that subsequently dies down (Chen, et al., 2007; Chen, 2008; Huang et al., 2015). In fact, Chen (2008) analyzed the non-stationary feature of extreme winds by considering a evolutionary random process excitation modeled as a zero mean stationary process modulated with a deterministic function of a similar form as that presented in Eq. 6.28.

6.3.1 Statistical Linearization Technique

Using the procedure described in Section 4.4, the variance of the non-stationary response is determined by solving the following:

$$\frac{d}{dt}\begin{bmatrix}\sigma_x & \sigma_{\dot{x}x}\\ \sigma_{\dot{x}x} & \sigma_{\dot{x}}\end{bmatrix} =$$

$$\begin{bmatrix}0 & 0\\ -{\omega_n}^2(1+3\lambda{\sigma_x}^2) & -\zeta_{eff}\end{bmatrix}\begin{bmatrix}\sigma_x & \sigma_{\dot{x}x}\\ \sigma_{\dot{x}x} & \sigma_{\dot{x}}\end{bmatrix} +$$

$$\begin{bmatrix}\sigma_x & \sigma_{\dot{x}x}\\ \sigma_{\dot{x}x} & \sigma_{\dot{x}}\end{bmatrix}\begin{bmatrix}0 & 0\\ -{\omega_n}^2(1+3\lambda{\sigma_x}^2) & -\zeta_{eff}\end{bmatrix} + 2\pi S_0 {f}^2(t)\begin{bmatrix}0 & 0\\ 0 & 1\end{bmatrix} \tag{6.8}$$

Eq. 6.29 is equivalent to the following set of differential equations,

$$\sigma_x = 2\sigma_{\dot{x}x}$$

$$\sigma_{\dot{x}x} = \sigma_{\dot{x}} - {\omega_n}^2(1 + 3\lambda\sigma_x)\sigma_x - \zeta_{eff}\sigma_{\dot{x}x}$$

$$\sigma_{\dot{x}} = -2\left[{\omega_n}^2\sigma_{\dot{x}x}(1 + 3\lambda\sigma_x) + \zeta_{eff}\sigma_{\dot{x}}\right] + 2\pi S_0 f^2(t) \tag{6.9}$$

The solution to Eq. 6.30 can be obtained by standard numerical methods such as the Runge–Kutta scheme (Shampine, 1994). Note that $f(t) = 1$ for all t in Eq. 6.30 for the transient response of the VEH subjected to a stationary stochastic process.

6.3.2 WPI Technique – Symmetric Potential

Next, Eq. 6.5 is solved using the WPI technique. The probability density functional for the white noise process is given by (e.g. Chaichian and Demichev, 2001):

$$\mathrm{W}[\ddot{x_b}] = \mathrm{Dexp}\left(-\int_{\mathrm{t_i}}^{\mathrm{t_f}} \frac{1}{2}\frac{{\ddot{x_b}}^2}{2\pi \mathrm{S_0}}\mathrm{dt}\right) \tag{6.10}$$

Then, Eq. 6.5 is substituted into Eq. 6.10 and the probability density functional $\mathrm{W}[\ddot{x_b}]$ is interpreted as the probability density functional $\mathrm{W[x(t)]}$ for $\mathrm{x(t)}$, yielding

$$\mathrm{W}[\ddot{x_b}] = \mathrm{Dexp}\left(-\int_{\mathrm{t_i}}^{\mathrm{t_f}} \frac{1}{4\pi \mathrm{S_0}}\left(\ddot{x} + \zeta_{eff}\dot{x} + {\omega_n}^2(x + \lambda x^3)\right)^2 \mathrm{dt}\right) \tag{6.11}$$

Next, the corresponding Lagrangian is given by

$$\mathrm{L}(\mathrm{x}, \dot{\mathrm{x}}, \ddot{\mathrm{x}}) = \frac{1}{4\pi \mathrm{S_0}}\left(\ddot{x} + \zeta_{eff}\dot{x} + {\omega_n}^2(x + \lambda x^3)\right)^2. \tag{6.12}$$

The E-L equation of Eq. 6.12 is in the following form:

$$\frac{\partial \mathrm{L}}{\partial \mathrm{x_c}} - \frac{\partial}{\partial \mathrm{t}}\frac{\partial \mathrm{L}}{\partial \dot{\mathrm{x}}_\mathrm{c}} + \frac{\partial^2}{\partial \mathrm{t}^2}\frac{\partial \mathrm{L}}{\partial \ddot{\mathrm{x}}_\mathrm{c}} = 0, \tag{6.13}$$

with the four boundary conditions

$$\mathrm{x_c}(\mathrm{t_i}) = \mathrm{x_i}, \dot{\mathrm{x}}_\mathrm{c}(\mathrm{t_i}) = \dot{\mathrm{x}}_\mathrm{i}, \mathrm{x_c}(\mathrm{t_f}) = \mathrm{x_f}, \dot{\mathrm{x}}_\mathrm{c}(\mathrm{t_f}) = \dot{\mathrm{x}}_\mathrm{f}, \tag{6.14}$$

Substituting Eq. 6.12 into Eq. 6.13 and considering Eq. 6.14 leads to,

$$\frac{d^4 x_c}{dt^4} + \left(2{\omega_n}^2 - {\zeta_{eff}}^2 + \lambda 6 {\omega_n}^2 {x_c}^2\right)\frac{d^2 x_c}{dt^2} + \left({\omega_n}^4 + \lambda 6 {\omega_n}^2 {\dot{x}_c}^2\right)x_c + \lambda 4 {\omega_n}^4 {x_c}^3 + \lambda^2 3 {\omega_n}^4 {x_c}^5 = 0 \tag{6.15}$$

along with the boundary conditions $\mathrm{x_c}(0) = 0, \dot{\mathrm{x}}_\mathrm{c}(0) = 0, \mathrm{x_c}(\mathrm{t_f}) = \mathrm{x_f}$ and $\dot{\mathrm{x}}_\mathrm{c}(\mathrm{t_f}) = \dot{\mathrm{x}}_\mathrm{f}$. The most probable path, $\mathrm{x_c}$, can be determined by solving the BVP of Eq. 6.15 numerically (e.g. De Coster and Habets, 2006).

To assess the transient response of the system subjected to a stationary excitation, the time, $\mathrm{t_f}$, in the boundary conditions, $\mathrm{x_c}(\mathrm{t_f}) = \mathrm{x_f}, \dot{\mathrm{x}}_\mathrm{c}(\mathrm{t_f}) = \dot{\mathrm{x}}_\mathrm{f}$, are simply updated to a time that is within the transient phase. For the non-stationary excitation, the Lagrangian (Eq. 6.12) is divided by the modulation function, $f(t)$:

$$\mathrm{L}(\mathrm{x}, \dot{\mathrm{x}}, \ddot{\mathrm{x}}) = \frac{1}{4\pi \mathrm{S_0}} \frac{1}{f^2(t)} \left(\ddot{x} + \zeta_{eff}\dot{x} + {\omega_n}^2 (x + \lambda x^3)\right)^2. \tag{6.16}$$

6.4 NUMERICAL EXAMPLE – SYMMETRIC POTENTIAL

The transient phase of the stationary response is computed first to evaluate the accuracy of statistical linearization and WPI techniques. The system parameters in Table 6-2 were used along with a spectral density, $S_0 = 0.1$, and a nonlinear coefficient, $\delta = 1000$.

Table 6-2: System Parameters – Symmetric Restoring Force Case

Parameter	Value
$\boldsymbol{m}$	$1.0\times10^{-3}\ kg$
$\boldsymbol{k}$	$1.0\times10^{3}\ N\ m^{-1}$
$\boldsymbol{c}$	$0.1N\ s\ m^{-1}$
$\boldsymbol{R}$	$1.0\times10^{3}\ \Omega$
$\boldsymbol{\theta}$	$-1.0\times10^{-2}\ N\ V^{-1}$

Figure 6-4 shows the displacement response PDFs at $t = 0.012$ (i.e. an arbitrary time in the transient phase).

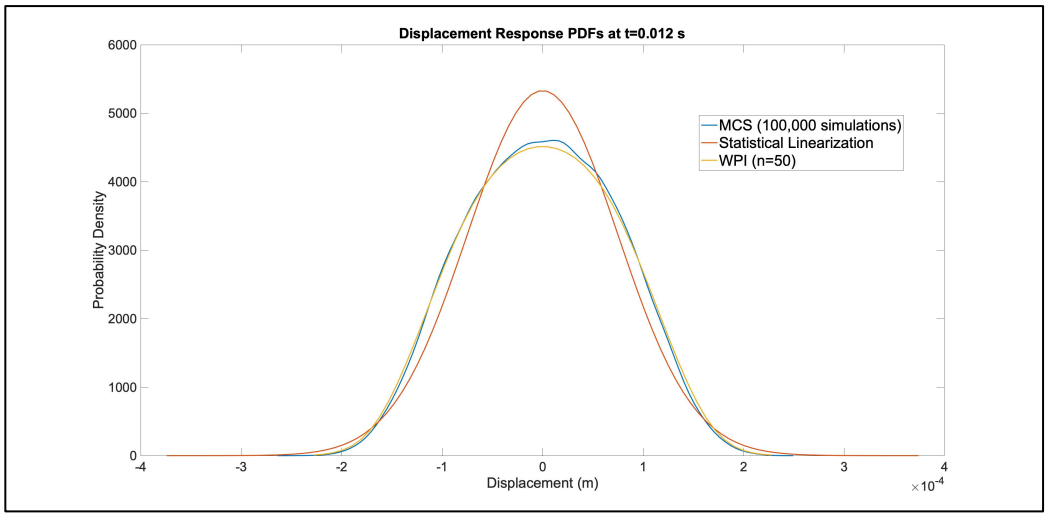

Figure 6-4: Displacement Response PDFs at t=0.012 s

As seen in Figure 6-4, the WPI approach provides a satisfactory level of accuracy when compared to the MCS solution, while the general shape of the response PDF derived using the statistical linearization technique is considerably different.

Next, the VEH system subjected to a time modulated white noise process is solved. The power spectral density function of the excitation is shown in Figure 6-5 for values of $a = 20$ and $b = 40$ in $g(t)$.

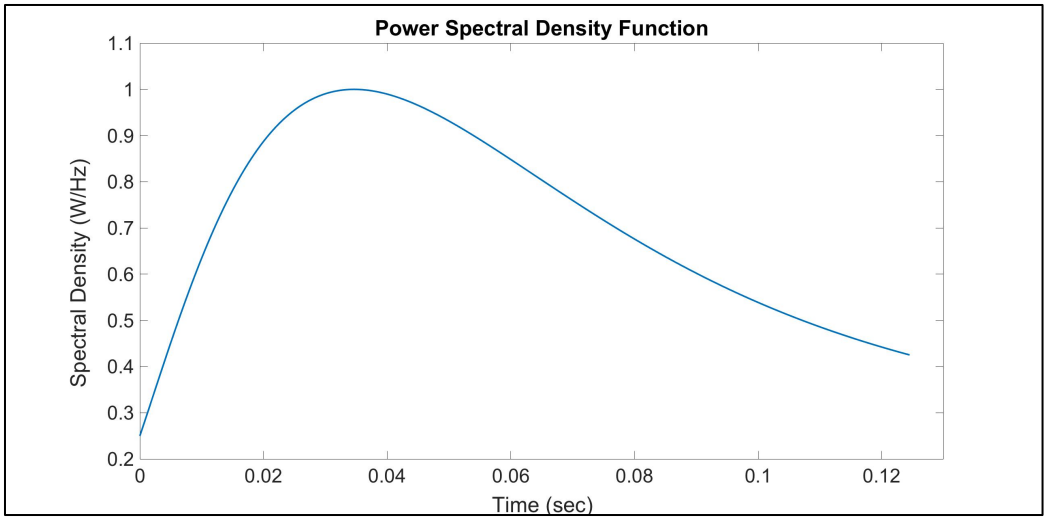

Figure 6-5: PSD Function of Time Modulated White Noise Process

The full displacement response PDFs derived using the statistical linearization and MCS approaches are presented in Figure 6-6 and Figure 6-7, respectively.

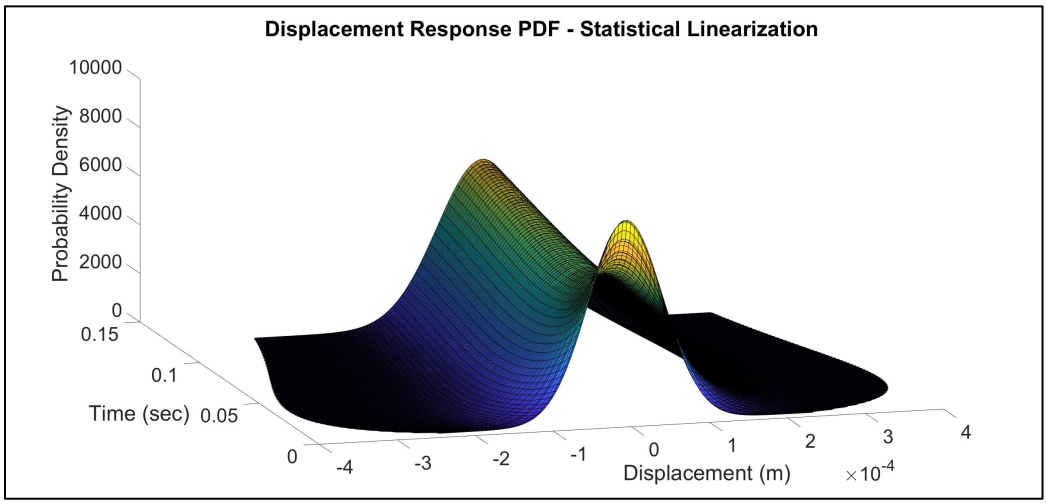

Figure 6-6: Displacement Response PDF (Statistical Linearization)

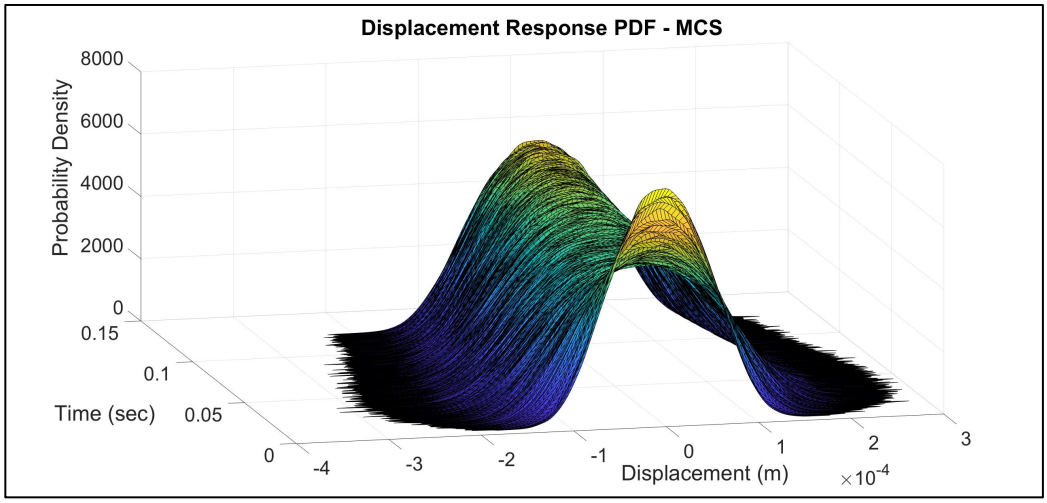

Figure 6-7: Displacement Response PDF (MCS)

The displacement response PDFs at the time of maximum variance are shown in Figure 6-8.

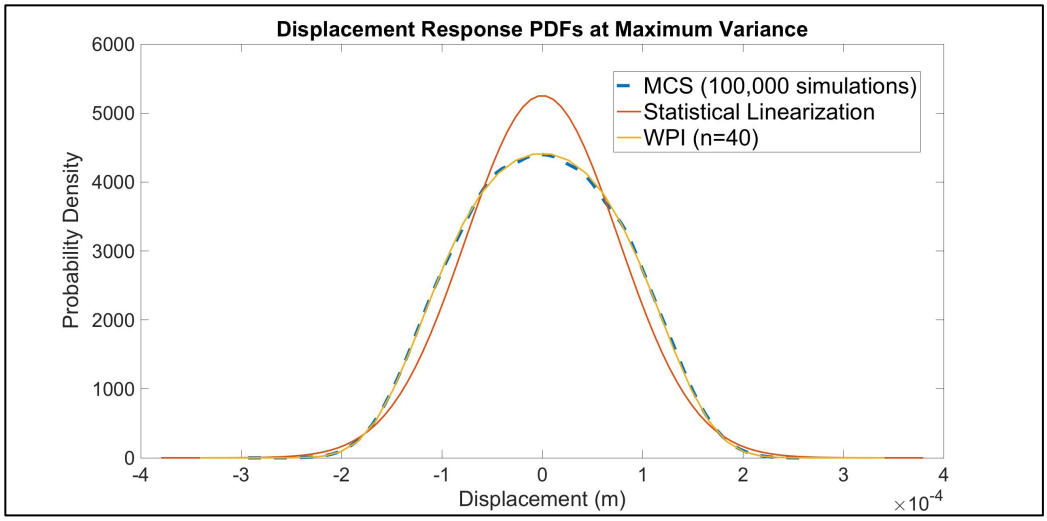

Figure 6-8: Displacement Response PDFs at Maximum Variance

As seen in Figure 6-8, again the WPI approach provides a satisfactory level of accuracy when compared to the MCS solution, while the general shape of the response PDF derived using the statistical linearization technique differs. The difference in shape is prevalent in the tail ends as seen in Figure 6-9 showing a zoomed in portion of the response PDF curves.

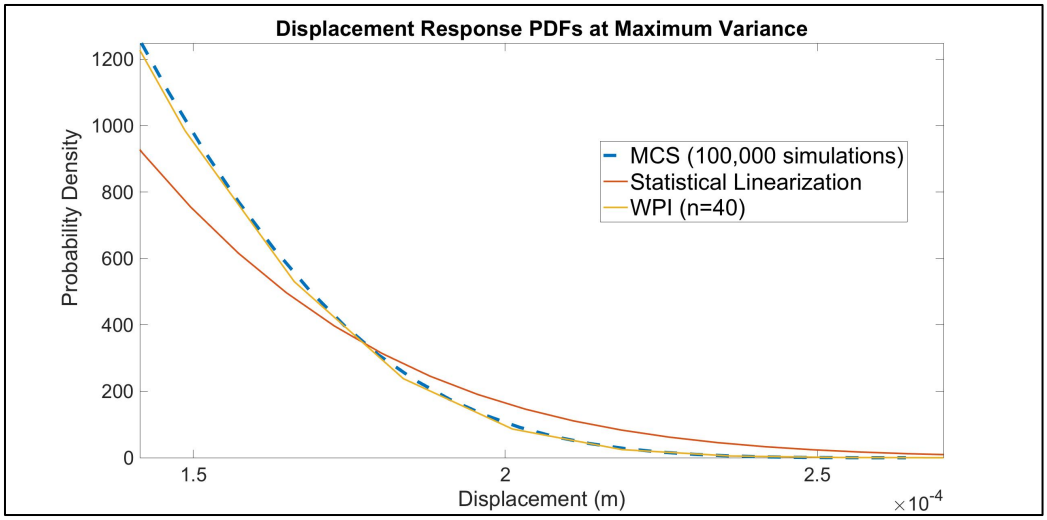

Figure 6-9: Displacement Response PDFs at Maximum Variance (tail ends)

6.4.1 Discussion - Symmetric Potential Case

The electrical load optimization of mono-stable Duffing harvesters excited by white noise was investigated in (Green et al., 2012) who demonstrated that the optimal load is not a function of the nonlinearity. This was confirmed in (He and Daqaq, 2016) who concluded that for cases of low inductance in electromagnetic harvesters (or low capacitance in piezoelectric harvesters) the nonlinear coefficient does not influence the power of the system. Specifically, the expected value of the electric quantity, voltage in the case of piezoelectric harvesters, and current in the case of electromagnetic ones, is independent of the shape of the potential function, which suggests that no matter how the potential function of the harvester is changed, it has no effect on the average output power. In fact, Langley (2014) has shown that the total power that can be harvested by nonlinear electromechanical systems subjected to white noise base accelerations whose internal forces are functions of the instantaneous state vectors depend only on the spectral density of the base acceleration and the total mass of the system, and not on the nonlinearity. However, (He and Daqaq, 2016) have demonstrated that when the inductance (or capacitance) is

not sufficiently small, the optimal power has a clear dependence on the nonlinearity term.

Although the power output is not affected by the nonlinearity for low inductance (or low capacitance) harvesters, the variance of the displacement can be reduced. Based on this, Green et al. (2012) suggested that the nonlinearity could help produce a more compact VEH device. Further, Langley (2014) concluded the same stating that there is not much a designer can do to improve the power performance but can affect the stroke and size of the device if there are practical reasons to do so. This provides the motivation for studying the displacement response. However, as stated in (He and Daqaq, 2015), this conclusion should be approached with caution since a reduction in variance does not necessarily prevent the instantaneous displacement from being large at some instants in time. Indeed, the variance of the displacement does not provide enough information regarding low probability events since the displacement response of the nonlinear system is not Gaussian. However, when the nonlinear coefficient is sufficiently low, a Gaussian assumption can produce fairly accurate results. For low nonlinearity cases the statistical linearization approach is desirable since it is extremely efficient (taking mere seconds to solve) and has been shown to be accurate even when considering the non-stationary response. However, for high nonlinearity cases, the response can deviate considerably from Gaussian, therefore, it is important to estimate the tail ends of the response PDF curve accurately. For high nonlinearity cases, the WPI approach has been shown to be both accurate and efficient when compared to the MCS method.

Further, it is worth noting that a mono-stable Duffing harvester with a symmetric potential always produces a lower average power than its linear counterpart. Thus, introducing hardening nonlinearities will inadvertently reduce the average

output power of the harvester when operated in a white noise environment (Daqaq et al., 2014).

6.5 ASYMMETRIC POTENTIAL

The potential energy function of nonlinear mono-stable harvesters can, in some cases, exhibit asymmetric behavior. For example, structural imperfections, initial curvature, and added masses produce a quadratic nonlinearity in beam-type harvesters. Also, in the process of intentionally introducing nonlinearities to the harvester through external design means, it is difficult to create a perfectly symmetric restoring force (He and Daqaq, 2016).

He and Daqaq (2016) considered VEHs with asymmetric potentials using the statistical linearization technique and found that when compared to symmetric potentials or linear systems, VEHs with asymmetric potentials produce higher optimal average power levels when exposed to white noise excitations. Therefore, given that asymmetries can come about inadvertently and that VEHs with asymmetric restoring force may produce higher optimal average power levels, it is useful to study the response of VEH systems with asymmetric restoring forces.

6.5.1 Asymmetric System Model

Eq. 6.3 is recast as considering an asymmetric potential,

$$\ddot{x} + \zeta_{eff}\dot{x} + {\omega_n}^2(x + \gamma x^2 + \lambda x^3) = \ddot{x}_b f(t) \tag{6.17}$$

where $\gamma = \frac{\varepsilon}{m{\omega_n}^2}$.

For values of $\delta \geq 0$, the restoring force $g(x)$ may lead to a bistable or mono-stable asymmetric potential depending on the magnitude of the quadratic

nonlinearity coefficient. In the current study, an example of a mono-stable asymmetric potential is considered. However, the approximate WPI can be solved considering bi-stable restoring forces as well.

6.5.2 WPI Technique – Asymmetric Potential

The corresponding Lagrangian is given by

$$\mathrm{L}(\mathrm{x},\dot{\mathrm{x}},\ddot{\mathrm{x}}) = \frac{1}{4\pi \mathrm{S}_0}\left(\ddot{x} + \zeta_{eff}\dot{x} + {\omega_n}^2(x + \gamma x^2 + \lambda x^3)\right)^2 \tag{6.18}$$

Substituting Eq. 6.18 into Eq. 6.13 and considering Eq. 6.14 leads to,

$$\frac{d^4 x_c}{dt^4} + (2\gamma^2 + 4\lambda {\omega_n}^2){x_c}^3 + 5\gamma\lambda {x_c}^4 + 3\lambda^2 {x_c}^5 + 2\gamma {\dot{x}_c}^2 + 2{\omega_n}^2\ddot{x}_c - {\zeta_{eff}}^2\ddot{x}_c +$$

$$x_c\left({\omega_n}^4 + 6\lambda {\dot{x}_c}^2 + 4\gamma\ddot{x}_c\right) + 3{x_c}^2(\gamma {\omega_n}^2 + 2\lambda\ddot{x}_c) = 0 \tag{6.19}$$

along with the boundary conditions $\mathrm{x_c}(0) = 0, \dot{\mathrm{x}}_\mathrm{c}(0) = 0, \mathrm{x_c}(\mathrm{t_f}) = \mathrm{x_f}$ and $\dot{\mathrm{x}}_\mathrm{c}(\mathrm{t_f}) = \dot{\mathrm{x}}_\mathrm{f}$. Again, the most probable path, $\mathrm{x_c}$, can be determined by solving the BVP of Eq. 6.15 numerically (e.g. De Coster and Habets, 2006).

6.5.3 Numerical Example – Asymmetric Potential

The system parameters in Table 6-1 were used along with a spectral density, $S_0 = 0.1$, and quadratic and cubic nonlinear coefficients, $\varepsilon = 700$ and $\delta = 1$, respectively. Note, C_p in Table 6-1 is considered to be negligible for the uncoupled model (Daqaq et al., 2014).

The power spectral density function of the excitation is shown in Figure 6-10 for values of $a = 8$ and $b = 16$ in $g(t)$.

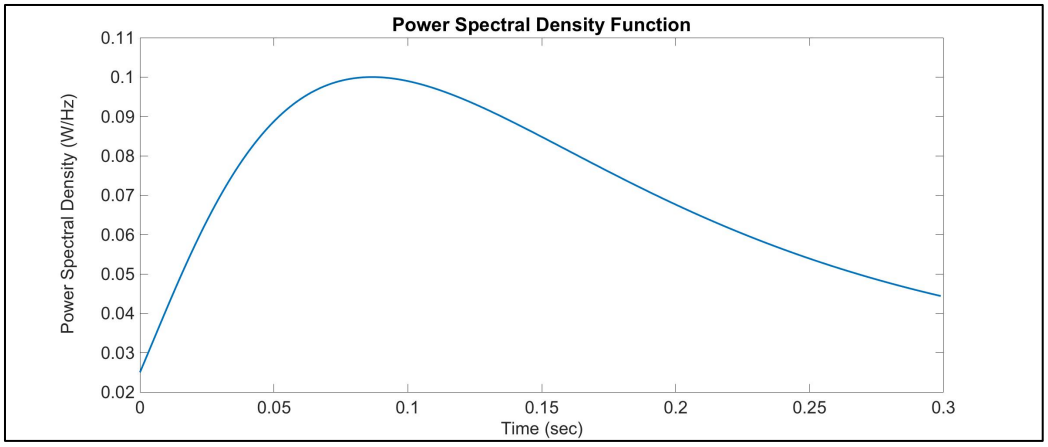

Figure 6-10: PSD Function of Time Modulated White Noise Process – Asymmetric Restoring Force Example

The full displacement response PDF derived using the MCS method is shown in Figure 6-11.

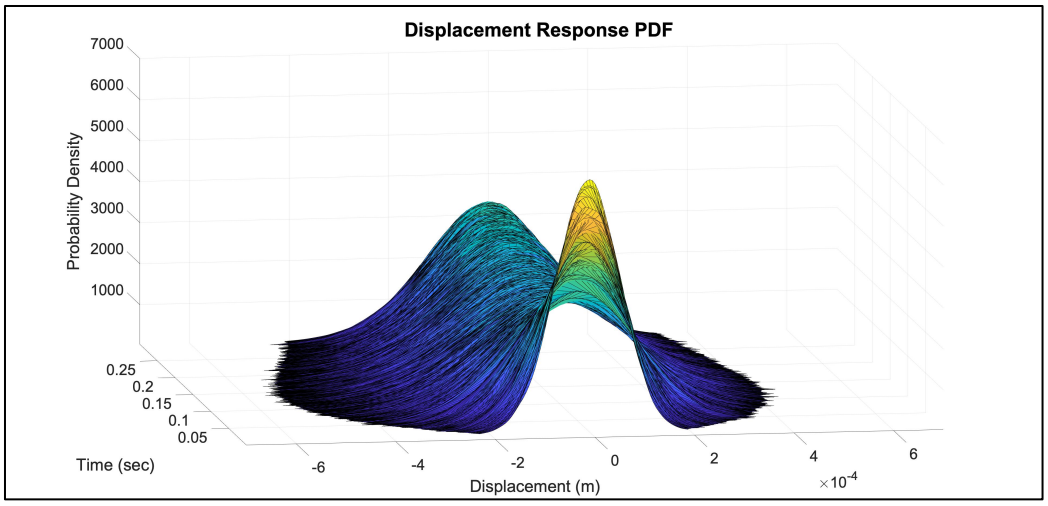

Figure 6-11: Full Displacement Response PDF - Asymmetric Restoring Force Case

The displacement response PDFs at the time of maximum variance derived using the WPI technique and the MCS method are shown in Figure 6-12. Additionally, the mean and variance estimated from the MCS were used to derive a Gaussian PDF for comparison.

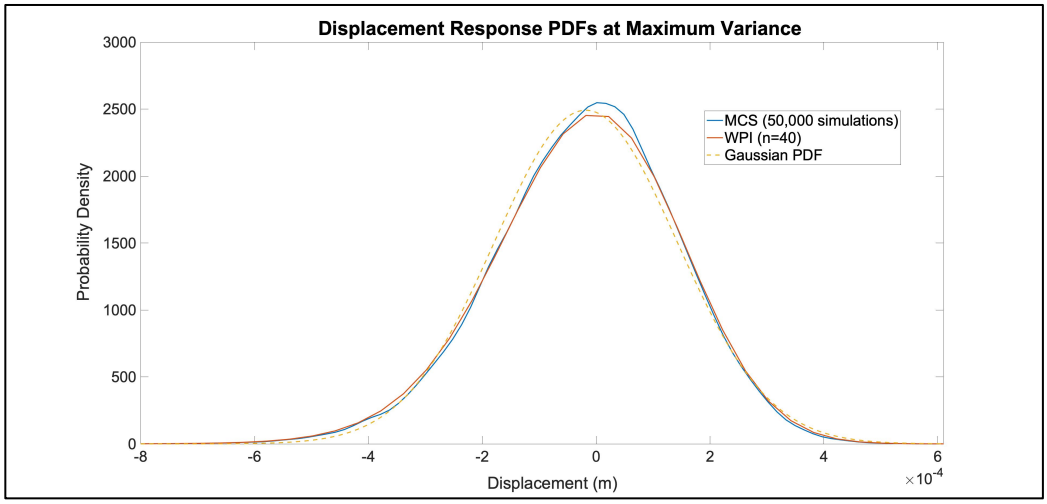

Figure 6-12: Displacement Response PDFs at Maximum Variance - Asymmetric Restoring Force Case

As seen in Figure 6-12, again the WPI approach provides a satisfactory level of accuracy when compared to the MCS solution, while the Gaussian response deviates from the nonlinear model. The difference in shape is prevalent in the tail ends as seen in Figure 6-13 showing a zoomed in portion of the response PDF curves.

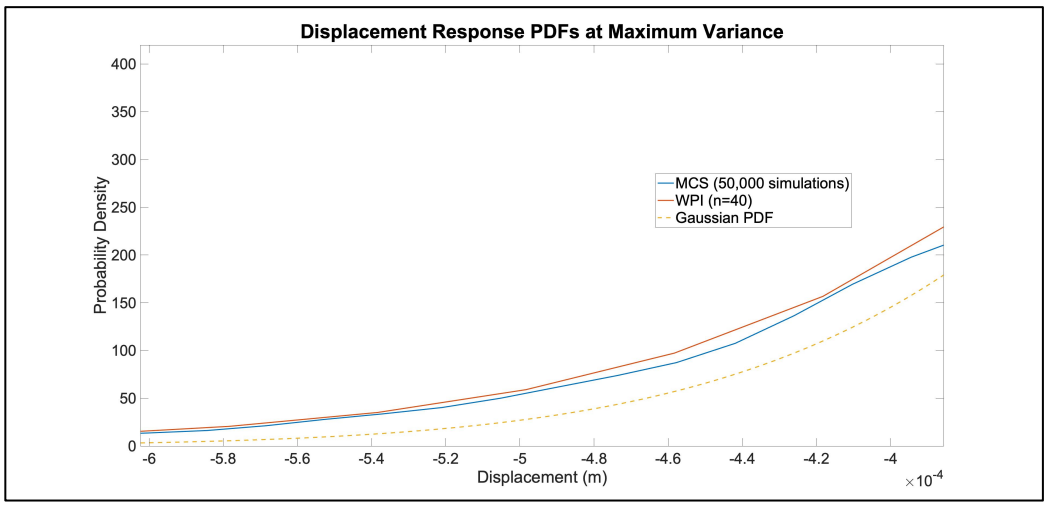

Figure 6-13: Tail Ends of Displacement Response PDFs - Asymmetric Restoring Force Case

6.6 SUMMARY

The stochastic responses of nonlinear VEHs were explored in this section. A cantilever piezoelectric VEH system was adopted (see Figure 6-2) and was

modeled as a SDOF system. The tip mass to distributed mass ratio is assumed to be sufficiently high enough for a SDOF system to accurately capture the response (Erturk and Inman, 2008b). Further, an uncoupled model is used since the electrical resistance is low (Erturk and Inman, 2008b). When the dynamics of the oscillator are decoupled from the circuit dynamics there is only a forward coupling effect. In other words, the mechanical oscillator influences the harvested circuit, but not vice versa.

An exact solution to Eq. 6.5 does not exist when assessing the non-stationary response; therefore, approximate solutions are required. First, a symmetrical nonlinear restoring force was considered and the response was derived using the statistical linearization, WPI and MCS techniques. The response derived using the statistical linearization technique deviated considerably from the MCS data when focusing on the tail ends of the curve, while a satisfactory level of accuracy was achieved using the WPI approach. It should be noted that the statistical linearization approach was the most efficient and only required mere seconds to derive the complete response PDF, while the WPI approach required approximately 45 minutes to solve $n^2 = 1600$ boundary value problems (for a single time instant), and the MCS approach took approximately 15 hours to solve 100,000 simulations.

It has been stated by several authors that the power output is not affected by the nonlinearity for low inductance (or low capacitance) harvesters that poses symmetric restoring forces (Green et al., 2012; Langley, 2014; Daqaq et al., 2014). However, the displacement variance can be reduced which can help produce a more compact VEH device (Green et al., 2012; Langley, 2014). Therefore, computing an accurate estimate of the displacement response is essential to designers as there may be geometrical constraints that need to be satisfied. However, the displacement response variance does not provide

enough information regarding low probability events since the displacement response of the nonlinear system is not Gaussian (see Figure 6-8). So, accurately estimating the shape of the tail ends of the response PDF curve is essential, and it appears that the WPI approach provides a satisfactory level of accuracy when compared to the MCS solution, while the general shape of the response PDF derived using the statistical linearization technique differs. It is worth noting, however, that when the nonlinear coefficient is sufficiently low, a Gaussian assumption can produce fairly accurate results.

He and Daqaq, (2016) have stated that VEHs with asymmetric potentials may produce higher optimal average power levels when compared to symmetric potentials or linear systems. Further, in the process of intentionally introducing nonlinearities to the harvester through external design means, it is difficult to create a perfectly symmetric restoring force, which can lead to asymmetry. Therefore, it is useful to study the response of VEH systems with asymmetric restoring forces.

The VEH system with asymmetric restoring force considered in the current study appeared to show a greater deviation from Gaussianity when compared to the response of the VEH with symmetric restoring forces. Therefore, caution should be exercised if low probability statistics are sought and linearization methods are used. Of course, a Gaussian assumption can be fairly accurate for cases with low nonlinear coefficient values. Finally, the WPI technique provides a satisfactory level of accuracy when compared to the MCS solution for both low and high nonlinear coefficient values.

7 ICE GOUGE DEPTH DETERMINATION

7.1 INTRODUCTION

Oil and gas (O&G) operators have been focusing their efforts on exploration and development of arctic regions the last several years as traditional fields are rapidly depleting (United States Geological Survey (USGS), 2008). It has been estimated that 22% of the world's undiscovered reserves are located in the arctic circle, 84% of which are located offshore (OG21 Strategy Report, 2006). One main concern with offshore oil and gas development in the arctic is seabed scouring due to iceberg impact with the soil (ice gouging). Offshore pipelines in the arctic are buried below the mud line so as to be protected from iceberg impact. An illustration of ice gouging is shown in Figure 7-1.

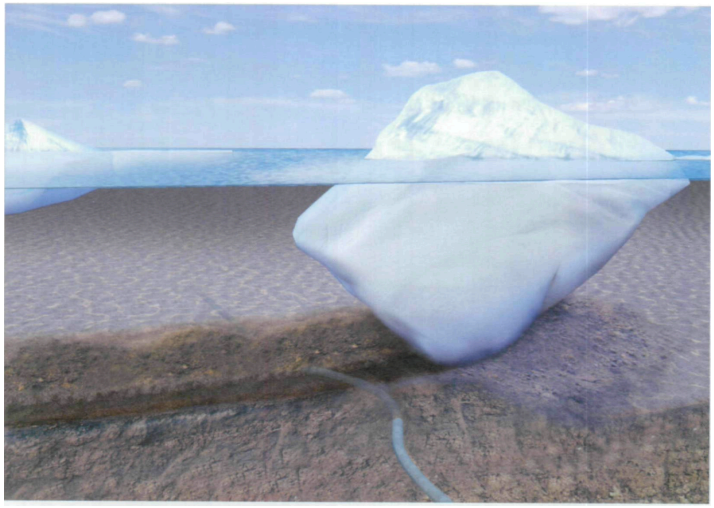

Figure 7-1: Illustration of Ice Gouging Event

The burial process involves trenching the seabed before laying the pipeline. However, trenching costs increase significantly with burial depth, potentially even exceeding the cost of the pipeline fabrication itself (Barrette, 2011).

Therefore, a sustained challenge in the O&G industry is the accurate prediction of the depth of the ice gouge, and consequent pipeline embedment design depth.

Seabed surveys can be used to directly measure the gouge depth (an example seabed survey is shown in Figure 7-2).

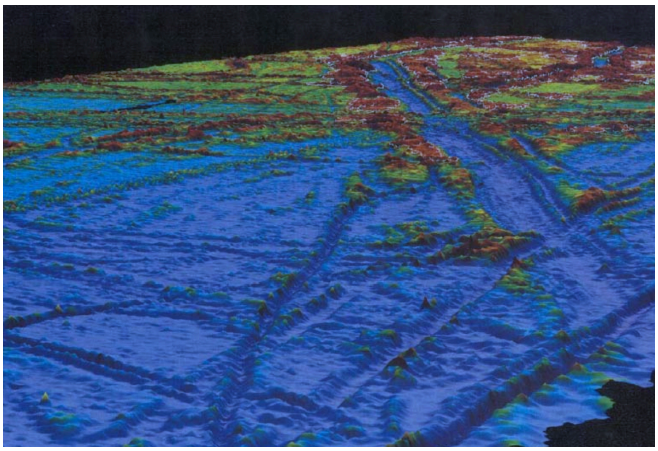

Figure 7-2: Seabed Survey

However, measurements of existing berg induced seabed scours may not accurately predict the potential future gouge event as infilling of the scour trenches occurs. Further, it is difficult to determine if the observed scours are recent or relics. Another approach is to conduct multiple seabed surveys over several years to determine scouring rates relative to time and space. However, this requires a tremendous amount of resources and is not feasible due to the high associated costs. Therefore, it is important to understand the mechanics of the grounding berg to predict realistic gouge depths using theoretical models.

Sophisticated finite element method (FEM) based models have been developed to predict the ice gouge behavior and the effects of ice gouging on buried pipelines (see Abdalla et al., 2008; Abdalla et al., 2009; Banneyake et al., 2011; Jukes et al., 2008; Konuk and Gracie, 2004; Konuk and Gracie; 2005; Phillips and Barrett, 2010). In (Liferov et al., 2007) a FEM based model was employed

in a parametric study to investigate the effect of different physical factors on gouge depth. A semi-empirical relationship, which can be construed as a “meta-model”, was derived to estimate gouge depth and utilized in a probabilistic analysis within a Monte Carlo simulation (MCS) context. FEM based approaches require significantly more computational effort when compared to more analytical approaches. Additionally, it can be argued that the overall accuracy of such detailed FEM approaches is not necessarily higher than that of more approximate analytical approaches. This is due to the high level of uncertainty involved in the selection of parameter values related to the system (e.g. iceberg shape/weight etc.) and to the excitation/environment (e.g. sea current characteristics). Clearly, because of this apparent inconsistency between a very detailed FEM modeling and a high degree of uncertainty regarding the involved parameter values, the desired outcome of overall enhanced accuracy is at least a debatable one. Furthermore, even if the effects of uncertainties were considered in these elaborate FEM models in a comprehensive manner via an appropriate stochastic modeling, determining the system stochastic response using brute force MCS based approaches would be, potentially, computationally prohibitive (Rubinstein, 2007; Au and Wang, 2014). A comprehensive discussion of some of the challenges in FEM based approaches is presented in (Palmer and Niedoroda, 2005).

In this regard, several researchers have proposed approximate analytical treatments of the ice-gouging problem. In (Chari, 1975) a model was developed that equates the kinetic energy of the moving berg to the work done in plowing into the soil. The energy is computed considering the mass of the berg and the environmental factors (sea current and current drag) while the soil resistance is determined based on a passive pressure mechanism at the face of the grounding berg; see also (Chari, 1979; Chari et al., 1980). Further, Been et al.

(1990) and Croasdale et al. (2005) considered the soil deformation ahead of the berg keel, assuming two-dimensional plane strain and relying on plasticity theory. In (Kioka and Saeki, 1995) a model of the grounding berg in sandy soils was developed based on experimental work that incorporates passive soil resistance on the front and sides of the berg and sliding resistance on the bottom. Lopez et al. (1981) used a differential equation that balances the forces of inertia, current drag and soil resistance to compute the gouge length. A comprehensive presentation of the various theoretical ice gouge models can be found in (Barrette, 2011; Walter et al., 1998).

The current work extends and generalizes the model proposed in (Lopez et al., 1981) circumventing some of its limitations. Specifically, first, the model proposed in (Lopez et al., 1981) exhibits an oscillatory response behavior, which, clearly, is not physically realistic for the ice-gouging problem. Therefore, an energy dissipation term is added to the model that prevents oscillatory behavior. The result can be construed as an “over-critically damped” nonlinear dynamical system (e.g. Chopra, 1995).

Second, most of the theoretical models in the literature (including the model in Lopez et al., 1981) are deterministic, and thus, it can be argued that they cannot capture many aspects of the ice gouge mechanism as the uncertainties inherent in the environment are not considered. Therefore, a natural extension/generalization to the proposed gouge model is to consider the variations in the environmental parameters that affect the response. In this regard, a stochastic treatment of the proposed dynamical system is considered by taking into account uncertainties related to the soil strength and the drag coefficient (independently); this yields second-order nonlinear stochastic differential equations (SDE) governing the evolution in time of the gouge length. Next, the recently developed Wiener path integral (WPI) technique for treating

certain random vibration problems (e.g. Kougioumtzoglou and Spanos, 2012; Kougioumtzoglou and Spanos, 2014) is applied to efficiently solve the SDEs governing the ice gouging motion; thus, computationally demanding MCS are circumvented. Specifically, a variational formulation is utilized to derive an Euler-Lagrange (E-L) equation governing the “most probable path”. The resulting boundary value problem (BVP) is then solved numerically and the response probability density function (PDF) for the gouge depth at a given point is obtained. Further, the accuracy of the WPI based solution approach is demonstrated by comparing the results to pertinent MCS data.

The model utilized in the proposed approach is a simplification of the gouging phenomenon, however, it requires significantly less computational time when compared to previously developed FEM based approaches. Further, as discussed in (Barrette, 2011), FEM based models require rigorous validation against quality data from physical simulations. Furthermore, conducting a probabilistic analysis utilizing a FEM based model in a MCS can be computationally prohibitive. The WPI technique adopted in the proposed approach is orders of magnitude less computationally demanding when compared to brute force MCS based approaches. The combination of a simplified model and the efficient WPI based solution establishes the proposed approach as a viable alternative to previous approaches, at least at a preliminary design level.

7.2 ICE GOUGE MODEL

The formulation in (Lopez et al., 1981) is delineated in the following subsection followed by the proposed enhancement to the model. A numerical example is presented comparing the two models and the results are discussed. Next,

modeling the soil strength and the drag coefficient (independently) as stochastic processes further extends the enhanced formulation governing the ice gouging. This leads to nonlinear second order stochastic differential equations governing the berg dynamics.

7.2.1 Equation of Motion Governing Ice Gouging

The berg is assumed to be freely drifting initially with a velocity equal to that of the propelling currents averaged over the immersed depth of the berg. As shallower water depths are reached the berg will tend to ground in the course of its travel. An illustration of the grounding berg is shown in Figure 7-3.

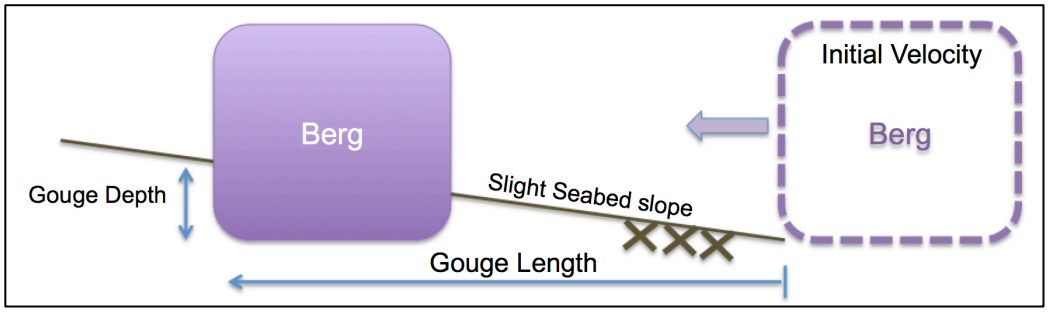

Figure 7-3: Schematic Representation of Ice Gouge Model

The forces acting on the berg during the gouging process are the hydrodynamic force from the current, the soil resistance and the inertial force of the berg. Balancing the forces yields the following expression (Lopez et al., 1981),

$$m\ddot{x} + P_s = f(t) \tag{7.1}$$

where m is the mass of the berg, P_s is the of soil resistance force, $f(t)$ is the hydrodynamic force and x is the gouge length. The most widely used expression for a hydrodynamic force is based upon Morison's equation (Morison et al., 1950),

$$f(t) = \rho V_b \dot{v} + (C_m - 1)\rho V_b(\dot{v} - \ddot{x}) + \frac{1}{2} C_d \rho A_b |v - \dot{x}|(v - \dot{x}) \tag{7.2}$$

where ρ is the density of seawater, V_b is the volume of the berg, A_b is the cross-sectional area of the berg normal to the drag force, C_m and C_d are the mass and drag coefficients, respectively, and v is the velocity of the current. Since the current velocity is assumed to be constant, Eq. 7.2 reduces to

$$f(t) = (C_m - 1)\rho V_b \ddot{x} + \frac{1}{2} C_d \rho A_b |v - \dot{x}|(v - \dot{x}). \quad (7.3)$$

The soil resistance force, P_s, is approximated as

$$\mathrm{P}_s = \mathrm{K_s d}^2 \quad (7.4)$$

where $\mathrm{K_s}$ is the coefficient of soil resistance and d is the gouge depth (see also Lopez et al., 1981). Note that Eq. 7.4 depicts the force required to push a smooth vertical wall into cohesionless soil and is based on Coulomb's passive earth pressure theory (Terzaghi et al., 1996). It has been shown in plowing force estimation studies (e.g. Coyne and Lewis, 1999) that Eq. 7.4 underestimates the plowing force as it ignores the shearing of the sidewalls and bottom surface as well as the effects of pore water flow. Therefore, Eq. 7.4 can be viewed as a conservative estimate of the soil resistance force and an appropriate first approximation for the given application.

In (Lopez et al., 1981) and in the ensuing analysis, a slight seabed indentation is assumed and the depth d is related to the length x of the gouge as $d = x tan\beta$ yielding the following equation for the soil resistance $\mathrm{P_s}$, i.e.,

$$\mathrm{P_s} = \mathrm{K_s x^2 tan^2 \beta} \quad (7.5)$$

where β is the seabed slope (assumed to be approximately constant over the space domain of the gouging event). Note also that seabed indentation observations indicate most gouge features are uniform in cross section over

long distances on often almost horizontal seabed configurations (Palmer et al., 1989).

Substituting Eq. 7.3 and Eq. 7.5 into Eq. 7.1 yields,

$$m\ddot{x} + \mathrm{K_s x^2 tan^2 \beta} = (C_m - 1)\rho V_b \ddot{x} + \frac{1}{2} C_d \rho A_b |v - \dot{x}|(v - \dot{x}) \tag{7.6}$$

Further, defining the ratios $A = \frac{\frac{1}{2} C_d \rho A_b}{m_e}$ and $B = \frac{K_s tan^2 \beta}{m_e}$, where

$$m_e = m + (C_m - 1)\rho V_b \tag{7.7}$$

Eq. 7.6 is rewritten as

$$\ddot{\mathrm{x}} + \mathrm{B x^2} = A[v - \dot{x}]^2. \tag{7.8}$$

Note that Eq. 7.8 is actually the equation proposed in (Lopez et al., 1981).

7.2.2 Modified Ice Gouge Model

Clearly, relying on the physics of the problem, it is anticipated that at time $\mathrm{t} = 0$ when the berg touches the seabed the conditions $\dot{x}(t = 0) = v$ and $x(t = 0) = 0$ are satisfied. Next, as the gouging process progresses, the velocity $\dot{\mathrm{x}}$ of the berg gradually decreases (monotonically) until it becomes zero. Obviously, (and since a constant velocity v of the current is assumed) a reversal of the sign of the berg velocity $\dot{\mathrm{x}}$ is not anticipated at any point during the gouging process.

Nevertheless, note that the form of Eq. 7.8 which can be construed as a nonlinear single degree of freedom oscillator excited by the forcing term $A[v - \dot{x}]^2$ suggests a solution of an oscillatory nature. Indeed, for the parameters values shown in Table 7-1 (the values are within typical ranges as presented in the Discussion section of reference Lopez et al., 1981), the model in (Lopez et al., 1981) yields a solution that is plotted in Figure 7-4. It can be

readily seen that according to Eq. 7.8 the berg oscillates. Clearly, this is not a physically realistic outcome; and thus, the dynamics modeling described by Eq. 7.8 needs to be modified. In this regard, a large enough energy dissipation term (i.e. damping term) is added to Eq. 7.8 to prevent any reversal in velocity; this yields

$$\ddot{x} + C\dot{x} + Bx^2 = A[v - \dot{x}]^2 \tag{7.9}$$

where C is the energy dissipation constant. Further, it can be argued that the motion of the berg resembles the non-oscillatory motion of an over-critically damped single degree of freedom oscillator (e.g. Chopra, 1995). In the following, a simple parametric study is performed to determine the lowest damping coefficient value C which prevents oscillatory motion; thus, being consistent with the physics of the problem. In this regard, in Figure 7-4 the solution of Eq. 7.9 is plotted for several values of the damping coefficient C and compared with the solution of Eq. 7.8 (model by Lopez et al., 1981).

Three energy dissipation constants are considered in the current example for solving Eq. 7.9. Note that although only three values are considered in the present example, the parametric study requires that an initial value is chosen arbitrarily and then ramped up in order to gauge the amount of damping required to prevent oscillatory behavior.

The equations are solved utilizing a standard fourth order Runge-Kutta scheme (Shampine, 1994) and the resulting gouge lengths as a function of time are shown in Figure 7-4.

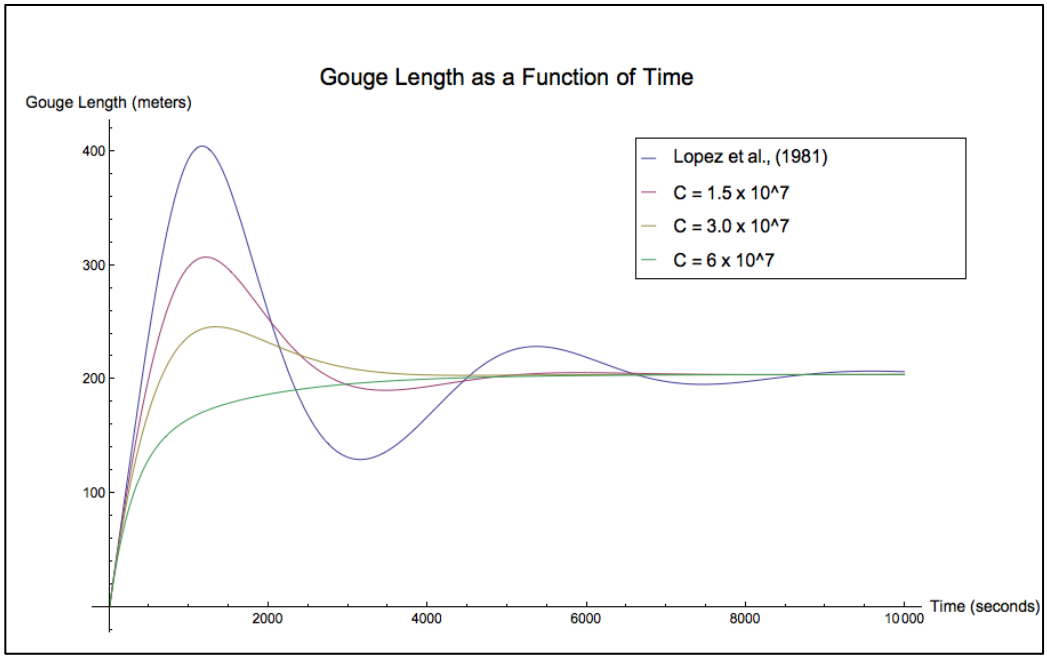

Figure 7-4: Model by Lopez et al., 1981 vs. Proposed Model

As can be seen in Figure 7-4, a constant $C = 6 \times 10^7$ is required to prevent oscillatory motion. Note that the solution derived using the model by (Lopez et al., 1981) yields the same final gouge length result. However, as previously mentioned, the response oscillates, and thus, does not portray the physics of the problem realistically. Further, due to the oscillatory nature of the response the computational cost related to the ODE solution is increased since more time is required for the solution to converge to the final gouge length.

The parametric exercise presented above can be performed for other system parameters as well. Additionally, the above exercise provides some insight regarding an approximate range of the response. This information can be used in the proposed approach to solve the SDE more efficiently (details regarding increasing the efficiency of the proposed approach are presented in Section 7.3.3). In the next subsection, the proposed model is extended to consider the uncertainties in soil strength and drag coefficient.

7.2.3 Stochastic Model

Offshore systems often exhibit random characteristics due to inherent uncertainties in offshore loading conditions (i.e. wind, wave, current, earthquake etc.) and soil properties. Even design standards and codes acknowledge the uncertainty in soil strength (see DNV, 2010; and DNV, 2012). Thus, to realistically capture the system behavior the inherent randomness must be appropriately modeled. This requires a suitable uncertainty quantification methodology with concepts and methods of statistics and probability theory (e.g. Ang and Tang, 2007). Stochastic procedures have been shown to provide a sound framework for a rational treatment of uncertainties (see Schuëller, 2007). Indicatively, probabilistic approaches have been developed that account for uncertainties in the design of pipeline systems (e.g. King et al., 2009; Kenny et al., 2007; Sicilia et al., 2014; Gomes and Beck, 2014).

Note, however, that the previous theoretical models developed for estimating gouge depths (i.e. Chari, 1975; Chari, 1979; Chari et al., 1980; Been et al., 1990; Croasdale et al., 2005; Kioka and Saeki, 1995; Lopez et al., 1981; Walter and Phillips, 1998) are purely deterministic; thus, neglecting the variations in soil properties and the drag coefficient, and utilizing deterministic “mean” (or “extreme” in some cases) values. Consequently, gouge depths may be overestimated when using deterministic approaches, which can lead to costly offshore pipeline burial campaigns. Therefore it is beneficial to model the uncertainties in the soil strength and the drag coefficient as more realistic gouge depths can be estimated, which may result in lower offshore installation costs.

In this regard, (Eq. 7.9) is modified by considering the randomness in the soil strength and Eq. 7.9 is re-written as

$$\ddot{x} + C\dot{x} + B[1 + w(t)]x^2 = A[v_0 - \dot{x}]^2 \qquad (7.10)$$

where $\mathrm{w(t)}$ represents a Gaussian, zero-mean white noise process possessing a power spectrum S_0. Note that a magnitude for the white noise intensity S_0 is chosen so as to ensure that the probability of a resulting negative soil resistance is negligible.

For the case of a random drag coefficient Eq. 7.9 is re-written as

$$\ddot{\mathrm{x}} + \frac{\mathrm{C}}{m}\dot{\mathrm{x}} + \mathrm{Bx}^2 = \mathrm{A}[1 + \mathrm{w(t)}][\mathrm{v}_0 - \dot{\mathrm{x}}]^2 \tag{7.11}$$

where, again, $\mathrm{w(t)}$ represents a Gaussian, zero-mean white noise process possessing a power spectrum S_0. The modeling of the uncertainty in soil strength and drag coefficient as Gaussian processes is recommended in (DNV, 2010). Also, it is noted that more sophisticated, than the Gaussian white noise, stochastic modeling of the soil strength can be utilized based on available measured data.

Clearly, Eq. 7.10 and Eq. 7.11 are nonlinear SDEs with no known exact solution. The basic elements of the recently developed Wiener Path Integral (WPI) technique presented in Section 5 will be used to solve the Eq. 7.10 and Eq. 7.11 in an efficient manner; thus, circumventing computationally demanding MCS.

7.3 APPLICATION OF WIENER PATH INTEGRAL APPROACH

In the next subsections the WPI approach presented in Section 5 is applied to the ice gouging problem considering both the random soil strength and random drag coefficient cases.

7.3.1 Random Soil Strength

Solving Eq. 7.10 for $w(t)$ yields,

$$w(t) = \frac{Av_0{}^2 - Bx^2 - \frac{c}{m}\dot{x} - 2Av_0\dot{x} + A\dot{x}^2 - \ddot{x}}{Bx^2}. \tag{7.12}$$

The probability density functional for the white noise process $w(t)$ is given by (e.g. Chaichian and Demichev , 2001)

$$W[w(t)] = D\exp\left(-\int_{t_i}^{t_f} \frac{1}{2}\frac{w(t)^2}{2\pi S_0}\,dt\right) \tag{7.13}$$

Next, Eq. 7.12 is substituted into Eq. 7.13 and the probability density functional $W[w(t)]$ is interpreted as the probability density functional $W[x(t)]$ for $x(t)$, yielding

$$W[w(t)] = D\exp\left(-\int_{t_i}^{t_f} \frac{1}{4\pi S_0}\left(\frac{Av_0{}^2 - Bx^2 - \frac{c}{m}\dot{x} - 2Av_0\dot{x} + A\dot{x}^2 - \ddot{x}}{Bx^2}\right)^2 dt\right). \tag{7.14}$$

Thus, the corresponding Lagrangian is given by

$$L(x, \dot{x}, \ddot{x}) = \frac{1}{4\pi S_0}\left(\frac{Av_0{}^2 - Bx^2 - \frac{c}{m}\dot{x} - 2Av_0\dot{x} + A\dot{x}^2 - \ddot{x}}{Bx^2}\right)^2. \tag{7.15}$$

The E-L equation of Eq. 7.15 is in the following form:

$$\frac{\partial L}{\partial x_c} - \frac{\partial}{\partial t}\frac{\partial L}{\partial \dot{x}_c} + \frac{\partial^2}{\partial t^2}\frac{\partial L}{\partial \ddot{x}_c} = 0, \tag{7.16}$$

with the four boundary conditions

$$x_c(t_i) = x_i, \dot{x}_c(t_i) = \dot{x}_i, x_c(t_f) = x_f, \dot{x}_c(t_f) = \dot{x}_f, \tag{7.17}$$

Substituting Eq. 7.15 into Eq. 7.16 and considering Eq. 7.17 leads to the E-L equation,

$$\frac{1}{2B^2m^2\pi S_0x_c^6}\Big(-20m\dot{x}_c^2\left(-(c+2Amv_0)\dot{x}_c+Am\dot{x}_c^2+m({v_0}^2-\ddot{x}_c)\right)+2Bm^2x_c^3(Av_0^2-A\dot{x}_c^2-2\ddot{x}_c)+2ABm^2x_c^4\ddot{x}_c-2x_c\Big(4Am(c+2Amv_0)\dot{x}_c^3-3A^2m^2\dot{x}_c^4-{\dot{x}_c}^2(c^2+4cmv_0+6A^2m^2v_0^2+8Am^2\ddot{x}_c)+m^2(A^2v_0^4-4Av_0^2\ddot{x}_c+3\ddot{x}_c^2)+2m\dot{x}_c(3(c+2Amv_0)\ddot{x}_c+2mx_c^{(3)})\Big)+x_c^2(-(c^2+4Acmv_0+6A^2m^2v_0^2)\ddot{x}_c+6Am(c+2Amv_0)\dot{x}_c\ddot{x}_c+6m^2\dot{x}_c^2(B-A^2\ddot{x}_c)+m^2x_c^{(4)})\Big)=0 \quad (7.18)$$

where $x_c^{(3)}$ and $x_c^{(4)}$ denote the third and fourth derivative with time. Further, the boundary conditions are $\mathrm{x_c}(0)=0$ and $\dot{\mathrm{x}}_\mathrm{c}(0)=\mathrm{v_c}$. The most probable path, $\mathrm{x_c}$, is determined by solving the BVP of Eq. 7.18 numerically (e.g. De Coster and Habets, 2006).

7.3.2 Random Drag Coefficient

Solving Eq. 7.10 for $\mathrm{w(t)}$ yields,

$$\mathrm{w(t)}=\frac{\mathrm{Av_0}^2+\mathrm{Bx}^2+\frac{\mathrm{c}}{\mathrm{m}}\dot{\mathrm{x}}+2\mathrm{Av_0}\dot{\mathrm{x}}-\mathrm{A}\dot{\mathrm{x}}^2+\ddot{\mathrm{x}}}{A[\mathrm{v_0}-\dot{\mathrm{x}}]^2}. \quad (7.19)$$

Then, using the same process as before leads to the E-L equation,

$$\frac{1}{2A^2m^2\pi S_0(v_0-\dot{x}_c)^6}\Big(2Bm^2{\dot{x}_c}^4+2B^2m^2{x_c}^3({v_0}^2-6v_0\dot{x}_c+5{\dot{x}_c}^2)-c^2{v_0}^2\ddot{x}_c+4Acm{v_0}^3\ddot{x}_c-10B^2m^2{x_c}^4\ddot{x}_c-2Bm{x_c}^2(v_0(4c-3Amv_0)+6(c+Amv_0)\dot{x}_c-3Am{\dot{x}_c}^2)\ddot{x}_c+10m^2{\ddot{x}_c}^3+2m{\dot{x}_c}^3(-2Bmv_0+Ac\ddot{x}_c)-2Bmx_c(v_0-\dot{x}_c)\Big((4c+7Amv_0){\dot{x}_c}^2-3Am{\dot{x}_c}^3+mv_0(Av_0^2-2\ddot{x}_c)-m\dot{x}_c(5Av_0^2+2\ddot{x}_c)\Big)+8m^2v_0\ddot{x}_cx_c^{(3)}+m^2{v_0}^2x_c^{(4)}-2\dot{x}_c\Big(\ddot{x}_c\Big(3cv_0(c+Amv_0)+4m^2x_c^{(3)}\Big)+m^2v_0x_c^{(4)}\Big)+{\dot{x}_c}^2\left(-3c^2\ddot{x}_c+m^2\left(2B{v_0}^2+x_c^{(4)}\right)\right)\Big)=0 \quad (7.20)$$

Usually, the number of BVPs to be solved is n^2. Consequently, the determination of the system response PDF can be computationally demanding.

However, for the ice-gouging problem, only n BVPs are required to compute the response PDF of maximum gouge depth due to the fact that the final velocity is known (i.e. $\dot{\mathrm{x}}_{\mathrm{c}}(\mathrm{t}_{\mathrm{f}}) = 0$). Note that based on numerical examples performed in this study, a value of n = 50 has been deemed more than adequate for determining the system response PDF with reasonable accuracy in most cases.

7.3.3 Numerical Example

Numerical examples are presented to demonstrate the efficiency of the developed approach. The system parameters listed in Table 7-1 along with a damping coefficient of $6.0\ x\ 10^7$ (derived previously and shown in Figure 7-4) are used for the current examples.

Table 7-1: Inputs Used in Numerical Example

Parameter	Value
Berg mass, m	$20 \cdot 10^9 \mathrm{kg}$
Drag coefficient, A	$10^{-3}\mathrm{m}^{-1}$
Soil resistance coefficient[1], B	$6 \cdot 10^{-9}\mathrm{m}^{-1}\mathrm{s}^{-2}$
Mean sea current velocity, $\mathbf{v}$	$0.5\frac{\mathrm{m}}{\mathrm{s}}$
Power Spectrum Values, $\mathbf{S_0}$	0.01 and 0.1

[1]The value of B considers a soil with relatively small cohesion, submerged unit weight of 2 kN/m^3, bottom slope of 1/100 and gouge width of 30 meters (e.g. Lopez et al., 1981).

Two power spectrum values were considered (a small value and a larger value) to observe the affect that the intensity of the white noise process has on the response. Further, the power spectrum values are such that the probability of a resulting negative soil resistance and a resulting negative drag coefficient are negligible. Furthermore, the parametric exercise used to compute the energy dissipation term provides some insight into the effective domain of the response PDF (i.e. approximate maximum and minimum gouge length/depth), and

provides an approximate time the response will reach a maximum displacement (or zero velocity). These improve the efficiency of the approach, as a relatively smaller amount of BVPs need to be solved to achieve the desired discretization density of the PDF, and an appropriate time instant can be chosen. In the following subsections, the numerical technique presented in Section 7.3 is employed considering a value of n=50 (i.e. number of BVPs).

7.3.3.1 Random Soil Strength

The resulting length response PDFs are shown in Figure 7-5.

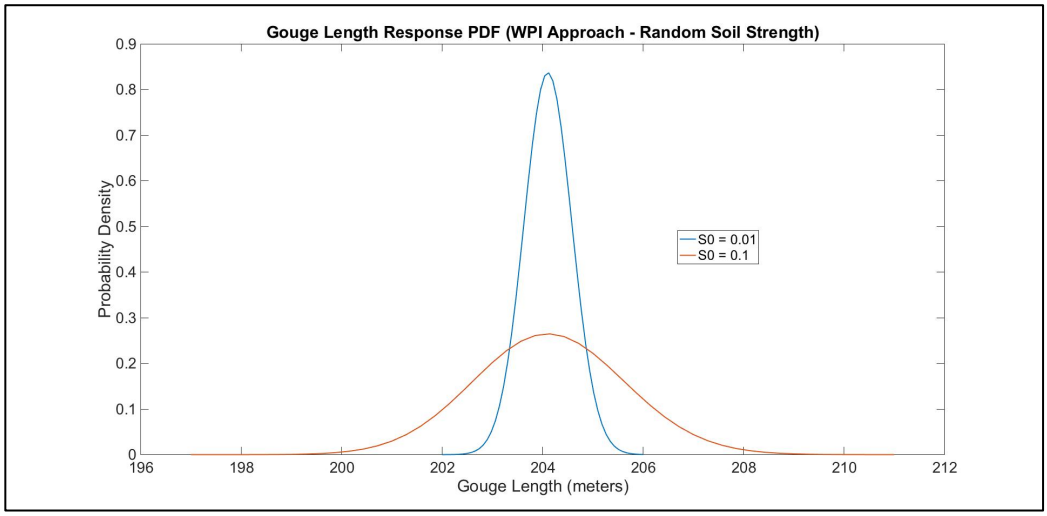

Figure 7-5: Gouge Length Response PDFs (WPI approach)

Both responses have the same mean value, however, the response derived considering the larger power spectrum value has a higher response variance (i.e. the response PDF is wider).

Since the gouge length PDF is computed, a transformation is conducted (see Section 2.1.2) to convert it to a response PDF for gouge depth (according to the relationship $\mathrm{d} = \mathrm{x}\tan\beta$) assuming a seabed slope of 1/100, a value within a typical range as presented in (Lopez et al., 1981).

To validate the approach, a Monte Carlo simulation is conducted and Eq. 7.10 is solved using a standard fourth order Runge-Kutta integration scheme (e.g.

Shampine, 1994) and utilizing 50,000 realizations. Figure 7-6 shows the gouge depth response PDFs derived using the WPI and MCS approaches for the case of $S_0 = 0.01$.

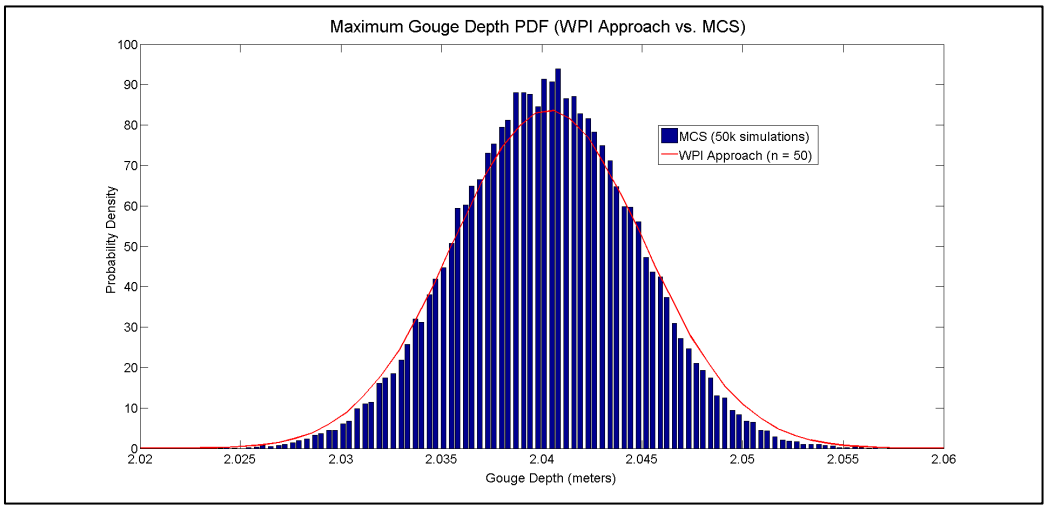

Figure 7-6: Maximum Gouge Depth Response PDF (WPI Approach vs. MCS)

As can be seen in Figure 7-6, a satisfactory level of accuracy is achieved using the WPI technique.

The approach can also be used to derive the response PDFs at different time instances if needed. Figure 7-7 shows the gouge depth response PDF as a function of time derived using the MCS and Figure 7-8 shows the comparison of the response PDFs derived using WPI and MCS approaches at various time instances.

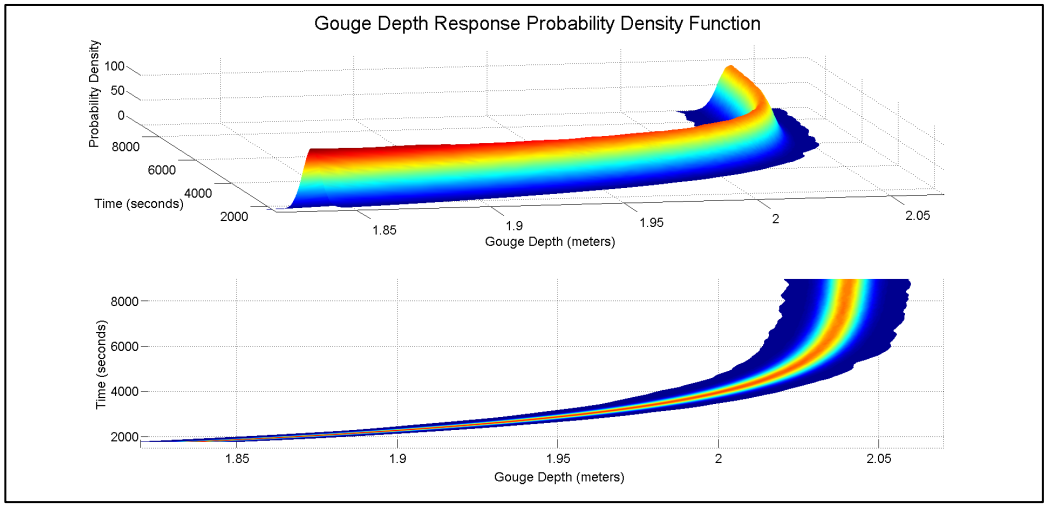

Figure 7-7: Gouge Depth Response PDF with Time (MCS)

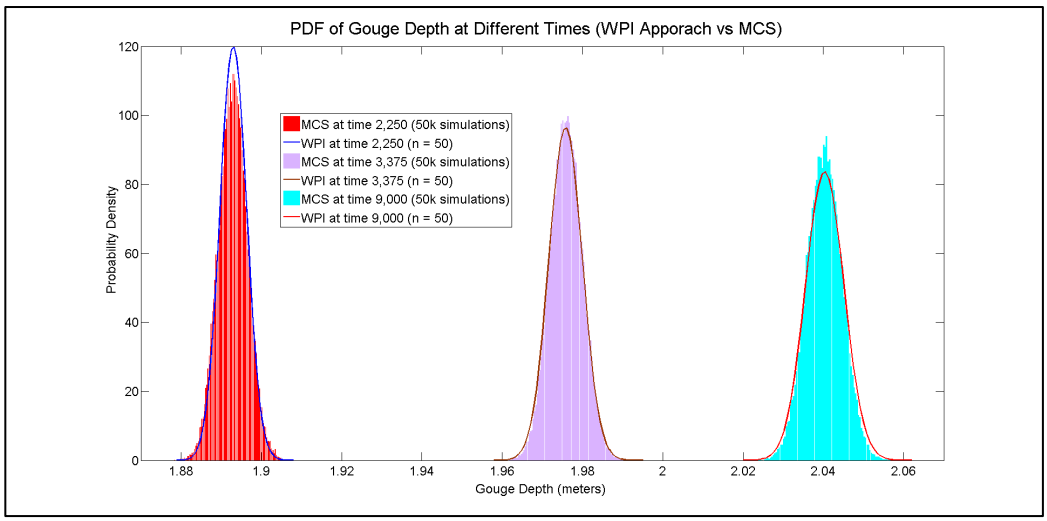

Figure 7-8: Gouge Depth Response PDF at Different Time Instances (WPI Approach vs. MCS)

As can be seen in the figures, a satisfactory level of accuracy is achieved with the WPI approach. It is worth noting that for Figure 7-8 an approximate range of values for the final velocity were required (i.e. $\dot{x}_{i,f,min}$, and $\dot{x}_{i,f,max}$) to solve n^2 BVPs and to compute the response PDFs at the different time instances. This, of course, is due to the fact that the final velocity is unknown at the intermediate time instances.

7.3.3.2 Random Drag Coefficient

The resulting depth response PDFs are shown in Figure 7-9.

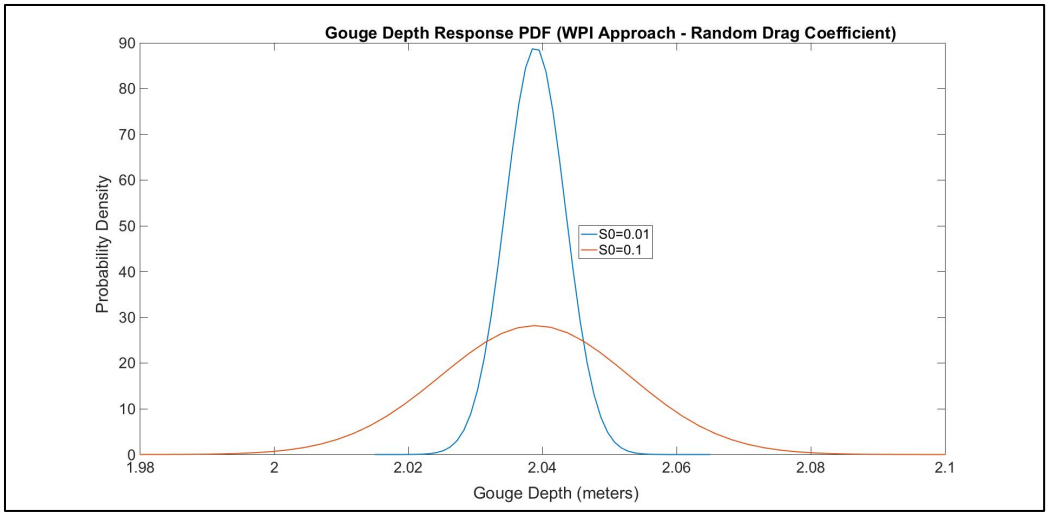

Figure 7-9: Gouge Depth Response PDFs (WPI approach)

Again, both responses have the same mean value, however, the response derived considering the larger power spectrum value has a higher response variance (i.e. the response PDF is wider).

Figure 7-10 shows the gouge depth response PDFs derived using the WPI and MCS approaches for the case of $S_0 = 0.1$.

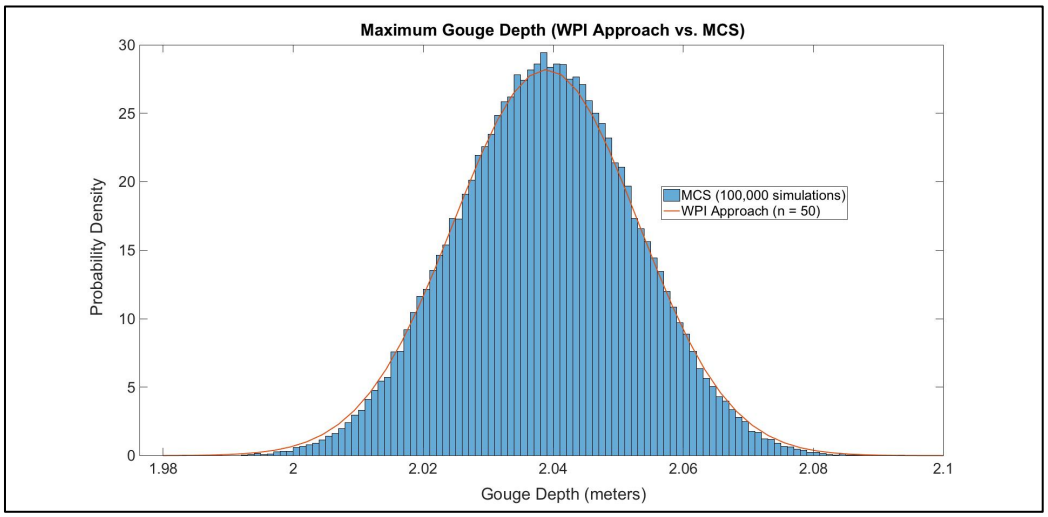

Figure 7-10: Maximum Gouge Depth Response PDF (WPI Approach vs. MCS)

As can be seen in Figure 7-10, a satisfactory level of accuracy is achieved using the WPI technique.

The gouge depth response PDFs derived for both the random soil strength and random drag coefficient cases considering $S_0 = 0.1$ are plotted in Figure 7-11.

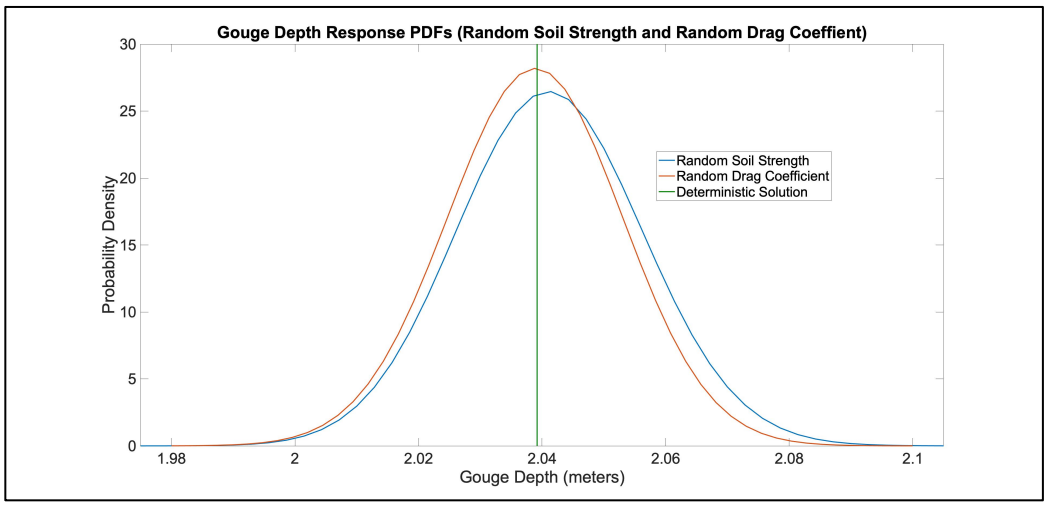

Figure 7-11: Gouge Depth Response PDFs (Random Soil Strength vs. Random Drag Coefficient)

As seen in Figure 7-11, the estimated mean gouge depth and variance are slightly larger for the case of the random soil strength (i.e. the peak of the PDF is shifted to the right and the PDF is slightly wider). The deterministic solution is also plotted for reference.

7.4 DISCUSSION

The maximum gouge depth response PDF is computed by solving n = 50 boundary value problems only. Obviously, the computational cost of the developed technique increases with an increasing value of n, or, in other words, when a relatively denser discretization map is utilized. Nevertheless, it is noted that to obtain reliable response PDF estimates via MCS, especially in the tails of the PDF where samples occur with low probability, the number of realizations to be produced and of subsequent numerical integrations of Eq. 7.10 and Eq. 7.11 need to be large (on the order of 10^6 simulations). To provide an order of magnitude for the example presented above, the 50 BVPs that were solved for

the WPI approach required only a few minutes (i.e. between 1 to 2 minutes) of computational time while the MCS approach required several hours (i.e. between 6 to 7 hours) of computational time to solve 50,000 simulations using the same machine.

Additionally, note that the proposed approach is befitting for determining the maximum gouge depth as only n BVPs are required versus n^2 (which would be the case in general stochastic response determination problems, e.g. Kougioumtzoglou and Spanos, 2012). This is due to the fact that the final velocity is zero.

Although the current study considered only the uncertainties in the soil strength and the drag coefficient, the model can be modified to consider the uncertainty in other parameters as well such as berg mass, current velocity etc. Further, it was found that the case considering the uncertainties in the soil strength resulted in a response PDF with a larger variance than the case considering the uncertainties in the drag coefficient. This may suggest that the gouge depth response is more sensitive to the uncertainties in the soil strength than the drag coefficient. However, more studies are required in order to confirm this conclusion.

Also, it is envisioned that future work will consider more sophisticated stochastic modeling as well as system modeling.

7.5 CONCLUDING REMARKS

Ice gouging has been identified as a concern for oil and gas development in the arctic and thus has prompted efforts to develop mathematical models of the gouging event (e.g. Walter and Phillips, 1998). Accurate theoretical models are

required to circumvent the costly seabed survey campaigns. In the present study, a previous formulation governing the ice gouging has been enhanced and then extended to consider the uncertainties in the soil strength and the drag coefficient. Further, the recently developed Wiener path integral technique for treating certain random vibration problems has been applied to solve the SDE governing the ice gouging motion. Specifically, a Lagrangian formulation in conjunction with a variational principle has been utilized to derive an Euler-Lagrange equation governing the most probable response trajectory. The boundary value problem has then been solved numerically and the corresponding response probability density function has been derived. The proposed approach is especially well suited for determining the maximum gouge depth as only n boundary value problems need to be solved as opposed to n^2 (which would be the case in general stochastic response determination problems, e.g. Kougioumtzoglou and Spanos, 2012), due to the fact that the final velocity is known (i.e. $\dot{\mathrm{x}}_{\mathrm{c}}(\mathrm{t}_{\mathrm{f}}) = 0$).

Further, the reliability of the approach has been demonstrated by comparing the results to those obtained by Monte Carlo simulations. The resulting PDFs computed via the WPI compare well to those computed using the more computationally demanding MCS-based approach.

The advantage of the proposed stochastic dynamics based approach over other approaches is computational efficiency, which hinges on the simplified model adopted to estimate the gouge depth coupled with the efficient WPI based solution used to conduct the stochastic analysis. The accuracy of sophisticated FEM based approaches is not necessarily higher than that of more approximate analytical approaches since a high level of uncertainty is involved in the selection of parameter values related to the system and to the excitation/environment. Further, parameter uncertainty is more prevalent in the

beginning stages of projects when in-situ data is limited or not available. As such, it is envisaged that the developed approach can be used during the “desk-top” study or “front-end” phases of projects given the high level of uncertainty involved in the selection of parameter values related to the system and to the excitation/environment in these phases. During the later stages of projects (i.e. detailed design, execution etc.) when in-situ data is gathered and the level of uncertainty is decreased, the use of more computationally demanding FEM based models is recommended. Nonetheless, the developed approach can provide a good first approximation of the gouge length/depth. Further, parametric studies are feasible using the developed approach since it is orders of magnitude more efficient than the common MCS-based approaches currently used in the industry for system response and reliability analysis.

Finally, note that although path integrals have reformulated and revolutionized theoretical physics, the engineering mechanics community has neglected their potential for uncertainty quantification of systems of engineering interest. It is hoped that the WPI will offer a potent new tool for treating complex offshore oil and gas problems where uncertainties are prevalent.

8 CONCLUSIONS

To realistically capture the behavior of a dynamic system the randomness inherent in virtually all dynamic problems must be considered. This requires stochastic analysis techniques. The goals of every stochastic dynamics based solution should be accuracy and computational efficiency. The most accurate and efficient method is to obtain the exact solution by solving the associated Fokker-Planck-Kolmogorov equation. However, the class of problems of nonlinear random vibrations that lend themselves to exact solutions is extremely limited. Moreover, exact solutions are rare or nonexistent for the non-stationary response of systems.

An accurate response can be derived using the Monte Carlo simulation method. However, in order to obtain reliable estimates of response variables, a sufficiently large sample size is required. This fact makes the method computationally expensive, especially in response analyses involving the estimation of rare events (e.g. failure probabilities). Nevertheless, given the strides made over the last few decades in computer power, and its simplicity, it can be seen that the MCS method will continue to be the most prevalent stochastic dynamics tool used in practice. In fact, “smart” MCS approaches have been developed recently (Au and Wang, 2014) to decrease the computation time. One such approach is the Subset Simulation method proposed by Au and Beck (2001). The idea behind their approach is to express the failure probability as a product of larger conditional failure probabilities by introducing intermediate failure events. With a proper choice of intermediate failure events, the conditional probabilities involved, become sufficiently large so

that they can be estimated efficiently by direct Monte Carlo simulation. Therefore, the problem of evaluating a small failure probability in the original probability space is replaced by a sequence of simulations of more frequent events in the conditional probability spaces. The approach has been shown to be computationally efficient and accurate when compared to the direct MCS method (Schueller and Pradlwarter, 2007).

The statistical linearization technique, which involves linearizing the equation of motion by replacing the original set of governing nonlinear equations with an equivalent set of linear equations, is extremely efficient to implement, and provides fairly good estimates of first and second moment statistics (e.g. mean and mean-square responses) when the damping is low. The technique can be extended to cope with the non-stationary response as well. However, due to the in-built assumption of Gaussianity, it doesn't accurately provide an estimate of the shape of the extreme tail ends of the response probability density function of nonlinear systems. Nevertheless, the approach is ideal for the beginning stages of projects when the parameters are not well established yet, complex systems can be simplified, and first and second moment statistics are sought.

One of the promising frameworks for solving random vibration problems relates to the concept of the Wiener path integral. The WPI has strongly impacted the field of theoretical physics, however, the engineering community has so far ignored its potential as a powerful stochastic dynamics tool. Recently, in (Kougioumtzoglou and Spanos, 2012) an approximate analytical WPI technique was developed based on a variational formulation and on the concepts of stochastic averaging/linearization for addressing certain stochastic engineering dynamics problems. In this regard, relying on the concept of the most probable path an approximate expression was derived for the non-stationary response probability density function. The aforementioned technique was enhanced in

(Kougioumtzoglou and Spanos, 2014) circumventing the approximations associated with the stochastic averaging/linearization treatment of the previous development and a novel WPI technique formulation/implementation was developed in (Kougioumtzoglou et al., 2015) that has drastically decreased the associated computational cost by several orders of magnitude, as compared to both the standard WPI technique and the MCS approach. Further, in recent work by (Psaros et al., 2018), the WPI technique was extended to account for non-white, non-Gaussian and non-stationary processes representing either the excitation of a MDOF dynamical system, or the media properties of a class of one-dimensional continuous systems. Although relatively accurate when compared to other techniques (e.g. statistical linearization), the WPI method is still approximate. The approximation is based on the fact that the most probable path is derived as opposed to the summation of all possible paths. There has been an ongoing effort to account for the fluctuations around the most probable path (see Chaichian and Demichev, 2001), which may increase the degree of accuracy.

The current thesis exploits approximate stochastic dynamics tools to solve engineering dynamics problems encountered in practice. In particular, the primary focus is directed towards the recently developed Wiener path integral technique, which has been shown to poses certain advantages over alternative well-established solution methodologies, namely, computational efficiency and accuracy. Two applications are investigated: the stochastic response of nonlinear vibratory energy harvesters, and, the depth determination of ice gouging events.

8.1.1 Stochastic Response of Nonlinear Vibratory Energy Harvesters

The motivation behind the development of VEHs is that compact and scalable electronic devices, such as wireless sensors, data transmitters and medical implants, are designed to function even with very low power levels. In this regard, VEHs aim at converting any available ambient energy into electricity, and eventually powering and enabling the independent operation of such devices. A main benefit of VEHs is that the need for re-charging and replacing batteries is circumvented. This is especially important considering in vivo biomedical implants such as pacemakers, where the replacement of batteries increases the risk of infection. Further, structural health monitoring applications have started benefiting from the utilization of wireless sensors powered by VEHs, resulting in reduced installation and maintenance costs as compared with alternative hard wired sensor configurations. Generally, VEHs use active materials (e.g. piezoelectric) and electromechanical coupling mechanisms to generate an electric potential in response to external/environmental excitations.

The majority of studies to date consider the excitations in a deterministic manner. However, in reality, most VEHs are subject to environmental excitations that have random and time-varying characteristics. Further, the few papers that consider stochastic excitations almost exclusively use the maximization of the average (mean) harvested power as the optimization criterion.

A cantilever piezoelectric VEH system was adopted for the current study and was modeled as a SDOF system. The tip mass to distributed mass ratio is assumed to be sufficiently high enough for a SDOF system to accurately capture the response (Erturk and Inman, 2008a). Further, an uncoupled model

is used since the electrical resistance is low (Erturk and Inman, 2008b). In other words the mechanical oscillator influences the harvested circuit, but not vice versa. Further, both symmetrical and asymmetrical nonlinear restoring forces were considered. An exact solution to the nonlinear stochastic differential equation does not exist when assessing the non-stationary response; therefore, approximate solutions are required. The results indicate that the adaptation of the recently developed approximate WPI technique for stochastic analysis is both computationally efficient and accurate when compared to the MCS based method.

8.1.2 Ice Gouge Depth Determination

Ice gouging has been identified as a concern for oil and gas development in the arctic and thus has prompted efforts to develop mathematical models of the gouging event. Accurate theoretical models are desirable to circumvent the costly seabed survey campaigns. Therefore, it is important to understand the mechanics of the grounding berg, as well as, consider the uncertainty inherent in the environment. Sophisticated finite element method based models have been developed to predict the ice gouge behavior, however, they require significantly more computational effort when compared to more analytical approaches. Further, FEM based methods can become computationally prohibited when utilized in conjunction with a stochastic framework. Therefore, approximate analytical treatments of the ice-gouge problem are appropriate.

The current work extended and generalized a model proposed in (Lopez et al., 1981) circumventing some of its limitations. Further, a stochastic model was developed taking into account the uncertainty in the environment, and the problem was solved using the WPI approach. The validity of the study was demonstrated by comparing the results to pertinent MCS data. The proposed

approach is orders of magnitude less computationally demanding when compared to brute force MCS based approaches. The combination of a simplified model and the efficient WPI based solution establishes the proposed approach as a viable alternative to previous approaches, at least at a preliminary design level.

8.2 FUTURE WORK

8.2.1 Sophisticated Stochastic Modeling

There is no doubt that more realistic solutions are obtained when considering the inherent randomness in dynamic systems. The current work has considered the uncertainties in the excitation (in the case of the VEH), and parameters (in the case of ice gouging) modeled as Gaussian white noise processes. In reality, systems subjected to the environment have random and time-varying characteristics (e.g. winds, waves etc.), and researchers have realized the need for modeling the uncertainties as *non-white* and even fully *non-stationary processes* characterized by evolutionary power spectrums. In this regard, future work should consider more sophisticated stochastic modeling approaches by including non-Gaussian media and excitation modeling. Once the uncertainties are properly modeled, and taking into account the work by (Psaros et al., 2018) which extends the WPI approach to account for non-white, non-Gaussian and non-stationary processes, the recent generalizations of the WPI technique can be adapted to handle these significantly more complex equations governing the behavior of the VEH and gouging phenomenon.

8.2.2 Ice Gouging Parametric Study

When estimating the gouge length/depth, it was observed that some parameters might influence the response more than others. Lopez et al. (1981) conducted parametric studies to assess the effect of the drag force and soil strength on the system response. They found that when the drag coefficient is sufficiently small it has a minimal influence on the response, and as the drag coefficient is increased its affect on the response is also increased only after a certain critical point is reached. Further, they found that for large soil strengths, the influence from the drag force diminishes completely. From these parametric studies, Lopez et al. (1981) derived a set of simple algebraic equations that can estimate the gouge length/depth of the berg. A useful extension of this study would be to conduct it in the stochastic domain. Specifically, the gouge length/depth can be derived for a range of values (e.g. mass, drag, soil strength etc.) while considering the uncertainty in other parameters in order to assess the influence on the response. This study can be useful for designers, as it would provide insight into how much detail is required when collecting in-situ data. For example, if variability in soil strength has a minimum influence on the response, then fewer soil borings may be required, and cost savings can be realized during the front-end of projects.

9 REFERENCES

Abdalla, B., Jukes, P., Eltaher, A., and Duron, B., 2008, “The Technical Challenges of Designing Oil and Gas Pipelines in the Arctic,” Oceans ‘08 MTS/IEEE, Quebec City, QC.

Abdalla, B., Pike, K., Eltaher, A., Jukes, J. and Duron, B., 2009, “Development And Validation Of A Coupled Eulerian Lagrangian Finite Element Ice Scour Model,” Proceedings 28th International Conference on Ocean, Offshore and Arctic Engineering, 5, pp. 87-95.

Abramowitz, M. and I. A. Stegun, 1972, Handbook of Mathematical Functions with Formulas, Graphs and Mathematical Tables. Washington: U.S. Govt. Off.

Adhikari, S., Friswell, M. I. and D.J. Inman, (2009), Piezoelectric energy harvesting from broadband random vibrations. Smart Materials and Structures, 18(11): 115005.

Adhikari, S., Friswell, M.I., Litak, G., Haddad Khodaparast, H., (2016), Design and analysis of vibration energy harvesters based on peak response statistics, Smart Mater. Struct. 25 (6).

Agdas, Duzgun, Michael T. Davidson, and Ralph D. Ellis. (2011). "Efficiency Comparison of Markov Chain Monte Carlo Simulation with Subset Simulation (MCMC/ss) to Standard Monte Carlo Simulation (sMC) for Extreme Event Scenarios." Vulnerability, Uncertainty, and Risk Analysis, Modeling, and Management, ASCE, Hyattsville, Maryland, 86-95.

Ali, S., Adhikari, S., and Friswell, M. I., (2010), “Piezoelectric Energy Harvesting With Parametric Uncertainty,” Smart Mater. Struct., 19(10), p. 105010.

American Institute of Steel Construction, (2016). Specifications for Structural Steel Buildings, ANSI/AISC 360-16.

Ang, A.S., Tang, W.H., 2007, Probability Concepts in Engineering, J. Wiley & Sons, NJ, Chap. 1 and Chap. 4.

Au, S.K., Beck, J.L., Estimation of small failure probabilities in high dimensions by subset simulation, Probab. Eng. Mech. 16 (4) (2001) 263–277.

Au S.K., Wang Y., 2014, Engineering Risk Assessment with Subset Simulation, J. Wiley & Sons, Singapore, Chap. 2.

Banneyake, R., Hossain, M. K., Eltaher, A., Nguyen, T., & Jukes, P., 2011, “Ice-Soil-Pipeline Interactions Using Coupled Eulerian-Lagrangian (CEL) Ice Gouge Simulations - Extracts From Ice Pipe JIP,” Offshore Technology Conference, OTC-22047-MS.

Barrette, P., 2011, “Offshore Pipeline Protection Against Seabed Gouging By Ice: An Overview,” Cold Regions Science and Technology, 69(1), pp. 3-20.

Beaman, F. J., and Wedrlck, J. K., (1981). Improved statistical linearization analysis and control of nonlinear stochastic systems. Part 1: Dyn. Syst. Measure Control, ASME 103, 14-21.

Beeby, S.P., Tudor, M.J., White, N.M., (2006). Energy harvesting vibration sources for microsystems applications, Measurement Science and Technology 17 (12) R175.

Beeby, S. P., Torah, R. N., Tudor, M. J., Glynne-Jones, P., O’Donnell, T., Saha, C. R., and Roy, S., (2007). “A Micro Electromagnetic Generator for Vibration Energy Harvesting,” J. Micromech. Microeng., 17(7), p. 1257.

Been, K., Kosar, K., Hachey, J., Rogers, B.T. & Palmer, A.C., 1990, “Ice Scour Models,” International Conference on Offshore Mechanics and Arctic Engineering, 5, pp. 179 - 188.

Caughey, T. K., (1963) Derivation and Application of the Fokker-Planck Equation to Discrete Nonlinear Dynamic Systems Subjected to White Random Excitation. Journal of the Acoustical Society of America, 35 (11).

Caughey, T.K., Ma, F., 1982, "The exact steady-state solution of a class of non-linear stochastic systems," International Journal of Non-Linear Mechanics, Vol. 17, 3, pp 137-142.

Chaichian M., Demichev A., 2001, Path integrals in Physics, Vol. I, Stochastic Processes and Quantum Mechanics, Institute of Physics Publishing, Bristol and Philadelphia.

Chari, T.R., 1975, “Some Geotechnical Aspects of Iceberg Grounding,” Ph.D. Thesis, Memorial University of Newfoundland, St. John's, Canada.

Chari, T.R., 1979, “Geotechnical Aspects of Iceberg Scours on Ocean Floors,” Canadian Geotechnical Journal, 16(2), pp. 379-390.

Chari, T.R., Peters, G.R., Muthukrishnaiah, K., 1980, “Hydrodynamic Effects on Iceberg Gouging,” Cold Regions Science and Technology, 1(3-4): pp. 223-230.

Chen, X. (2008). “Analysis of alongwind tall building response to transient nonstationary winds.” J. Struct. Eng., 134(5), 782–791.

Chen, J., Hui, M. C. H., and Xu, Y. L. (2007). “A comparative study of stationary and non-stationary wind models using field measurements.” Bound. Layer Meteorol., 122(1), 105–121.

Cheng, M., Chen, Y., Wei, H. and W. Seah, 2013, Event-driven energy-harvesting wireless sensor network for structural health monitoring. Proceedings of the 2013 IEEE 38th Conference on Local Computer Networks (LCN), Sydney (Australia).

Chopra, A. K., 1995, Dynamics of Structures Theory and Applications to Earthquake Engineering, Prentice Hall, Upper Saddle River, NJ. Chap. 3.

Coyne, J.C., Lewis, G.W., 1999, "Analysis of Plowing Forces for a Finite-Width Blade in Dense, Ocean Bottom Sand," OCEANS '99 MTS/IEEE, 1, pp. 1-10.

Crandall, S.H., Mark, W.D., 1963, Random Vibration in Mechanical Systems, Academic Press, London.

Crandall, S.H., (1980). Non-Gaussian closure for random vibration of non-linear oscillator. Int. J. Nonlin. Mech. 15, 303-313

Crandall, S.H., (1985). Non-Gaussian closure for stationary random vibrations. Int. J. Nonlin. Mech. 20, 1-

Croasdale, K., Comfort, G. & Been. K., 2005, “Investigation of Ice Limits to Ice Gouging,” Proceedings. 18th International Conference on Port and Ocean Engineering Under Arctic Conditions, 1, pp. 23 - 32.

Daqaq MF, Masana R, Erturk A, Dane Quinn DD. (2014), On the Role of Nonlinearities in Vibratory Energy Harvesting: A Critical Review and Discussion. ASME. Appl. Mech. 66(4).

De Coster C., Habets P., 2006, Two-Point Boundary Value Problems: Lower and Upper Solutions, Elsevier, Amsterdam, Chap. 1.

Det Norske Veritas, 2010, Environmental Conditions and Environmental Loads, DNV-RP-C205.

Det Norske Veritas, 2012, Statistical Representation of Soil Data, DNV-RP-C207.

Det Norske Veritas, 2013, Submarine Pipeline Systems, DNV-OS-F101.

Di Matteo A., Kougioumtzoglou I. A., Pirrotta A., Spanos P. D., Di Paola M., 2014, “Non-Stationary Stochastic Response Determination Of Nonlinear Oscillators with Fractional Derivatives Elements via the Wiener Path Integral,” Probabilistic Engineering Mechanics, 38, pp. 127-135.

Di Paola M, Santoro R. (2008). Path integral solution for nonlinear system enforced by Poisson white noise. Probab Eng Mech; 23:164–9.

duToit N. E., Wardle B. L., (2007) Experimental verification of models for microfabricated piezoelectric vibration energy harvesters AIAA J. 45 1126–37

Elvin, N. G., Lajnef, N. and A.A. Elvin, 2006, Feasibility of structural monitoring with vibration powered sensors. Smart Materials and Structures, 15(4): 977-986.

Erturk A and Inman D J (2008a) On mechanical modeling of cantilevered piezoelectric vibration energy harvesters J. Intell. Mater. Syst. Struct. 19 1311–25.

Erturk A and Inman D J (2008b) Issues in mathematical modeling of piezoelectric energy harvesters Smart Mater. Struct.17 065016.

Ewing G. M., 1985, Calculus of Variations with Applications, Dover, New York, Chap. 4.

Feynman R. P., 1948, “Space-Time Approach to Non-Relativistic Quantum Mechanics,” R. M. Phys., 20, pp. 367-387.

Galambos, T.V., Ellingwood, B., MacGregor, J.G. and Cornell, C.A. (1982), “Probability- Based Load Criteria: Assessment of Current Design Practice,” Journal of the Structural Division, ASCE, Vol. 108, No. ST5, pp. 959–977.

Gazis, N., & Kougioumtzoglou, I. A. (2015). A Stochastic Dynamics Approach for Ice Gouge Depth Determination. International Society of Offshore and Polar Engineers (ISOPE).

Gazis N, Kougioumtzoglou IA, Patelli E. (2017). Ice Gouge Depth Determination Via an Efficient Stochastic Dynamics Technique. ASME. J. Offshore Mech. Arct. Eng. 2016;139(1).

Gomes, W., T. Beck, A., 2014, “Optimal Inspection and Design of Onshore Pipelines Under External Corrosion Process,” Structural Safety, 47, pp. 48-58.

Green, P.L., Worden, K., Atallah, K., Sims, N.D., (2012), The benefits of Duffing-type nonlinearities and electrical optimisation of a mono-stable energy harvester un- der white Gaussian excitations. Journal of Sound and Vibration, 331(20):4504 4517.

He, Qifan & F. Daqaq, Mohammed. (2015). Electric load optimization of a nonlinear mono-stable duffing harvester excited by white noise. Meccanica. 51. 10.1007/s11012-015-0289-7.

Huang, G., Zheng, H., Xu, Y., and Li,Y. (2015), Spectrum models for nonstationary extreme winds. Journal of Structural Engineering. 10.1061/(ASCE)

Ibrahim, R. A., (1985), Parametric Random Vibration. John Wiley, New York.

Igusa T, Der Kiureghian A. Response of uncertain systems to stochastic excitations. ASCE Journal of Engineering Mechanics 1988;114(3):812–32.

Iwan, W.D., Mason, A.B., (1980) “Equivalent linearization for systems subjected to non-stationary random excitation,” International Journal of Non-Linear Mechanics, Vol. 15, Issue 2, pp 71-82.

Jukes, P., Eltaher, A., Abdalla, B. and Duron, B., 2008, “The Design and Simulation of Arctic Subsea Pipelines – Ice Gouging Formulations,” 4th Annual Arctic Oil & Gas Conference, Oslo, Norway.

Kazakov, I.E. (1965). Generalization of the Method of Statistical Linearization to Multidimensional Systems, Auto. Remote Control, 26, 1201-1206.

Kenny, S., Barrett, J., Phillips, R. and Popescu, R., 2007, “Integrating Geohazard Demand and Structural Capacity Modeling within a Probabilistic Design Framework for Offshore Arctic Pipelines,” Proceedings Seventeenth International Ocean and Polar Engineering Conference (ISOPE), Lisbon, Portugal, ISOPE2007-SBD-03.

King, T., Phillips, R., Barrett, J., Sonnichsen, G., 2009, “Probabilistic Pipeline Burial Analysis for Protection Against Ice Scour,” Cold Regions Science and Technology 59(1), pp. 58–64.

Kioka, S., Saeki, H., 1995, “Mechanics of Ice Gouging.” Proceedings 5th International Offshore and Polar Engineering Conference (ISOPE), 2, pp. 398-402.

Kolmogorov, A.N., (1965), Foundations of the Theory of Probability, Chelsea, New York.

Kong F., Spanos P. D., Li J., Kougioumtzoglou I. A., 2014. Response evolutionary power spectrum determination of chain-like MDOF nonlinear structural systems via harmonic wavelets, International Journal of Non-Linear Mechanics, vol. 66: 3-17

Konuk, I.S. and Gracie, R., 2004, “A 3-Dimensional Eulerian FE Model for Ice Scour,” International Pipeline Conference, Calgary, Alberta, IPC2004-0075, pp. 1911-1918.

Konuk, I.S., Yu, S. Gracie, R., 2005, “An ALE FEM Model of Ice Scour,” Proc. 11th International Conference of the International Association of Computer Methods and Advance in Geomechanics, Turin, Italy, 3, pp. 63-70.

Kougioumtzoglou I. A., 2013, “Stochastic Joint Time-Frequency Response Analysis of Nonlinear Structural Systems,” Journal of Sound and Vibration, 332, pp. 7153-7173.

Kougioumtzoglou I. A., Spanos P. D., 2009, “An Approximate Approach for Nonlinear System Response Determination Under Evolutionary Stochastic Excitation,” Current Science, 97, pp. 1203-1211.

Kougioumtzoglou I. A., Spanos P. D., 2012, “An Analytical Wiener Path Integral Technique for Non-Stationary Response Determination of Nonlinear Oscillators,” Probabilistic Engineering Mechanics, 28, pp. 125-131.

KougioumtzoglouI A , Spanos PD. (2013a). Response and first-passage statistics of nonlinear oscillators via a numerical path integral approach. ASCE J Eng Mech;139:1207–17.

Kougioumtzoglou I. A., Spanos P. D., (2013b), “Nonlinear MDOF System Stochastic Response Determination via a Dimension Reduction Approach,” Computers and Structures, 126, pp. 135-148.

Kougioumtzoglou, I. A., Spanos P. D., 2014, “Nonstationary Stochastic Response Determination of Nonlinear Systems: A Wiener Path Integral Formalism,” J. Eng. Mech., 10.1061/(ASCE)EM.1943-7889.

Kougioumtzoglou I. A., Di Matteo A., Spanos P. D., Pirrotta A., Di Paola M., 2015. An efficient Wiener path integral technique formulation for stochastic response determination of nonlinear MDOF systems, ASME Journal of Applied Mechanics, vol. 82, 101005: 1-7.

Kougioumtzoglou I. A., Spanos P. D., 2016. Harmonic wavelets based response evolutionary power spectrum determination of linear and nonlinear oscillators with fractional derivative elements, International Journal of Non-Linear Mechanics, vol. 80: 66-75.

Kougioumtzoglou I. A., 2017. A Wiener path integral solution treatment and effective material properties of a class of one-dimensional stochastic mechanics problems, ASCE Journal of Engineering Mechanics, vol. 143 (6), 04017014: 1-12.

Langley, R.S., (2014), A general mass law for broadband energy harvesting, J. Sound Vib. 333 (3) (2014) 927–936, http://dx.doi.org/10.1016/j.jsv.2013.09.036.

Li J., Chen j., 2009, Stochastic Dynamics of Structures, J. Wiley & Sons, Singapore.

Liferov, P., Shkhinek, K. N., Vitali, L., & Serre, N., 2007, “Ice Gouging Study - Actions And Effects,” Port and Ocean Engineering Under Arctic Conditions POAC-07, Dalian, China, ISBN 978-7-5611-3631-7, pp. 774-786.

Lin, Y. K. (1967). Probabilistic theory of structural dynamics, McGraw Hill, New York.

Lopez, R., Chari, T.R., Moore, E., Peters, G.R., Zielinski, A., 1981, “Environmental Factors Affecting Iceberg Scour Estimates,” Cold Regions Science and Technology, 4(1), pp. 55-61.

Lutes, L. D., & Sarkani, S. (2004). Random vibrations: Analysis of structural and mechanical systems. Amsterdam: Elsevier.

Mann, B. P., and Sims, N. D., 2008, “Energy Harvesting From the Nonlinear Oscillations of Magnetic Levitation,” J. Sound Vib., 319, pp. 515–530.

Marano, G. C., Greco, R. and Sgobba, S. 2010. A comparison between different robust optimal design approaches: Application to tuned mass dampers. Probabilistic Engineering Mechanics, 25(1): 108-118.

Meimaris A., Kougioumtzoglou I. A., Pantelous A., 2017. A closed form approximation and error quantification for the response transition probability density function of a class of stochastic differential equations, Probabilistic Engineering Mechanics, doi.org/10.1016/j.probengmech.2017.07.005 (In Press).

Morison, J.R., Johnson, J.W., Shaaf, S.A., 1950, “The Force Exerted by Surface Waves on Piles,” Journal of Petroleum Technology, 2, pp. 149-154.

Naess. A., Johnsen, J.M., (1993). Response statistics of nonlinear, compliant offshore structures by the path integral solution method, Probabilistic Engineering Mechanics, Vol. 8, Iss. 2, Pp. 91-106.

Newland, D.E., 2005, An Introduction to Random Vibrations, Spectral and Wavelet Analysis, Dover Publications Inc.

Noori, M., Saffar, A., Davoodi, H., A comparison between non-gaussian closure and statistical linearization techniques for random vibration of a nonlinear oscillator, Comput. Struct. 26 (6) (1987) 925–931

OG21 Strategy Report, 2006, “Technology Strategy for the Arctic,” Technical Report, Oil and Gas in the 21 Century, The Research Council of Norway.

Palmer, A., Konuk, I., Love, J., Been, K. and Comfort, G., 1989, “Ice Scour Mechanics,” A Research Paper prepared for Canada Oil and Gas Lands Administration and Gulf Canada Resources Ltd.

Palmer, A.C., Niedoroda, A., 2005, “Ice Gouging and Pipelines: Unresolved Questions,” Proceedings of the 18th Conference on Ports and Ocean Engineering Under Arctic Conditions (POAC), Potsdam, NY, USA, 1, pp. 11–22.

Pate-Cornell, E. (1994), “Quantitative Safety Goals for Risk Management of Industrial Facilities,” Structural Safety, Elsevier, Vol. 13, No. 3, pp. 145–157.

Phillips, R., Barrett, J. and Al-Showaiter, A., 2010, “Ice Keel-Seabed Interaction: Numerical Modeling Validation,” Offshore Technology Conference, OTC2010-20696.

Pirrotta A, Santoro R. Probabilistic response of nonlinear systems under combined normal and Poisson white noise via path integral method. Probab Eng Mech 2011;26:26–32.

Pishro-Nik, H. (2014), "Introduction to probability, statistics, and random processes", available at https://www.probabilitycourse.com, Kappa Research LLC.

Priestley M. B., 1965. Evolutionary spectra and non-stationary processes, Journal of the Royal Statistical Society, vol. 27: 204-237.

Priestley M. B., 1988. Non-linear and non-stationary time series analysis, Academic Press, San Diego.

Psaros, A.F., Brudastova, O., Malara, G., Kougioumtzoglou, I.A., (2018). Wiener Path Integral based response determination of nonlinear systems subject to non-white, non-Gaussian, and non-stationary stochastic excitation, Journal of Sound and Vibration, Vol. 433, 314-333.

Roberts, J.B., (1981). Response of nonlinear Mechanical Systems to Random Excitation: Part II; Equivalent Linearization and Other Methods, Shock Vib. Digest, 12, 15-29.

Roberts J. B., Spanos P. D., 1986. Stochastic Averaging: An Approximate Method of Solving Random Vibration Problems, International Journal of Non-Linear Mechanics, vol. 21: 111-134.

Roberts J. B., Spanos P. D., 2003. Random Vibration and Statistical Linearization. New York: Dover Publications.

Roundy S., Wright P. and Rabaey J. (2004) Energy Scavenging for Wireless Sensor Networks with Special Focus on Vibrations (Boston, MA: Kluwer–Academic).

Rubinstein R. Y., Kroese D. P., 2007, Simulation and the Monte Carlo Method, John Wiley & Sons, Hoboken.

Schuëller GI, Pradlwarter HJ, Koutsourelakis PS. A critical appraisal of reliability estimation procedures for high dimensions. Prob Eng Mech 2004;19(4):463–74.

Schueller GI, Pradlwarter HJ. Benchmark study on reliability estimation in higher dimensions of structural systems - an overview. HJ. Benchmark study on

Schuëller, G.I., 2007, “On the Treatment of Uncertainties in Structural Mechanics and Analysis,” Computers and Structures, 85, pp. 235–243.

Shampine, L. F., 1994, Numerical Solution of Ordinary Differential Equations, Chapman & Hall, New York, Chap. 4.

Shampine, L.F., Gladwell, I., and Thompson, S., (2003).
Solving ODEs with MATLAB, Cambridge University Press

Shinozuka M., Deodatis G., 1991. Simulation of stochastic processes by spectral representation, Applied Mechanics Reviews, vol. 44, no4: 191-203.

Sicilia, C., Bonnet, E., & Cooper, P. A., 2014, “Probabilistic Lateral Buckling Assessment,” Proceedings Twenty-fourth International Ocean and Polar Engineering Conference (ISOPE), Busan, Korea, 25, pp. 241-246.

Socha, L. (2008). Linearization Methods for Stochastic Dynamic Systems. Springer, Berlin, Heidelberg

Soong, T. T., and Grigoriu, M. (1993). Random vibration of mechanical and structural systems, Prentice Hall, New Jersey.

Spanos, P. T. D. (1981a). Stochastic linearization in structural dynamics. Appl. Mech. Rev. 34:1-8

Spanos, P. T.D. (1981b) “A method for analysis of non-linear vibrations caused by modulated random excitation,” International Journal of Non-Linear Mechanics, Vol. 16,1, pp 1-11.

Spanos P T D, Lutes L D 1987 A primer of random vibration techniques in structural engineering. Shock Vib.Dig.19(4):3-9

Spanos P. D., Kougioumtzoglou I. A., 2014, “Survival Probability Determination of Nonlinear Oscillators Subject to Evolutionary Stochastic Excitation,” Journal of Applied Mechanics, 81, pp. 1-9.

Spanos, P. D., and Kougioumtzoglou, I. A. (2012). “Harmonic wavelets based statistical linearization for response evolutionary power spectrum determination.” Probab. Eng. Mech., 27(1), 57–68.

Spanos, P. D., and Kougioumtzoglou, I. A. (2014). “Survival probability determination of nonlinear oscillators subject to evolutionary stochastic excitation.” J. Appl. Mech., 81(5), 1–9.

Spanos P. D., Kougioumtzoglou I. A., dos Santos K. R. M., Beck A. T., 2018. Stochastic averaging of nonlinear oscillators: Hilbert transform perspective, ASCE Journal of Engineering Mechanics, vol. 144 (2), 04017173: 1-9.

Spanos P. D., Zeldin B. A., 1998. Monte Carlo treatment of random fields: A broad perspective, Applied Mechanics Reviews, vol. 51, no3: 219-237.

Terzaghi, K., Peck, R. B., and Mesri, G., 1996, Soil Mechanics in Engineering Practice, 3rd Edition, Wiley, New York, Chap. 8.

Tomicek, D., Tham, Y., Seah, W. and R. Rayudu, 2013, Vibration-powered wireless sensor for structural monitoring during earthquakes. Proceedings of the 6th International Conference on Structural Health Monitoring of Intelligent Infrastructure (SHMII-6 2013), Hong Kong (P.R. China)

United States Geological Survey (USGS), 2008, “90 Billion Barrels of Oil and 1,670 Trillion Cubic Feet of Natural Gas Assessed in the Arctic.”

Walter, D. J., Phillips, R., 1998, “PRISE – Force models for Drained and Undrained Steady State Ice Scouring,” Technical Report, C-CORE Publications 98-C33.

Wiener N., 1921, “The Average of an Analytic Functional,” Proc. Natl. Acad. Sci. USA 7(9): 253-260.

Wirsching, P.H., Paez, T.L., Ortiz, K., 2006, Random Vibrations: Theory and Practice, Dover Publications Inc.

Zhu WQ., Stochastic Averaging Methods in Random Vibration. ASME. Appl. Mech. Rev. 1988;41(5):189-199.